Prenatal development of the human entorhinal cortex

Šimić, Goran; Krsnik, Željka; Knezović, Vinka; Kelović, Zlatko; Mathiasen, Mathias Lysholt; Junaković, Alisa; Radoš, Milan; Mulc, Damir; Španić, Ena; Quattrocolo, Giulia; ...

Source / Izvornik: **Journal of Comparative Neurology, 2022, 530, 2711 - 2748**

Journal article, Accepted version
Rad u časopisu, Završna verzija rukopisa prihvaćena za objavljivanje (postprint)

https://doi.org/10.1002/cne.25344

Permanent link / Trajna poveznica: https://urn.nsk.hr/urn:nbn:hr:105:401778

Prenatal development of the human entorhinal cortex

Goran Šimić,[1]* Željka Krsnik,[1] Vinka Knezović,[1] Zlatko Kelović,[2] Mathias Lysholt Mathiasen,[3] Alisa Junaković,[1] Milan Radoš,[1] Damir Mulc,[4] Ena Španić,[1] Giulia Quattrocolo,[5] Vanessa Jane Hall,[3] Laszlo Zaborszky,[6] Mario Vukšić,[1] Francisco Olucha Bordonau,[7] Ivica Kostović,[1] Menno P. Witter,[5] Patrick R. Hof[8]

[1]Department of Neuroscience, Croatian Institute for Brain Research, University of Zagreb Medical School, Zagreb, HR 10000, Croatia

[2]Department of Anatomy, University of Zagreb Medical School, Zagreb, HR 10000, Croatia

[3]Department of Veterinary and Animal Sciences, Faculty of Health Sciences, University of Copenhagen, Frederiksberg C, DK 1870, Denmark

[4]Psychiatric Hospital Vrapče, University of Zagreb Medical School, Zagreb, HR 10090 Zagreb, Croatia

[5]Kavli Institute for Systems Neuroscience and Centre for Neural Computation, Norwegian University of Science and Technology, Trondheim, NO 7491, Norway

[6]Center for Molecular and Behavioral Neuroscience, Rutgers, the State University of New Jersey, Newark, NJ 07102, USA

[7]Department of Medicine, School of Medical Sciences, Universitat Jaume I, Castellón de la Plana, ES 12071, Spain

[8]Nash Family Department of Neuroscience and Friedman Brain Institute, Icahn School of Medicine at Mount Sinai, New York, NY 10029, USA

***Correspondence**

Goran Šimić

Department of Neuroscience, Croatian Institute for Brain Research

University of Zagreb Medical School, Šalata 12, Zagreb HR-10000, Republic of Croatia

Email: gsimic@hiim.hr

Abstract

Little is known about the development of the human entorhinal cortex (EC), a major hub in a widespread network for learning and memory, spatial navigation, high-order processing of object information, multimodal integration, attention and awareness, emotion, motivation, and perception of time. We analyzed a series of 20 fetal and 2 adult human brains using Nissl stain, acetylcholinesterase (AChE) histochemistry, and immunocytochemistry for myelin basic protein (MBP), neuronal nuclei antigen (NeuN), a pan-axonal neurofilament marker, and synaptophysin, as well as postmortem 3T MRI. In comparison to other parts of the cerebral cortex, the cytoarchitectural differentiation of the EC begins remarkably early, in the 10th week of gestation (w.g.). The differentiation occurs in a superficial magnocellular layer in the deep part of the marginal zone, accompanied by cortical plate (CP) condensation and delamination of the deep part of CP. These processes last until the 13-14th w.g. At 14 w.g. the superficial lamina dissecans (LD) is visible, which divides the CP into the lamina principalis externa (LPE) and interna (LPI). Simultaneously, the rostral LPE separates into vertical cell-dense islands, whereas in the LPI, the deep LD emerges as a clear acellular layer. In the 16th w.g., the LPE remodels into vertical cell-dense and cell-sparse zones with a caudorostral gradient. At 20 w.g., NeuN immunoreactivity is most pronounced in the islands of layer II cells, whereas migration and differentiation inside-out gradients are seen simultaneously in both the upper (LPE) and the lower (LPI) pyramidal layers. At this stage, the EC adopts for the first time an adult-like cytoarchitectural organization, the superficial LD becomes discernible by 3 T MRI, MBP-expressing oligodendrocytes first appear in the fimbria and the perforant path (PP) penetrates the subiculum to reach its molecular layer and travels along through the CA fields to reach the suprapyramidal blade of the dentate gyrus, whereas the entorhinal-dentate branch perforates the hippocampal sulcus about 2-3 weeks later. The first AChE reactivity appears as longitudinal stripes at 23 w.g. in layers I and II of the rostrolateral EC and then also as AChE-positive in-growing fibers in islands of superficial layer III and layer II neurons. At 40 w.g., myelination of the PP starts as patchy MBP-immunoreactive oligodendrocytes and their processes. Our results refute the possibility of an inside-out pattern of the EC development and support the key role of layer II prospective stellate cells in the EC lamination. As the early cytoarchitectural differentiation of the EC is paralleled by the neurochemical development, these developmental milestones in EC structure and connectivity have implications for understanding its normal function, including its puzzling modular organization and potential contribution to consciousness content (awareness), as well as for its insufficiently explored deficits in developmental, psychiatric and degenerative brain disorders.

Keywords

acetylcholinesterase, Alzheimer's disease, consciousness, cytoarchitecture, entorhinal cortex, lamina dissecans, perforant path, periallocortex, schizophrenia, temporal lobe epilepsy

Abbreviations

ab, angular bundle

ACh, acetylcholine

AChE, acetylcholinesterase

ACx, archicortex (archipallium)

al, alveus

Amy, amygdala

AP, alvear pathway

BLA, basolateral nucleus of the amygdala

BrDU, bromodeoxyuridine

CA, Cornu Ammonis

CL, caudolateral entorhinal area

CP, cortical plate

CRC, Cajal-Retzius cells

CRL, crown-rump length

DG, dentate gyrus (including fascia dentata and "CA4" [hilus of the dentate fascia])

E, embryonic day

EC, entorhinal cortex

E_C, caudal subarea of EC

E_{CL}, caudal limiting subarea of EC

E_I, intermediate subarea of EC

E_{Lc}, lateral caudal subarea of EC

E_{Lr}, lateral rostral subarea of EC

E_{MI}, medial intermediate subarea of EC

E_O, olfactory subarea of EC

E_R, rostral subarea of EC

fMRI, functional magnetic resonance imaging

FOV, field of view

GE, ganglionic eminence

HA, area uncinata

HB, area parauncinata

HC, area rhinalis limitans

HRP-WGA, horseradish peroxidase-conjugated with wheat-germ agglutinin

HIPP, hippocampus

hs, hippocampal sulcus

In, insula

IZ, intermediate zone

LD, lamina dissecans

LD1, superficial lamina dissecans

LD2, deep lamina dissecans

LEC, lateral entorhinal cortex

LPE, lamina principalis externa

LPEd, lamina principalis externa - deep part

LPEs, lamina principalis externa - superficial part

LPI, lamina principalis interna

MBP, myelin basic protein

MEC, medial entorhinal cortex

MP-RAGE, magnetization-prepared rapid acquisition gradient echo

MRI, magnetic resonance imaging

MZ, marginal zone

Neo, prospective neocortex (isocortex, in figures, denotes temporal neopallium)

NEX, number of excitations

OA, occipital lobe, area A

OB, olfactory bulb

ots, occipitotemporal sulcus

PAM, periamygdaloid area

PaS, parasubiculum

P, putamen

PCW, postconceptional weeks

PHC, parahippocampal cortex

PP, perforant path

ppc, prepiriform cortex

pr, prorhinal cortex

PRC, perirhinal cortex

PrS, presubiculum

RM, rostromedial entorhinal area

RS, rhinal sulcus

SD1-7, stage of cell differentiation

SGL, subpial granular layer

SP, subplate zone

SUB, subiculum

SVZ, subventricular zone

T, thalamus

TE, time to echo

TF, temporal lobe, area F

TG, temporal lobe, area G

TH, temporal lobe, area H

TR, repetition time

VIBE, volumetric interpolated brain examination

VTA, ventral tegmental area

VZ, ventricular zone

w.g., weeks of gestation

wm, white matter

1. Introduction

The entorhinal cortex (EC) is a multimodal area in the temporal lobe that receives projections from many other cortical association areas and limbic structures. As the main interface between the hippocampal formation and the neocortex, it is a major hub in a widespread network for learning and memory, spatial navigation, high-order processing of object information, multimodal integration, attention, and perception of time (for review, see Buzsáki & Tingley, 2018; Alexander et al., 2020). The EC also interfaces between the hippocampus and the amygdala as its circuits are heavily involved in the processing of

emotional and social stimuli (Wahlstrom et al., 2018; Guthman et al., 2020; for review, see Šimić et al., 2020, 2021).

Brodmann was the first to realize that, together with the presubiculum (PrS) and parasubiculum (PaS), the EC belongs to a special part of the cortex (the periallocortex) in between the six-layered homogeneous isocortex and the inhomogeneous allocortex (a "different cortex", meaning different from six-layered isocortex, comprising the two-layered paleocortex and three-layered archicortex) (Brodmann, 1909; Insausti et al., 2017). Although the EC is a multilaminar cortex, it is highly atypical in comparison to other cortical areas. In the isocortex, larger neurons are found in the deeper (infragranular) layers, whereas smaller neurons predominantly occupy supragranular layers II and III (Solodkin & Van Hoesen, 1996). In the EC however, the largest, entorhinal projection neurons are found in layer II, whereas smaller neurons reside in the deeper layers. Thus, it has been proposed that the EC, together with PrS and PaS, is formed from both the allo- and isocortical plates, where deeper layers are formed from the allocortical origin and the superficial layers develop from the isocortex (Filimonoff, 1947; Rakic & Nowakowski, 1981). As these supposedly fuse during the development of the EC, a cell-free remnant of the allocortical molecular layer parallel to the pial surface forms a distinct lamina dissecans (LD) in between. Due to this unique cytoarchitectural feature of the EC, PrS, and PaS this type of cortex has been termed by many different names, most commonly as periallocortex, mesocortex, periarchicortex, juxtallocortex, and schizocortex ("split cortex") (Rose 1926, 1927a, 1927b). Herein, we use the term periallocortex. The laminar structure of the EC, as well as of the adjacent PaS and PrS also differs from the isocortex as the transition between the isocortex and periallocortical EC is not sharp, but comprised of an intervening temporopolar, perirhinal, and parahippocampal proisocortex (sometimes also called the paralimbic cortex). This transition cortex has six layers, as the isocortex, but retains some periallocortical features, such as prominent layers II and V, lacking or having a thin layer IV, and having lesser columnarity than the isocortex (Insausti et al., 2017).

In humans, the EC is the part of the cerebral cortex that occupies the rostral parts of the parahippocampal gyrus and the entire uncinate gyrus (Figure 1). Rostrally, the EC borders the amygdaloid complex and the perirhinal cortex (PRC, area 35). Laterally, throughout its whole rostrocaudal extent the EC is separated from the temporal polar and temporal fusiform regions (areas TF, TG, and TH of von Economo & Koskinas, 1925) by the PRC (areas TGa and THa of von Economo & Koskinas) in the medial bank of the rhinal sulcus and its caudal extension – the medial occipitotemporal sulcus, also known as the collateral sulcus (Figure 1a,b). Due to high variability, the rhinal and collateral sulcus could be also separated, both on the surface and in-depth (Fig. 3 of Insausti et al., 1995; Fig. 2 of Huntgeburth & Petrides, 2012). This rhinal sulcus should not be confused with a furrow at the most rostral part of the medial temporal lobe separating the piriform and perirhinal cortices (Insausti et al., 1995; Ding & Van Hoesen, 2010). Medially, the EC is separated from the periamygdaloid area (PAM) by the semiannular sulcus, whereas the caudal half of the EC borders with the PaS (Insausti et al., 1995). The EC also includes two small gyri located on the medial aspect of the uncus: the semilunar gyrus located medially, and the ambiens gyrus located laterally. The ambiens gyrus is separated from other parts of the uncus by the internal rhinencephalic sulcus, and from the semilunar gyrus by the semilunar sulcus. Based on its position, the EC is included in the cortical structures of the so-called outer ring (Isaacson, 1982) of the great limbic lobe (*le grand lobe limbique*) of Broca (Broca, 1878; Pessoa & Hof, 2015). The hippocampal formation, parahippocampal gyrus, and cingulate gyrus form most of the limbic cortex.

Brodmann (1909) first divided the human EC into two basic fields, areas 34 and 28 (Brodmann, 1909; Šimić & Hof, 2015). Area 34 (gyrus ambiens) belongs to the medial EC (Insausti et al., 2019), whereas area

28 was further divided into the lateral (28a) and medial part (28b). Based on complex cytoarchitectural criteria, Rose (1926, 1927a, 1927b) divided the human EC into 23 fields, Sgonina (1938) into 5 subregions with 12 fields, Vogt & Vogt (1919) into 10 fields, and Braak (1972) into 16 fields. Applying different criteria over time has resulted in a variety of subdivisions and descriptions of EC layers. Stephan (1975) proposed a simple fundamental division of the EC into a lateral and medial part, adding to these the perirhinal area (Brodmann's area 35). While most authors, including Stephan (1975), have tried to match the division of the human EC to the division generally accepted in experimental animals, it should be emphasized that this part of the cerebral cortex in humans is more complex and has reached, both in size and cytoarchitectural differentiation, a level not found in any animal. Von Economo & Koskinas were the first who acknowledged this fact and divided the EC in the rostrocaudal direction into ´H´ fields: HA, HB, and HC (von Economo & Koskinas, 1925, Figure 1a,b). In all areas designated by von Economo & Koskinas the first letter represents lobe, in this case, 'H' represents the hippocampal lobe.

The simple division of EC in experimental animals proposed by Stephan (1975) and Van Hoesen & Pandya (1975) according to cytoarchitecture corresponds to a large extent to the division of von Economo & Koskinas. These authors proposed a subdivision in which the HA occupies the most ventral part of the uncus up to the terminal segment of the band of Giacomini where it appears on the upper lip of the uncal sulcus and is more or less equivalent to the lateral (area 28a of Brodmann). In addition, the HC is the most variable part located more posteriorly and medially representing the caudal narrowed end of the EC that borders the TF and TH areas (the first letter 'T' representing the temporal lobe) and largely corresponds to the medial (area 28b of Brodmann), whereas the HB corresponds to the intermediate part in between the HA and HC (Figure 1a,b). These cytoarchitectural zones of the EC gradually transform into each other, so it is difficult to determine the exact borders among them, but this way of dividing the EC allows a simultaneous comparison with the division of Van Hoesen & Pandya (1975), which is significant because it includes, in addition to cytoarchitecture, afferent and efferent connections. Although in a smaller part of this work we will use the nomenclature of EC that is based on the division of von Economo & Koskinas into three basic cytoarchitectural areas – area HA (area uncinata), HB (area parauncinata), and HC (area rhinalis limitans), because the use of area 28 has been largely discontinued, in those parts of the text related to the functional relevance of different parts of EC we will use its subdivision into only two components that stem from research on experimental animals: the MEC and LEC (Witter et al., 2017; Witter & Amaral, 2021).

By complementing connectivity fingerprints and functional roles of scene and object information of the rodent MEC and LEC with high-resolution fMRI scanning of sensitivity to spatial vs non-spatial stimuli in healthy human volunteers, MEC- and LEC-corresponding subregions in humans have been roughly identified (Maass et al., 2015; Navarro Schröder et al., 2015). The anterior parts of the human EC contain mostly the homolog of the rodent LEC, the posterior parts contain the human homolog of the rodent MEC, and the central part contains a partial overlap of the posteromedial and anterolateral human EC of medial (septal) and lateral (temporal) rodent subdivisions, respectively (Maass et al., 2015; Navarro Schröder et al., 2015). These findings confirmed the von Economo and Koskinas supposition that the human EC is functionally divided primarily along the anteroposterior axis. Simplified, the MEC occupies the posteromedial portion of EC, predominantly receives allocentric spatial information from the parahippocampal cortex (PHC; Insausti et al., 1987a; Suzuki & Amaral, 1994; Insausti & Amaral, 2008), and contains a high proportion of the grid, border, head-direction, and speed cells, whose activity is modulated by spatial location (Hafting et al., 2005), running direction (Sargolini et al., 2006), borders (Solstad et al., 2008), and speed (Kropff et al., 2015), respectively. On the other hand, the LEC occupies the rostrolateral

portion of EC, and predominantly receives inputs from the PRC (Brodmann's areas 35 and 36) about object-related information associated with egocentric spatial processing, high-order processing of object information, attention, multimodal integration, motivation, emotion, and time perception (Insausti et al., 1987a; Suzuki & Amaral, 1994; Insausti & Amaral, 2008; Van Strien et al., 2009; Rowland et al., 2016; Witter et al., 2017; Nilssen et al., 2019). The subdivision of EC into MEC and LEC also has a foundation in the expression of different genes in these two areas as the anatomical organization and connectivity patterns are largely conserved across species (Canto et al., 2008; for a comprehensive description and mapping, see Ding et al., 2022). While this division generally suffices to describe the functional architecture of EC and allows an anatomical interpretation of the different phenotypes of MEC and LEC), for various species more complex proposals have been published (see Discussion in Witter & Amaral, 2021). This holds true for the human EC as well, where other partitions of the human EC are in use, especially those in which the EC is subdivided into seven or eight cytoarchitectural subfields (olfactory – E_O, lateral rostral – E_{Lr}, rostral – E_R, medial intermediate – E_{MI}, intermediate – E_I, lateral caudal – E_{LC}, caudal – E_C, and caudal limiting subfield - E_{CL}) by Insausti and collaborators (Insausti et al., 1995; Insausti et al., 2017; Figure 1c) and the one where the EC is divided into the five main subfields (prorhinal – Pr, lateral – 28L, intermediate – 28I, medial – 28M, and sulcal – 28S subdivision) by Krimer and coworkers (Krimer et al., 1997).

There are also significant differences among authors regarding the basic terminology of the laminar division of EC, and some of these differences are shown in Table 1. In this work, we adopt the basic laminar division into 6 layers, which was first proposed by Lorente de Nó (1933). Stephan accepted and proposed this division as the best solution (Stephan, 1975). According to this concept, the EC consists of the following 6 layers: I - *stratum moleculare*, II - *stratum stellare*, III - *stratum pyramidale* + *substratum dissecans* (superficial LD), IV - *stratum magnocellulare* + *substratum dissecans* (deep LD), V - *stratum parvocellulare*, and VI - *stratum multiforme*. According to Rose, the superficial LD divides the EC into two main layers: an external (*lamina principalis externa*, LPE) and an internal (*lamina principalis interna*, LPI) layer (Rose 1926, 1927a, 1927b).

Early investigations of the sequence of neuron birth using ^{3}H-thymidine and ^{3}H-proline autoradiography, the Fink-Heimer method for degenerating axon terminals, and the Timm silver sulfide method (Zimmer & Haug, 1978; Bayer, 1980; Loy, 1980) in rat and rhesus monkey suggested that cells in the LEC are generated, on average, earlier than those in the MEC, which are, in turn, formed earlier than those in the para- or presubiculum (Schlessinger et al., 1978; Nowakowski & Rakic, 1979, 1981). However, a recent more delicate and more elaborated study in mouse, based on temporally restricted pharmacogenetic silencing have revealed that maturation and synaptogenesis of the entorhinal-hippocampal network rely on an excitatory activity-dependent signal that originates in the stellate cells of the MEC and then spreads sequentially and unidirectionally from MEC towards LEC (Donato et al., 2017). As assessed through monitoring of the doublecortin (a microtubule-associated protein uniquely associated with immature neurons) expression, stellate cells in layer II of the MEC were the first to mature, followed by pyramidal cells in MEC layer II, CA1, DG, subiculum, layer V of MEC and LEC and layer II of the LEC. One of the latest studies that used bromodeoxyuridine (BrDU) labeling in the porcine brain, which, in comparison to rodents, better corresponds to the timing of neurogenesis in humans (7-17 w.g., Kostović et al., 2019), has revealed that the deeper layers of the MEC (V/VI) form first, but in parallel and thereafter the superficial MEC layers (II/III), with some layer II neurons forming last; a process termed parallel lamination (Liu et al., 2021). In comparison to the neocortex, parallel lamination of the MEC suggests that lamination

of the EC differs significantly from the classic inside-out lamination of the neocortex (Bayer, 1980; Liu et al., 2021).

One of the fundamental features of EC development is that it does not have a single cortical plate (CP) from the early stages of development. Namely, inside the CP there is a clear acellular zone that divides the CP into two cellular laminae. An analysis of serial Nissl-stained sections of EC at about 13 w.g. reveals the concomitant appearance of a monolayer between the CP and the marginal zone (MZ) and multi-laminated spread of the deep part of the CP, which is the earliest sign of area-specific cytoarchitectural differentiation of all pallial regions that have the typical CP (Kostović et al., 1993), including the whole prospective parahippocampal and cingulate gyri.

However, the prenatal development of the human EC remains poorly understood. Despite an abundance of work on its connectivity and functions, surprisingly little is known about its prenatal development. One study used implants of carbocyanine dye crystals in either the EC or the DG of the 19-22 w.g. human brain (Hevner & Kinney, 1996). These authors reported two stages of EC development, one before the investigated period, in which the main reciprocal connections between EC and CA fields are configured, and one after the investigated period, in which entorhinal projections into the molecular layer of the DG are developed. Therefore, the general aim of our study is to investigate the development of laminar structure and connectional fiber systems of the human EC, and to reveal unknown details about the prenatal development of fiber systems and myelination, using histochemical and immunohistochemical methods as well as MRI imaging. Specifically, we analyzed the development of the EC cytoarchitectural lamination in the brains of human fetuses using serial sections stained for Nissl substance. We determined periods of intensive fiber in-growth and neuronal differentiation in different cytoarchitectural parts and layers of EC. We correlated the appearance and development of EC layers with the known timinglikend laminar distribution of afferent fiber systems during human fetal development. We determined the first appearance of AChE-positive axons in the human fetal EC as an indicator of afferent fiber in-growth of these potential cholinergic fibers into the EC. We investigated the columnar, alternating termination of individual afferent fiber systems in the context of cellular and acellular zones in the EC. Finally, we assessed the development of the entorhinal projection pathways to the hippocampus and revealed the temporal and spatial sequence of myelination of those major fiber pathways of the EC, providing a comprehensive overview of the events governing the development and connectivity of the EC leading to its establishment as a distinct cortical domain.

2. Materials and methods

2.1. Human brain tissue

Permission to conduct the analyses performed in this work was obtained on multiple occasions from the Central Ethical Committee, formerly the Institutional Review Board, of the University of Zagreb Medical School. Postmortem brain tissues were collected from the early 1970s to the present and are a part of the Zagreb Neuroembryological Collection (Kostović et al., 1991; Judaš et al., 2011; Krušlin et al., 2014). It is generally very difficult to obtain high-quality human fetal postmortem brain material and to achieve optimal tissue staining. Therefore, such material is of high value. However, archive material loses its quality and clarity over time.

All the brains (Table 2) were obtained within 6-8 h after death during autopsy and preserved in 10% neutral buffered formalin, as described previously (Kostović et al., 1991; Judaš et al., 2011; Krušlin et al., 2014). From each specimen, coronal slabs from the right hemisphere (or the whole telencephalon in the youngest specimens) were used for AChE histochemistry and immunocytochemistry. Coronal or horizontal slabs from the left hemisphere were used for paraffin or celloidin embedding and Nissl staining.

2.2. Nissl staining

After fixation, the brains were cut in the frontal (coronal) or horizontal plane into 8-10 mm-thick slabs and frozen or dehydrated through a graded series of increasing concentrations of ethanol (70, 96, and 100%; twice 12 h each) and passed through a mixture of diethyl ether and absolute alcohol solution (50/50 vol/vol) for 180 minutes twice, and then embedded in either 2% celloidin (Cedukol, Merck, Darmstadt, Germany, cat. no. 4363) or paraffin (Histowax, Jung, Nussloch, Germany). Frozen slabs were sectioned at 70 µm, whereas the dehydrated blocks were embedded in 2% celloidin for 24 h. After the medium had hardened, the paraffin or celloidin or blocks were cut on a Reichert sliding microtome (Reichert, Vienna, Austria) into 15 ± 2 µm- or 25 ± 2 µm-thick sections, respectively. After mounting and deparaffinization, xylene was removed with 100% ethanol. The sections were collected in 70% ethanol, placed in 50% ethanol, then in 5% ethanol for 2 minutes and in distilled water for 5 minutes, and finally in 0.5% cresyl-violet in distilled water until adequate staining was achieved. Then the sections were placed in distilled water twice for 5 minutes and through a graded series of alcohol solutions (50% ethanol, 70% ethanol with 2-4 drops of 25% acetic acid in distilled water, 70% ethanol, and 95% ethanol) for 10 minutes each. Finally, the sections were placed in an ether-alcohol solution (2 parts of ether and 1 part of absolute alcohol) for 5 minutes, rinsed with xylene for 5 minutes, and mounted with a cover glass using Permount mounting medium (Thermo Fisher Scientific, Waltham, MA, USA).

To assess the "functional maturity" of individual layers, we used light-microscopy criteria to assess cell differentiation according to Rakic (1968): the degree of basophilia of the nucleus and the rough endoplasmatic reticulum, metachromaticity of the nucleolus, the intensity of cytoplasmic staining, nucleocytoplasmic index, and the appearance of Nissl granules (rough endoplasmatic reticulum). Using these criteria, neuronal development can be divided into seven stages of differentiation (SD1-7, Figure 2 and Table 3).

2.3. AChE histochemistry

After removal from the skull, the brains were fixed for 24-72 h by immersion in 0.1 M sodium phosphate buffer containing 1% glutaraldehyde and 2% paraformaldehyde at 4-6° C. After fixation, the blocks were cut into 8-10 mm-thick coronal or horizontal slabs and frozen by CO_2. Sections (70 or 80 µm-thick) were cut on a freezing microtome or a cryostat and collected in phosphate-buffered saline (PBS). Free-floating sections were stained for AChE by using the Lewis modification of the acetylthiocholine iodide method of Koelle and Friedenwald, as described previously (Šimić et al., 1999). To verify the specificity of the reaction for AChE, and not butyrylcholinesterase (BuChE), either incubation in a medium without substrate was performed or specific inhibitors were used. Treatment of adjacent sections in an incubation medium containing tetraisopropylpyrophosphoramide (isoOMPA, 10^{-4} M final concentration) was used for the inhibition of BuChE and 1,5-bis-(4-allyl-dimethylammoniumphenyl)-pentane-3-one dibromide (BW284C51, 10^{-5} M, Sigma-Aldrich, Munich, Germany) for the inhibition of AChE. Eserine (10^{-4} M) was used for simultaneous inhibition of both AChE and BuChE. As eserine inhibited all staining, whereas isoOMPA had little effect, this indicated that the reaction obtained is due to the true AChE. The reaction product was developed with sodium sulfide in 0.2 M acetic acid after incubation for up to 24 h. Some sections were also processed by the Karnovsky-Roots "direct coloring" method (Karnovsky-Roots, 1964) as described by Broderson and coworkers (Broderson et al., 1974) and modified by Tago and coworkers (Tago et al., 1986).

2.4. Immunocytochemistry

The brains were fixed by immersion for 1-2 h in the 4% paraformaldehyde in 0.1 M phosphate buffer and cut in 10 µm-thick coronal slabs, which were left overnight in freshly prepared fixative. After the cryoprotection and sectioning to 70-80 µm-thick sections, free-floating sections for immunocytochemistry were processed according to the avidin-biotin method (Hsu et al., 1981) using a Vectastain ABC kit (Vector Laboratories, Burlingame, CA, USA). We used commercially available antisera against MBP (monoclonal antibody, dilution 1:1000 BioLegend, San Diego, CA, USA, cat. no. 808401, RRID: AB_2564741), NeuN (neuronal nuclear antigen, polyclonal antibody, dilution 1:1000, Abcam, Cambridge, UK; cat. no. ab104225, RRID: AB_10711153), a pan-axonal neurofilament marker (antibody SMI-312, dilution 1:1000, BioLegend/Covance, San Diego, CA, USA, cat. no. 837901, RRID: AB2314906), and synaptophysin (a major synaptic vesicle protein, monoclonal antibody, dilution 1:100, Dako cat. no. M7315, RRID: AB_2687942). Adjacent Nissl-stained sections were used for the delineation of layers.

2.5. *Ex vivo* 3 T MRI protocol

Before histological processing, some fetal brains or hemispheres were, after fixation by immersion in 4% paraformaldehyde in 0.1 M phosphate buffer (pH 7.4), scanned with a 3 T magnetic resonance imaging (MRI) device (Magnet TrioTim and Magnet PrismaFit, Siemens, Germany), using high-resolution MP-RAGE (magnetization-prepared rapid acquisition gradient echo) T1 sequence, according to the following standardized protocol. To acquire the high spatial resolution and high-contrast T1 weighted images, we modified the commercially available volumetric interpolated brain examination (VIBE) sequence (Rofsky et al., 1999) by reducing the field of view (FOV), increasing the resolution and number of excitations, modifying the time to echo (TE), repetition time (TR), and flip angle. The final parameters used for MRI acquisition were: TR=14.5 ms, TE=5.4 ms, number of excitations (NEX) 5, flip angle 12°, voxel size = 0.5 x

0.5 x 0.5 mm, acquisition time – on average about 1.5 h per brain, depending on size). Of the larger number of scanned fetal brains aged 13-40 w.g., here we chose a brain of 20 w.g. to illustrate the specific time-point at which the superficial LD can be observed.

3. Results

3.1 Stage 1 (8-9 weeks of gestation, CRL 20-50 mm): cytoarchitecturally undifferentiated EC

The base of the periallocortex, the prospective EC, occupies the medial part of the lower wall of the telencephalon bilaterally in the area of the future inferior (temporal) horn of the lateral ventricles. The amygdaloid nucleus is already developing in this area. The pallium of this part of the telencephalon is made of layers that are identical to the layers of the lateral neopallium, with identifiable MZ, CP, intermediate zone (IZ) and matrix (ventricular, VZ, and subventricular zone, SVZ). The thinner CP is sharply limited by the IZ, and more medially it becomes thinner and disappears in the area of the future archipallium. At this stage, cytoarchitectural differentiation of the EC has not yet begun. As the EC cannot be delineated, it can only be defined based on thinning of the CP in the area of the medial part of the lower wall of the telencephalon.

3.2. Stage 2 (10-13 weeks of gestation, CRL 50-80 mm): CP condensation in the prospective EC

At this stage, the first cytoarchitectural differentiation of the periallocortex begins. For the first time, the future EC can be demarcated from the surrounding regions. The lateral border of the EC is different from the compact CP of the temporal neopallium (Figure 3).

Rostrally and medially, the EC continues into the periamygdaloid (PAM) and prepiriform areas. The criterion for delimiting the EC from these regions is that the EC extends to the point where the well-organized CP ends (indicated by the black arrow in Figure 4a). Caudally and medially, the EC borders the archipallium (Figures 3a, 4a). At the border with the archipallium, the superficial magnocellular zone below the marginal layer disappears, and the deep parts of the CP of the archipallium are not delaminated. This means that, in comparison with the periallocortex of the prospective EC, the CP of the archipallium lags in differentiation. Posteriorly, the CP of the EC continues into the compact CP of the temporal neopallium.

3.2.1 Lamination pattern

At this stage, the laminar development of the EC is characterized by a single compact CP, the first appearance of the superficial magnocellular zone below the MZ, and the initial delamination of the deep layers of the CP of the EC. In the rostral parts of the EC, a narrow cellular zone appears between the superficial, condensed part of the CP and the MZ. It is separated from the CP by a cellularly sparse zone (Figure 3a,b). This narrow cellular zone is not continuous, but is interrupted in some places, and consists of 2-3 rows of irregularly spaced cells (indicated by arrows in Figure 3b). These cells are mostly triangular and polymorphic in body shape, differently oriented, mostly oblique and horizontal, while some are inverted. They have a large, brightly colored nucleus with a visible nucleolus, a rich cytoplasm around the

nucleus, and relatively developed processes. According to Rakic's classification, these cells can be classified as SD5. We call this cell zone the superficial magnocellular zone, which is present at this stage only in the EC, while it is absent in the surrounding regions. In the caudal parts of the EC, the superficial magnocellular zone is not present.

The superficial, main part of the fetal CP consists at this stage of densely packed differentiated bipolar cells of the same characteristics as the lateral neopallium CP cells. The deeper part of the CP is not compact and sharply demarcated from the intermediate zone, as is the case in the lateral neopallium. In the deeper parts of the CP within the EC, several cell-dense and sparse zones (indicated by arrows in Figures 3c, 4c) lie below the superficial, compact part of the medial part of the neopallium, which is not observed in the lateral neopallium. The cell-dense zones are made of one to several rows of undifferentiated bipolar cells (SD1-2). Based on the analysis of Nissl preparations, it can be assumed that these cell-dense zones represent waves of migrating neurons, and an increase in their number in fetuses with CRL of 80 mm (compare Figures 3c, 4c) indicates progress in neuronal migration into the CP. Delamination of the deeper parts of the CP is less likely at this stage to be an indication of the in-growth of afferent fibers into the deeper parts of the CP.

3.2.2 Cytoarchitectural zones

Two cytoarchitecturally different parts can be distinguished, already at this stage in the EC, a rostral part, characterized by the presence of a superficial magnocellular zone between the MZ and the compact part of the CP, and stratification of the deep parts of the CP (Figure 3a,b), and a caudal part, in which the magnocellular zone between the MZ and the CP is not well-developed. The deep portion of the CP is similarly delaminated in both parts of the EC (Figures 3c, 4c).

3.3. Stage 3 (14-16 w.g., CRL = 80-120 mm): delamination of the primary CP and beginning of LD formation

In contrast to Stage 2, the CP of the prospective EC in this stage expands significantly. The caudolateral EC in its full extent borders the temporal neopallium, which, in contrast to the delaminated CP of the EC, is characterized at this stage by a compact CP (Figures 5, 6a).

Rostrally and medially the EC borders with PAM that has no CP but a diffuse cellular zone below the MZ (Figure 5a,b). Caudomedially, the CP of the EC is compact and borders the future parasubiculum (PaS). In the caudal and medial parts of the EC within the LPI, another narrow acellular zone appears and continues medially into the PaS (Ding & Van Hoesen, 2010, 2015), corresponding to the first appearance of the deep LD (dis 2, Figure 6b,c). Therefore, the caudal EC has both the superficial (dis 1) and deep LD (dis 2). The deep LD (dis 2) of the EC continues into the PaS, where it is more pronounced (Figure 6b,c). For interpretation of these observations, one should know that acellular zones that are not stained by the Nissl method consist of branches of basal dendrites of cells located above these zones and of dense bundles of horizontal afferent axons ending on the basal dendrites of those cells - a conclusion first made by Lorente de Nó (1933) based on Golgi preparations. As such, these zones belong to the layers above them. Therefore, dis 1 belongs to LPE (more precisely to layer III, which consists of medium-sized pyramidal cells; as layer III is wide and very consistent throughout the EC, the superficial LD is readily visible). The deep LD, dis 2, belongs to LPI (more precisely to layer IV that is made of large pyramidal cells

variably distributed through the EC, making the deep LD less conspicuous). The parasubiculum's large and densely packed pyramidal cells are a constant feature there. Hence, dis 2 is more visible in the PaS than in the EC. From sections analyzed in the caudal part of the EC (Figure 6b,c), EC layer IV and LPE fuse into superficial layers II and III of the PaS, so that beneath lies a single LD in continuation with the deep LD of the EC, making it appear as if the LD of the PaS continued into the dis 1 of EC and not into the dis 2, as both lie beneath layer III.

3.3.1 Lamination pattern

The laminar development of the EC at this stage is characterized by the differentiation of the CP into two main cell layers, the lamina principalis externa (Rose's LPE, external principal layer) and the lamina principalis interna (Rose's LPI, internal principal layer), which are separated by an acellular zone corresponding to the first appearance of the superficial LD (dis 1, Figures 5, 6, 7a). At the same time within the LPI appears the deep LD (dis 2, Figure 6b,c), but only in the caudomedial part of EC (Figure 6b,c). Another important event at this stage is the beginning of the differentiation of the LPE in the rostral parts of the EC into vertical cell-dense zones (cell islands) and vertical cell-sparse zones in between them, which indicates the beginning of the in-growth of afferent fiber bundles into the LPE of the CP.

In the rostral parts of the EC, near the border with the PAM, the LPE consists of two cellular zones: a superficial (LPEs) narrow one, located below the MZ (superficial magnocellular layer) and a deeper (LPEd), wider one, corresponding to the main part of the LPE of the CP (Figure 5b,c). The two zones are separated from each other by a narrow, cell-sparse layer. These irregular, oval, acellular zones appear to encroach both cellular layers of the LPE and thus separate them into, irregular vertical cell-dense and cell-sparse groups (indicated by arrows in Figure 7b-e). In contrast to the previous stage (Stage 2), the superficial zone of the LPE consists of two cell types: large cells with a large clear nucleus, rich in cytoplasm and developed extensions (SD5), and smaller cells with dark nuclei, in which several basophilic granules can bee seen (SD1-2). All cells of the deep cellular zone of the LPE are still undifferentiated (SD1-2) (Figure 7b,c).

The organization of the LPE into two cell zones and vertical groups (islands) of cells is not present in the caudal parts of the EC. At the level of the ventral hippocampus, the LPE is sharply demarcated from the MZ and the superficial LD, and has all the characteristics of the CP of the lateral neopallium: it consists of densely packed undifferentiated bipolar cells (SD1-2) (Figure 6). Beneath the LPE, a deep layer of the CP can be distinguished, the LPI (of Rose), which is most developed at this stage in the caudal and lateral parts of the EC (Figure 6a,b). The two main layers of the CP (LPE and LPI) are separated from each other by a narrow, cell-sparse zone that narrows laterally and caudally and disappears at the border with the temporal neopallium (Figure 6a) and extends medially to the border with the prospective PaS (Figure 6a,b). This cellularly sparse zone, which first appears at this stage, corresponds to the superficial LD.

In the rostral parts of the EC, the LPI narrows and disappears toward the border with the PAM (Figure 5a,b). It is made of densely packed bipolar cells that are not differentiated (SD1-2). The superficial boundary with the LD is sharp, while in the deeper parts of the LPI, several slightly denser and rarer zones of bipolar cells are seen, suggesting that the process of condensation of the CP is still ongoing (Figures 5b, 6a,b, 7a). In the caudal parts of the EC at the level of the ventral hippocampus and the lateral parts of the EC, the LPI is sharply demarcated with the superficial LD and the intermediate zone (Figure 6a,b). Towards the lateral and caudal border with the temporal neopalium, the deeper parts of the LPI become increasingly sparse and gradually transform into the most superficial parts of the IZ corresponding to the

subplate zone (SP), while the superficial parts of the LPI gradually continue into deep parts of the CP of temporal neopallium (Figure 6a,b).

3.3.2 Cytoarchitectural parcellation

This stage is defined by three basic cytoarchitectural zones within the EC, with a rostral (rostromedial, RM) part characterized by one LD located between the LPE and LPI and by initial differentiation of the superficial parts of the LPE into vertical cell-dense and cell-sparse zones (Figure 5b), a caudolateral part (CL) with one (superficial) LD separating the LPE and LPI, which are both compact and undifferentiated (indicated as CL in Figures 5b, 6b), and a caudomedial (CM) part (Figure 6b) with a superficial and a deep LD, the latter one appearing within the LPI.

3.4 Stage 4 (16-20 w.g., CRL 120-170 mm): transformation of the fetal lamination and in-growth of the PP into the hippocampal formation

At this stage, the boundaries of the EC with surrounding regions remain unchanged. The narrowed anterior part of the EC can be recognized in most rostral parts of the temporal lobe between the temporal neopallium laterally and the periamygdaloid area (PAM) medially (Figure 8a). The temporal neopalium is characterized by a sharply demarcated, broad CP. At the transition to the EC, the CP suddenly becomes laminated (Figure 8a-c), whereas medially, where the EC continues into the PAM, the marginal zone (MZ) expands, and, instead of the CP, the cell zone of large differentiated cells of the PAM can be seen (Figure 8a). Towards the posterior part of the EC, the CP transforms into the compact CP of the lower aspect of the temporal lobe.

3.4.1 Lamination pattern

The most significant features of the EC at this stage are an increase in the extent of the EC, the expansion and progress in differentiation within both main layers (LPE and LPI) of the CP of the EC (but LPE more than LPI), the appearance of distinct cellular islands (clusters) of cells in the superficial and deep cellular zones of the LPE, and an expansion of the LD. The MZ of the EC at this stage has the same width and the same characteristics as the MZ in the lateral neopallium. The surface part of the MZ is occupied by a narrow layer of undifferentiated cells (SD1) and corresponds to the so-called subpial granular layer (SGL, Figure 9a).

The differentiation of the LPE into cell islands, the onset of which was described in the previous stage (Stage 3) in the rostral parts of the EC, continues in this stage and also extends to the more caudal parts of the EC. Below the MZ, in the rostral parts of the EC, a clearly defined narrow, discontinuous cell zone (future layer II) is seen organized into irregular islands of cells (Figure 8a,b; islands are indicated by arrows). These islands are separated from each other by clear acellular zones that extend from the MZ to the deep cellular zone of the LPE (LPEd). The islands of the cells of the superficial cellular zone of the LPE (LPEs) are continuous with the islands of the cells of the LPEd (Figures 8a,c,d, 9a). These deep "connecting" parts of the islands have a lower cell density but are clearly distinguished from the clear zones that separate them. The clear zones probably correspond to the in-growing bundles of axons into the superficial parts of the CP.

Similarly to Stage 3, two types of cells can be distinguished within the islands of cells of the LPEs: a small number of large polymorphic cells with a large, clear nucleus, rich cytoplasm, and developed extensions (SD5, shown by arrows in Figure 9b), and a larger number of small dark cells with granular chromatin in the nucleus and almost without cytoplasm (SD1-2, Figure 9b). Compared to the previous stage, the number of undifferentiated cells in the islands of the LPEs increases, making large polymorphic cells being relatively difficult to detect.

At this stage, the discontinuity of the deep cell zone (future layer III) of the LPE (LPEd) can also be observed. This is especially pronounced in the rostral parts of the EC, while such organization disappears caudally. The cells of the LPEd are grouped into islands that are recognizable by a higher density of cells without cytoplasm and with a dark, round nucleus (SD1-2, Figures 8a,b,d, 9a). As previously described, these islands of undifferentiated cells of the LPEd are, as a rule, in continuity with the islands of the superficial cellular zone of the LPE. In the caudal parts of the EC, the described organization into islands of the superficial (magnocellular) and deep cellular zones of the LPE (LPEs and LPEd) of the CP is lost. Here, only two relatively compact cellular zones of the LPE (superficial and deep, Figure 9c) can be seen. Further caudally, at the level of the transition from the ventral to the dorsal hippocampus, these two zones merge into a single cell layer of the LPE.

Another major fetal layer of the CP, the lamina principalis interna (LPI), is poorly developed in the rostral parts of the EC at this stage, at the level of the amygdaloid nucleus (Figure 8a,b). The LPI can only be recognized as a thickening of IZ cells, and probably corresponds to the SP layer in the neocortex. Medially, the LPI narrows and disappears at the border with the PAM (Figure 8a,b). Throughout the entire width of the EC, the LPI is separated from the LPE by a cell-sparse zone corresponding to the superficial LD (Figures 8b,c, 9c). Caudally, the LPI expands increasingly, and at the level of the ventral hippocampus, it is fully developed, sharply limited by the superficial LD and IZ, and it possesses all the characteristics of the deep parts of the CP of other parts of the pallium (Figure 9c). Laterally and caudally, the LPI is continuous with the superficial parts of the IZ of the temporal neopallium, representing the SP layer.

In the caudal and medial parts of the EC, there is another acellular zone described already in the previous stage within the LPI at the level of the ventral hippocampus. This zone is corresponding to the deep LD, which continues medially into the PaS. Throughout the entire width of the EC, the LPI consists mainly of small undifferentiated cells with dark nuclei (SD1-2) and only of a very small number of more differentiated cells (SD3-4).

3.4.2 Cytoarchitectural zones (subareas)

Four cytoarchitectural zones of the EC can be distinguished at this stage, i.e. rostral, central, caudomedial, and caudolateral zones. The rostral zone locates at the level of the amygdaloid nucleus. This zone is characterized by the organization of the superficial and deep cellular zones of the LPE into islands of cells (LPEs and LPEd). The LPI is poorly developed in this part and only one (superficial) lamina dissecans is present (Figure 8a). In the central zone, found at the level of the ventral hippocampus, the organization of the superficial and deep cellular zone of the LPE into islands of cells is lost, because they form relatively continuous layers. The LPI is significantly wider here than in the rostral part. Only the superficial LD is present (between LPE and LPI). In the caudomedial part, the LPE forms a relatively compact layer, such that it lacks two separate cellular parts. Within the LPI there is a deep LD. As such, there are two LDs in this part of the EC. The caudolateral zone extends along the entire level of transition between the ventral and dorsal hippocampus. The LPE is organized as a single compact layer. Only a superficial LD is present.

3.4.3 In-growth of the perforant path into the hippocampal formation and onset of myelination

We assessed the in-growth of the perforant path (PP) into the hippocampal formation at 20 w.g. using an antibody against a pan-axonal neurofilament marker (Figure 10). At this stage, the temporoammonic (main) branch of PP does not penetrate the hippocampal sulcus yet. Rather, as in other species, it penetrates the subiculum after separating from the angular bundle and travels through the stratum lacunosum-moleculare of the CA1, CA2, and CA3 fields to reach first the suprapyramidal blade of the DG (Figure 10a,b,d). This indicates that the first PP fibers are coming into the DG through the stratum lacunosum-moleculare of the Ammon's horn and not through the hippocampal sulcus, thus taking the same route as seen in other species (Ramón y Cajal, 1911; Witter et al., 2000).

In our materials, the penetration and crossing of PP fibers through the hippocampal sulcus can be seen only about three weeks later, at 23 w.g. (Figure 11), when the entorhinal projection to the hippocampus via the temporoammonic branch also reaches the infrapyramidal blade of the DG. Together with other changes in that period, we noticed a strongly increased expression of vimentin along the PP fibers, especially in the subiculum's CP. In addition, at 20 w.g., MBP-immunoreactive oligodendrocytes first appear in the fimbria, and two to three weeks later (at 22-23 w.g.) myelin patches are also present in the alveus. For more details, see the descriptions of the following stages below.

3.4.4 Visualization of the synaptophysin and NeuN immunoreactivity at 20 w.g.

In this mid-fetal stage (16-20 w.g.), the allocortical zones are at their developmental peak. The CP of the EC consists of a recognizable LPE with entorhinal islands (Figure 12a). Below the LPE is the LD, and further the LPI. The MZ is slightly thinner than in the subiculum and CA fields of the hippocampus, but still thicker than the adjacent parts of the temporal neocortex. Synaptophysin immunoreactivity shows that synaptogenesis is most intense in the MZ and is positive throughout the thickness of the MZ, LD, and SP (Figure 12b). At this stage, only the upper parts of EC islands are immunoreactive for synaptophysin (Figure 12b). NeuN immunoreactivity shows the laminar organization of postmitotic neurons in the EC layers and is most pronounced in the islands of layer II cells (Figure 12c). Migration and differentiation gradients are seen in both the upper (LPE) and the lower (LPI) pyramidal layers as well as layer II, where less differentiated cells are found in the more superficial portions in each of these compartments (Figure 12c). At this stage, for the first time, the EC adopts an adult-like cytoarchitectural organization.

3.5 Stage 5 (20-30 w.g., CRL = 180-280 mm): initial formation of definitive lamination

This stage of development includes fetal brains of 20-30 w.g., which is about 185-280 mm of CRL. At this stage, layers of CP of the EC corresponding to those in the adult brain are already formed. The cytoarchitectural zones seen in the adult human EC appear. In addition, the first appearance and characteristic arrangement of acetylcholinesterase-reactive fibers in the EC are seen at this stage, which indicates the potential in-growth of cholinergic axons into the EC.

The development of the EC at this stage is described below in four substages, at 22 w.g. (CRL = 200 mm), 23 w.g. (CRL = 220 mm), 25.5 w.g. (CRL = 245 mm), and 28 w.g. (CRL = 270 mm). Additionally, longitudinal stripes of entorhinal islands in horizontal sections in a 33 w.g. fetal brain (8 lunar months, CRL = 300 mm) are illustrated.

3.5.1 Situation at 22 w.g. (CRL = 200 mm)

At 22 w.g, the EC occupies the same position in the temporal lobe as in the previous stage. The EC borders rostromedially the PAM, caudomedially the PaS, and laterally and posteriorly with the temporal neopallium. However, an increase in the rostrocaudal and mediolateral extent of the EC is now visible.

3.5.1.1 Description of lamination, borders, and cytoarchitectural zones

The most significant characteristics of the EC development at this stage are a general decrease in cell density within the CP with a consequent increase in the proportion of neuropil, and progress in cell differentiation. In Nissl-stained coronal sections (Figure 13a,b), it is possible to discern the MZ (layer I), the superficial layer of CP (LPE), within which future layers II and III can be recognized, the superficial LD and the deep layer of CP (LPI), in which a deep LD is present in the medial parts of the EC. The superficial part of the MZ contains the SGL whose cells are at a low degree of differentiation (SD1-2, Figure 14a).

The LPE is bounded by the MZ and superficial LD along the entire width of the EC. In the rostral parts of the EC, at the level of the amygdaloid complex, LPE can be divided into superficial and deep cellular zones, which will become layers II and III, respectively (Figure 14a). This layer is characterized by the segregation of cells into vertical islands, as indicated by arrows in Figure 13a,b.

Below the marginal zone, narrow, irregular islands of cells can be seen, which contain differently oriented large polymorphic cells with a bright nucleus, rich in the cytoplasm, and with branched extensions (SD5, marked by arrows in Figure 14b), and small less differentiated ones (SD1-2). As already described, these cellular islands are separated from each other by bright acellular spaces of unequal size (Figures 13a,b, 14a).

Laterally, towards the temporal neopallium, islands become increasingly sparse and eventually disappear (Figures 13a,b, 14c,d). Nissl-stained sections show that the acellular zones separating the islands of the superficial cellular zone of the LPE extend into the MZ (Figure 14a). These zones penetrate the deep cellular zone of the LPE to different depths (Figures 13a,b, 14a).

The narrow islands of cells below the marginal layer are often separated from the deep cellular zone of the LPE (layer III) by narrow, cell-sparse zones (Figures 13b, 14a), while in some places this transition has no visible boundary. The pattern of cellular islands separated by acellular zones in the rostral parts of the EC is repeated in the deep cellular zone LPE. In this way, the deep cellular zone of the LPE is also organized into irregular vertical, cell-dense zones separated from each other by narrow vertical, cell-sparse zones (Figures 13a,b, 14a). The deep parts of the vertical, cell-dense zones are more cell-sparse and dominated by neurons at a higher SD with a bright nucleus in which the nucleolus is visible, and in some of them, the first appearance of cytoplasm and extensions can be observed (SD3-4), while in the superficial parts smaller cells of a lower degree of differentiation predominate (SD1-2, Figure 14a,b).

The LPE of the CP within the caudal parts of the EC, at the level of the ventral hippocampus, is also characterized by islands of cells of unequal size below the MZ. These islands are separated by acellular zones from the deep cellular zone of the LPE, which is no longer organized into vertical groups but forms a single continuous layer (Figure 14c,d). Within the LPE one can distinguish the deeper (wider), cell-sparse

part of differentiated cells (SD3-4), and the superficial (narrower) part that consists of undifferentiated cells (SD1-2). The vertical acellular zones between the islands of the superficial cellular zone LPE (prospective layer II) do not penetrate deep into the deep cellular zone (i.e. layer III), but only separate the superficial, undifferentiated part of layer III, into cell-dense groups (Figure 14c,d).

The islands of cells below the MZ in the caudal direction become increasingly sparse and are finally lost. In these caudal parts of EC, the LPE is relatively continuous, and contains a narrower superficial, cell-dense population of predominantly undifferentiated neurons (SD1-2) and a wider deep, cell-sparse population of differentiated neurons, Figure 14a,b). Contrary to coronal sections, where these zones look like irregularly distributed islands of unequal size in horizontally cut sections, it can be seen that the islands of the superficial LPE zone are not true "islands", but rather longitudinal strips extending approximately in the rostrocaudal direction, and separated by longitudinal acellular zones (Figure 15a,b).

At this stage, the LPI is less developed in the rostral parts of the EC than in the caudal parts (compare Figures 13a,b to 14c,d). It is separated from the LPE by an acellular layer corresponding to the superficial LD. In most rostral parts of the EC, the LPI narrows and disappears toward the PAM border (Figure 13a). In the caudal level of the ventral hippocampus, the LPI is far wider, and medially it continues into the PaS. In the caudomedial parts of the EC, a narrow bright layer is present within the LPI, which medially continues into the PaS (Figure 14c), and corresponds to the deep LD. Laterally and caudally LPI continues into the deep parts of the CP that correspond to the SP layer, and into the superficial parts of the temporal neopallium. Throughout the whole EC extent, the LPI contains relatively differentiated cells (SD3-4), and rich neuropil.

3.5.1.2 Histochemical presence of AChE-positive axons

At this stage, no AChE reactivity is visible in the EC. The characteristic bilaminar arrangement of the AChE-positive reaction is seen in the adjacent temporal neocortex. There, a thin AChE-labeled band is seen in the MZ, whereas the thick AChE-positive bundle of fibers coming from the basal forebrain (medial septum, nuclei of the diagonal band, and basal nucleus in the substantia innominata) occupies the deep part of the IZ and the outer part of the outer fiber zone of the SVZ of the temporal neopallium (Figure 16), as recently described by Ding et al. (2022) and is lost at its border with the EC (arrow in Figure 16). Likewise, the AChE-positive fiber system of the external capsule, located in the deep part of the IZ also extends only to the border of the temporal neopallium with the EC.

3.5.2 Situation at 23 w.g. of gestation (CRL = 220 mm)

At this stage, there is a further increase in the EC size proportionally to the growth of the temporal lobe and further cytoarchitectural differentiation of the EC layers. The boundaries of the EC with the surrounding structures remain mostly unchanged from previous stages.

3.5.2.1 Lamination pattern

The most significant features of the laminar development of the EC at this stage progress in the formation of definitive layers and cell differentiation, further differentiation of the cells in islands of the superficial LPE, and significant expansion of the deep acellular part of the future layer II (Figure 17a,b).

Within the LPE, three layers can be distinguished that correspond to the layers of the EC in an adult human brain. The superficial half of the MZ is occupied by the SGL consisting of densely distributed undifferentiated cells (SD1-2, Figure 17c). The deep part of the MZ is cell-sparse, sharply demarcated from the islands of layer II, and is continuous with the acellular vertical zones separating the islands of layer II neurons (Figure 17c). The cell islands of the superficial LPE are most pronounced in the rostral and central parts of the EC, while in the caudal and lateral parts of EC, they are lost (Figure 17a,b,d).

On coronal Nissl-stained sections, islands are of unequal size through the EC, separated from each other by cell-sparse, vertical zones of unequal size, which in the rostromedial part of the EC penetrate the deep LPE, into the prospective layer III (Figure 15c). At this stage, the islands of layer II neurons show large polymorphic, well-differentiated cells (SD5-6), and small, poorly differentiated cells (SD1-2). Unlike the previous stage (22 w.g.), there is a significant expansion of the acellular spaces that separate the islands from the deep cellular zone of the LPE (Figure 17d). Thus, in the LPE there is a reduction of the superficial part, so it makes only one-fifth to one-sixth of layer III (arrows in Figure 17c). It contains undifferentiated cells (SD1-3), but a small number of pyramidal cells appear at this stage with a higher degree of differentiation (SD4-5). The deep, wider part of layer III (the deep cellular zone of the LPE) consists of pyramidal-shaped cells with a large bright nucleus, a narrow cytoplasm around the nucleus, and developed extensions (SD5). The superficial cellular zone of LPE (layer III) of the rostral part of the EC (area HA) is also organized here into vertical, cell-dense groups separated by vertical acellular zones that extend from the prospective layer II to different depths of layer III. Below layer III, there is a superficial LD, which displays the same characteristics as in the previous stage (Figure 15a,b). The LPI is compact in the lateral and caudal parts of the EC. In the superficial parts of the LPI, pyramidal-shaped cells (SD5), although discerned, do not yet fully form a clear layer V such as that seen in adults. The deep part of the LPI consists of smaller bipolar or polymorphic cells (SD4-5). In the medial parts of EC (areas HA_2 and HB_2), a deep LD (dis 2) is present in the LPI and separates the surface part of the LPI with pyramidal cells (layer V) from the deep part of the LPI (layer VI).

3.5.2.2 Cytoarchitectural zones

At this stage, cytoarchitectural zones corresponding to cytoarchitectural zones in the adult human EC (areas HA, HB, and HC of von Economo & Koskinas) can be distinguished. These cytoarchitectural zones have more or less the same characteristics as at the 22 w.g. stage (compare Figure 15a and b at 23 w.g. with the description and Figures 13, 14, and 16 of the previous stage at 22 w.g.).

3.5.2.3 AChE-positive axons

The first AChE-positive staining in the EC appears at this stage. Throughout the whole extent of EC, the most intense AChE-positive reaction is present in the superficial portion of the MZ corresponding to the SGL (horizontal white arrow in Figure 17c). AChE-positive cell bodies are observed in this layer, mainly horizontally oriented with respect to the surface of the cortex, which may represent Cajal-Retzius cells (CRC). A slight increase in AChE reactivity occurs in the superficial part of the LPE. Here, weak and diffuse AChE-positive vertical zones appear, extending from the surface of the cortex to the superficial part of the

deep cellular zone of the LPE (layer III, compare to Figure 20d,e). Compared to Nissl-stained sections, AChE-negative zones correspond to vertical acellular zones between islands of cells of the superficial LPE. A slight increase in AChE reactivity is also present in the deeper layers of the EC. Between the LPE and LPI, a completely unstained LD is observed. At this stage, a pronounced AChE reactivity can be observed in the MZ corresponding to the bundle of AChE-positive axons in the cortex of the uncus, near the border with the EC (white arrow in Figure 17e). To some extent, these AChE-positive bundles of axons are extending from the uncus to the superficial layers of the EC. In serial sections in the ventral direction, they are continuous with sublenticular structures.

3.5.3 Stage 25.5 w.g. (CRL = 245 mm)

In contrast to the previous stages, an expansion of AChE-positive reactivity in the MZ in the rostral and lateral parts of the EC (white arrows in Figure 17d) and an increased number of AChE-positive cell bodies in the MZ is seen. Vertical AChE-positive bands appear to extend from the AChE-positive MZ of the LPE In the rostral and lateral parts of the EC (black arrows in Figure 18). The appearance of these vertical bands indicates the beginning of the in-growth of AChE-positive axons into the islands of the superficial LPE.

3.5.4 Stage 28 w.g. (CRL = 270 mm)

At this stage, a shallow furrow corresponding to the RS appears between the temporal neopallium and the EC, in the rostral part of the temporal lobe (Figure 19a). The vertical cellular zones of the LPE and the superficial LD mark the border between the EC and the temporal neopallium. Other boundaries remain unchanged from the previous stage.

3.5.4.1 Lamination pattern

At this stage, the EC is characterized by further maturation of neurons within all layers and an expansion of these layers, the presence of vertical cellular zones of still undifferentiated cells in the MZ and superficial parts of the LPE. The deep parts of the LPE differentiate into a pronounced pyramidal layer III and LPI into the deep polymorphic layers V and VI.

In the LPE of the rostral and central parts of the EC, the irregularly distributed vertical cellular zones are most noticeable at this stage. They extend as cell-dense bands from the SGL to different depths of the deep LPE (arrows in Figure 19a). These vertical cellular zones are composed of densely distributed small undifferentiated cells (SD1-3) in the MZ, islands of stellate neurons of the superficial LPE, acellular zones below the islands of layer II, and in the superficial part of the deep LPE. They are separated by vertical acellular spaces of unequal width that extend from the MZ to different depths of the deep LPE (Figure 19a). Within the vertical cellular zones, islands of large stellate neurons of layer II can be recognized, which, unlike the previous stage, have more abundant cytoplasm and more branched extensions (SD6). Also, well-developed pyramidal neurons (SD6) are seen in the deep part of the vertical zones belonging to the superficial parts of layer III. In this part of the future layer III, small, undifferentiated cells are few, as this layer consists mainly of large, differentiated pyramid-shaped neurons (SD6).

In the caudal and lateral parts of the EC, the vertical cellular zones of undifferentiated cells are smaller. The deep parts of these zones are reduced to a narrow superficial part of the deep LPE made of undifferentiated cells. Beneath the LPE the superficial LD separates the LPE from the LPI. The superficial part LPI now exhibits differentiated large pyramidal cells (SD6). In the lateral and caudal portions of the EC, this layer is sharply demarcated from the deep, polymorphic portion of the LPI. In the medial parts of the EC, the deep LD is present within the LPI and separates the layer of large pyramidal cells from the deep polymorphic part of the LPI (SD4-6).

3.5.4.2 Cytoarchitectural zones

At this stage, the extent and appearance of EC cytoarchitectural zones are equivalent to the adult patterns described in the 22 w.g. stage.

3.5.4.3 AChE-positive axons

A marked development of the AChE-positive fibers occurs at this stage. This development is probably closely related to the in-growth of AChE-positive axons into the CP of the EC. In contrast to temporal neopallium, at the transition of temporal neopallium to EC (in the region of the RS), there is an increase in AChE reactivity in the MZ and the superficial part of LPE and a sudden loss of reactivity in the SP zone (Figures 19b, 20a-c). The most intense AChE reactivity in EC at this stage is present in the MZ and the superficial zone of the LPE (layer II, Figures 19b, 20a-e).

The deeper layers of the CP in the EC show a lower intensity of AChE reactivity (Figure 20a-e). MZ (layer I) and LPE (future layers II and III) are characterized by two different types of AChE reactivity. The superficial part of the MZ and the SGL has a higher intensity of AChE reaction than the deep part (Figure 20c-f). AChE-positive horizontal neurons can be recognized (arrows in Figure 20f).

The AChE reactivity of MZ is gradually decreasing medially and is lost at the border with PAM (Figure 20a). In the deep part of this layer, the LPE shows distinct AChE-positive vertical zones alternating with bright zones of low AChE reactivity (Figures 19b, 20b-e). Dark AChE-positive zones correspond to the vertical cell-dense zones of undifferentiated cells encompassing the MZ, islands of stellate neurons of layer II, and the superficial part of layer III. These zones extend from the superficial part of the MZ to different depths of the LPE.

In the neuropil of the AChE-reactive vertical zones, weakly AChE-positive stellate-shaped neurons can be seen and correspond to large islands of layer II (arrows in Figure 20f). The bright AChE-negative zones correspond to the acellular zones located between the islands of cells of the superficial LPE that extend from the MZ to the deep LPE.

The deep LPE shows a marked lower intensity of AChE reactivity and is separated from the LPI by an AChE-negative LD (Figure 19b). In the rostral parts of EC dark AChE-positive and light AChE-negative vertical zones are present from the superficial part of the LPE to the LD where the deep part of layer III is also organized into vertical cell-dense groups. The darker, AChE-positive vertical zones within this layer are continuous with the AChE-positive zones in the superficial LPE. Weakly AChE-positive pyramidal cells and dark, AChE-positive polymorphic neurons are seen in the neuropil of this layer (Figure 21a,b).

The LPI is characterized by weak and diffuse AChE reactivity. In this layer, we observed weakly stained pyramidal neurons and darkly stained polymorphic neurons (Figure 21c,d). Laterally and caudally the LPI is continuous with the AChE-positive SP layer of the temporal neopallium. It is separated from the LPE by

an AChE-negative superficial LD, whereas in the medial part of the LPI another narrow, the AChE-negative layer corresponds to the deep LD (Figure 20b,e).

3.6. Stage 6: definitive lamination and formation of adult-like cytoarchitectural zones (neonatal stage and adult appearance, 31-40 w.g.)

The laminar structure of the EC in humans at this stage is relatively well known and does not change significantly in comparison to the previous stage, except for further volume increase. We will focus our description on the further development of fibers and myelination patterns using acetylcholinesterase reactivity and MBP immunocytochemistry.

3.6.1 Myelination of the EC fiber systems at the neonate stage

Most of the human fiber systems at the neonate stage are not myelinated, except the posterior limb of the internal capsule. MBP immunocytochemistry revealed that at this stage MBP-expressing oligodendrocytes are present in the alveus and fimbria, but the perforant and alvear pathways are not yet myelinated. However, there are patchy MBP-immunoreactive oligodendrocytes and fibers along the temporoammonic branch of the perforant path, especially in the subicular region (Figure 22).

3.6.2 AChE histochemistry in neonatal and adult human EC

The intensity of AChE reactivity in the cortex of the anterior part of the parahippocampal gyrus displays its lowest intensity in layer III (including the superficial LD), and its highest reactivity in the islands of neurons of layer II. This part of the parahippocampal cortex corresponds to the rostral (area HA) and central parts (area HB) of the EC.

Layer II neurons are markedly AChE-positive in areas HA and HB. Their star-shaped cell bodies and the initial parts of their dendrites are visible. The neuropil between the perikarya of layer II neurons is also AChE-positive, but of lower intensity than these neurons. In addition, rare AChE-positive axons can be identified in the islands' neuropil. The neuropil in the acellular zones between the islands of layer II shows a significantly lower intensity of the AChE reactivity, as in layer III.

The layer I neuropil above the layer II islands is markedly AChE-positive, comparable to the layer II neuropil between the islands. In layer I, horizontally oriented, darkly AChE-positive bipolar neurons are present, likely CRC. Layer III shows the weakest intensity of the AChE reactivity in the EC neuropil, with a few AChE-positive axons and a small number of AChE-positive neurons, mostly pyramidal.

The LD cannot be distinguished on AChE preparations from layer III. Layer III is sharply bordered by layer IV which, unlike adjacent layers, shows a slightly higher intensity of AChE reactivity. Within layer IV, a dense plexus of AChE-positive axons without a specific orientation and a large number of dark, AChE-positive pyramidal neurons are observed. Between layers IV and VI, which exhibit a comparable intensity of AChE reactivity, Layer V appears as a lightly stained zone, containing rare axons. Layer VI contains a rich plexus of AChE-positive axons emerging from the white matter, as well as a large number of AChE-positive pyramidal and horizontal bipolar neurons.

In the most caudal part of the EC (area HC), AChE-positive layer II neurons are no longer grouped into islands but form a relatively continuous layer. There is no segregation of the AChE reactivity of layers I and II into vertical alternating zones. AChE reactivity in the neuropil of layer II is of the same intensity as in the layer II islands in the rostral EC. Layers I and III in the caudal part have the weakest AChE reactivity. The deep layers IV-VI have the same characteristics as in the rostral part of EC. In the lateral parts of the EC, layers III and V, which are usually the brightest, become thinner near the RS. In the entorhinal aspect of the RS, layer II expands significantly. The AChE-positive islands extend over the entire width of layer II and are elongated. In the neocortical aspect of the RS, the islands of layer II disappear. The AChE reactivity in layer I is lower than on the EC side.

Based on the analysis of serial coronal sections, the vertical AChE-positive zones of layers I and II in the rostral EC are not organized as vertical cylinders but are longitudinal AChE-positive bands extending in the anteroposterior direction. We also performed an analysis of AChE preparations cut tangentially to the surface of the EC. From serial reconstructions it became apparent that areas HA and HB are characterized by longitudinal AChE-positive bands in layers I and II, which vary in width, winding in different directions, often adopting X- or Y-shaped patterns, communicating with each other or ending abruptly (Figure 23a-f). On tangentially cut Nissl preparations of the EC, the neurons of layer II are also not organized into islands, but into longitudinal strips that extend in the anteroposterior direction and coincide with the AChE-positive bands.

4. Discussion

4.1 Cytoarchitectural indices of the EC development

To understand the development of the EC in detail, we examined its cytoarchitecture using Nissl staining, AChE histochemistry, and immunohistochemistry for a pan-axonal neurofilament marker, NeuN, MBP, and synaptophysin, in a series of postmortem samples of 20 fetal and 2 adult human brains. As nuclear chromatin patterns develop in parallel with morphological and cytoplasmic differentiation (García-Cabezas et al., 2018), Nissl staining was the basis for all our analyses. We reveal several major events in the development of the human EC.

The first major event is the earliest EC cytoarchitectural differentiation of the superficial magnocellular layer in the MZ in the 10th w.g. (Kostović et al., 1993), followed by the early condensation of the EC CP and simultaneous delamination of its deep part that last from the 10th w.g. until the 14 w.g. In that period, the magnocellular layer is made up of cells that, according to their degree of differentiation, belong to the most mature neurons of the telencephalon (see Table 3). Interestingly, this clearly shows that the first cytoarchitectural differentiation of the cerebral cortex begins in the periallocortex, not the archicortex (hippocampus). Moreover, the rostromedial location of the first appearance of the superficial magnocellular zone, which is the forerunner of the future EC islands, indicates that the cytoarchitectural differentiation in the human brain starts at the interface of the rostrolateral and posteromedial parts of EC, which corresponds to the border between MEC and LEC in animals. This subareal differentiation within the EC begins with uneven development of a fiber-rich LD and with the appearance of characteristic cell islands of the prospective layer II in the rostromedial EC at the subpial depths where large promoter neurons reside (Kostović et al., 1993). These large promoter neurons are probably the counterpart of the early-born stellate neurons in the dorsomedial mouse EC, which drive the maturation of other components of the entorhinal-hippocampal circuitry (Donato et al., 2017). At caudal levels, the LPI of the EC is continuous with the upper SP of the adjacent neocortex in the 13-week-old fetus, that is, during the stage of neocortical SP formation. As the SP zone forms by a gradual spread of neurons from the deep CP after the arrival of the first wave of afferent fibers (Kostović & Rakic, 1990), a similar process may occur in the LPI of the entorhinal CP. The unique feature of this process in the EC appears to be the precocious onset of fiber in-growth into the CP, the incomplete spread of the CP, and the paucity of thalamocortical fibers. Therefore, it may be speculated that the poor development of the SP in the EC is a decisive factor in the paucity of the thalamocortical projection, the SP being crucial in dynamical interactions that provide both spatial and temporal cues necessary for the normal formation of the thalamocortical connections (Shatz, 1992). Recent research findings in non-human primates revealed that most SP neurons generated in the VZ initially migrate radially, together with future layer VI neurons. During midgestation, SP cells become secondarily displaced and spread into the expanding SP zone, possibly as a result of an invasion of monoamine, basal forebrain, thalamocortical, and corticocortical axons (Duque et al., 2016).

The second major event appears in the period from the 14th to 16th w.g. The superficial magnocellular zone is transformed due to the arrival of a large number of small differentiated cells in that zone. The LPE of the CP of the most rostral parts of the EC begins to separate into vertical cell-dense groups separated by oval acellular zones, indicating the in-growth of afferent fibers into the most rostral parts of the EC. Afferent fibers also grow into the deep parts of the hitherto compact CP, which is manifested by the appearance of a bright acellular layer in the CP. This layer corresponds to the first appearance of the

superficial LD, which possibly indicates the first in-growth of afferents from the thalamus. The superficial LD divides the CP into the LPE and LPI. In the medial parts of the EC, in the LPI there appears as a clear acellular layer corresponding to the first appearance of the deep LD, which most probably indicates a growth of afferent fibers from the hippocampus. Electron microscopic analysis of the hippocampus shows that the distribution of synapses in 15- and 16.5-week-old fetuses is restricted to the MZ and SP, which contain dendritic branches of pyramidal and large non-pyramidal neurons, with a much higher density of synapses in the MZ than in the SP (Kostović, 1975; Kostović et al., 1989), just the opposite of the neocortex (Kostović & Molliver, 1974). Accordingly, in this stage, the MZ becomes characteristically enlarged in the hippocampus, whereas the SP becomes the thickest layer in the neocortex. In the 16th w.g. the process of differentiation of the LPE into vertical cell dense and cell sparse zones continues and spreads in the rostrocaudal direction and both LDs are getting thicker, probably due to the in-growth of afferent fibers from the amygdaloid nucleus. At this stage, the EC can be divided into four basic cytoarchitectural zones (rostral, central, caudomedial, and caudolateral), which, with minor modifications, can be seen throughout the rest of the intrauterine development and in adults. The rostral and central parts correspond to the rostrolateral EC in the adult brain, i.e. LEC, whereas the caudomedial and caudolateral parts correspond to the posteromedial EC in the adult brain and are likely equivalent to the MEC in animal species (cf. Maass et al., 2015; Navarro Schröder et al., 2015).

The third major event is the penetration of the main (temporoammonic) branch of the PP into the subiculum by the 20th w.g., reaching the suprapyramidal blade of the DG. Only about 2-3 weeks later the main branch of PP perforates the hippocampal sulcus to enter into the molecular layer of the DG directly. This is highly consistent with previous observations of carbocyanine DiI crystals injected into either the DG or the EC of the fixed human brains at the midgestational period (Hevner & Kinney, 1996). In that work, anterograde and retrograde labeling from the subiculum and CA1 field to the EC and vice versa showed that these reciprocal connections are consistently present at 19 w.g. In contrast, at 22 w.g. the perforant pathway had only limited anterograde labelings in the molecular layer of the DG, thus reaching only a rudimentary stage of development. These findings are highly similar to our observations and suggest that the piercing fibers of the PP crossing the hippocampal sulcus to directly reach the molecular layer of the DG occurs substantially later as a secondary process contributing to the trisynaptic pathway. At the same time, between the 20th and 23rd w.g., an intensive differentiation of the EC takes place, the vertical cellular zones in the MZ and the superficial part of the LPE containing a large number of small, undifferentiated cells appear, and the superficial LD becomes discernible by 3 T MRI. Therefore, the first stage at which the EC assumes a near-adult organization is at about 22 w.g. (CRL=200 mm). Taking into account the most pronounced cytoarchitectural features, such as the presence of cell islands and LDs, at this stage four, main EC parts can be distinguished, namely, rostral, central, medial, and laterocaudal subareas. However, their boundaries are still not sharply defined and only partially resemble the cytoarchitectural zones of the adult human (von Economo & Koskinas, 1925) and non-human primates (van Hoesen & Pandya, 1975).

The fourth major event is the first AChE reactivity in the prospective EC occurring in the 23 w.g. as a bundle of intensely AChE-positive fibers in the superficial part of the MZ. These axons run across the MZ of the uncus and are continuous with the sublenticular structures, suggesting that they originate from the basal telencephalon or brainstem tegmentum. At 25 w.g. AChE-positive axons begin to grow into the deep parts of the MZ and the most superficial parts of the CP in the form of vertical AChE-positive bands. In the 28th w.g., there is a definite in-growth of AChE-positive axons from the superficial part of the MZ into the vertical cellular zones of the MZ and the superficial cellular zones of the LPE, which is manifested by the

alternating distribution of AChE reactivity in the EC superficial layers I and II. Similar to cytochrome oxidase staining (Solodkin & Van Hoesen, 1996), the deep layers show a significantly lower intensity of AChE reactivity, but the presence of a large number of AChE-positive neuron bodies in the deeper layers of the CP is noticeable. Our serial reconstruction shows that AChE reactivity in layers I and II of the rostral parts of the EC (subareas HA and HB) is organized into longitudinal strips reminiscent of ocular-dominance columns in the visual cortex (Hubel & Wiesel, 1969; Wiesel et al., 1974). The alternating, columnar distribution of reactivity to AChE is probably an indication of the early in-growth of dopaminergic mesencephalic projections from the ventral tegmental area (VTA). In the later stages of development (20-28 w.g.), there are indicators of the thalamic source of afferent axons, which is manifested by the appearance and development of both LD and the differentiation of the CP (see below).

Finally, the fifth major event is the patchy myelination of the PP in the form of MBP-immunoreactive immature oligodendrocytes and their processes at term (40th w.g.). These five milestones are summarized in Table 4.

Our cytoarchitectural findings show that there are four cytoarchitectural layers in the human fetal EC: one superficial, two intracortical, and one deep (below the CP). The most superficial of these four layers is the MZ, which is already present in the earliest investigated stages in the 9th and 10th w.g. We detected the presence of large differentiated cells in the MZ very early – around the 9th and 10th w.g. as well as the appearance of differentiated islands of cells below the deep MZ around 13-14 w.g.

The EC is unique in that it shows a distinct cytoarchitectural differentiation, by the appearance and development of two intracortical layers, the LDs (Rose 1926, 1927a, 1927b; Lorente de Nó, 1933; Stephan, 1975). The superficial LD arises around the 14th w.g., consistent with previous findings (Rose 1926, 1927a, 1927b; Filimonoff, 1947; Macchi, 1951; Kahle, 1969). Experimental studies in rats and cats have shown that the superficial LD receives fibers from nuclei of the medial thalamus, such as the thalamic nucleus reuniens (Herkenham, 1978; Wouterlood et al., 1990) and the commissural rhomboid nucleus (Ohtake & Yamada, 1989; Vertes et al., 2006), and from the lateral amygdaloid nuclei (Krettek & Price, 1977), perirhinal (Van Hoesen & Pandya, 1975; Burwell & Amaral, 1998; Shi & Cassell, 1999), medial prefrontal (Leichnetz & Astruc, 1976; Apergis-Schoute et al., 2006), and caudal orbitofrontal cortex (Van Hoesen et al., 1975; Kondo & Witter, 2014). Projections from the basolateral complex of amygdaloid nuclei (lateral, basal, and accessory basal nucleus) that terminate in the superficial LD were confirmed in cats (Krettek & Price, 1977) and non-human primates (Pitkänen et al., 2002).

A deep LD emerges at the 14th w.g., which is an indicator of maturation and development of neural connections, including dendritic growth and axon in-growth. It was present exclusively in the medial EC. While early description reported a late onset of the deep LD in the 7th month of gestation (Rose, 1926, 1927a, 1927b), our findings are consistent with the observations of Filimonoff (1947) and Macchi (1951). Experimental studies have shown that the deep LD contains afferent fibers from the CA1 field of the hippocampus (Swanson et al., 1978; Witter & Amaral, 2021), the perirhinal (Van Hoesen & Pandya, 1975), and the prefrontal cortex (Leichnetz & Astruc, 1976). Regarding the projection from the hippocampus, it should be noted that already at the 15th w.g. the hippocampus contains relatively mature pyramidal neurons, which show a relatively high degree of differentiation (Kostović, 1975). Additionally, as seen from DiI tracing, projections from the CA1 and subicular field to the EC are already present at the 19th w.g. in the developing human brain (Hevner & Kinney, 1996).

The deepest layer of the EC differentiates very early below the CP with a decrease in cell density, and a plexiform appearance, in parallel to the MZ. The lateral and caudal EC adjacent to the neocortex has an

especially developed deep layer that corresponds to the SP, as defined in the neocortex (Kostović & Molliver, 1974). In contrast, the medial and rostral EC contains a completely undeveloped SP. The SP in the caudal and lateral EC shows continuity with the external capsule and the ventral internal capsule. The SP is the main source of afferent fibers of the fetal cortex in the early developmental period (Kostović, 2020), consistent with the early onset of synapses in that layer in both the neocortex and cingulate gyrus (Judaš et al., 2010). It must be noted that the generation of the LDs is earlier than the differentiation of the cortical projections arriving at them. As we have observed, the LD is already present when the CP of the laterally located PRC has not yet started to differentiate, which is in accordance with the findings of heavy labelings in the EC at 20 w.g. in layers both above and below the LD (but not neocortex) after DiI injection into the CA1 and subiculum (Hevner & Kinney, 1996).

4.2 Histochemical indices of the development of EC connections

AChE axon reactivity may be temporary and related to axon growth and differentiation as well as to nonenzymatic roles, and thus is not necessarily related to the cholinergic nature of the axon (Filogamo & Marchisio, 1971; Karczmar et al., 1973, 1980; Silver, 1974; Slotkin et al., 2009). It has been shown that acetylcholinesterase can also occur in adult monoaminergic neurons (Lewis & Schon, 1975; Butcher, 1977; Albanese & Butcher 1979, 1980; Butcher & Talbot, 1978; Meibach & Weaver, 1979). We observed the presence of AChE reactivity in fibers, in the neuropil, and the neuronal perikarya.

AChE fiber reactivity was present in the MZ and the SP. The reactivity of the MZ was continuous only in its superficial part, while the deep layers of the MZ contained alternating zones of AChE reactivity. The reactivity of the superficial part of the marginal zone decreased significantly in the later stages of development, so it can be considered a temporary reactivity, related to axonal in-growth (Kostović-Knežević et al., 1979). The origin of fibers in the superficial MZ remains uncertain, as there are no conclusive experimental data from non-human primates. However, it can be assumed that some of these fibers come from the area of the nucleus basalis complex or even from the tegmentum of the mesencephalon based on the relationship (continuity) of AChE-positive fibers in the marginal zone of the anterior EC to AChE-positive areas of the mediobasal telencephalon.

Serotonergic and noradrenergic fibers are known to access the neocortex along the ventral amygdalofugal pathway (also called the "entorhinal pathway"). In the rhesus monkey, many of these fibers enter the MZ of the EC (Fallon et al., 1978; Köhler et al., 1980) together with a contingent of afferent fibers from the basal and lateral amygdaloid nuclei that travel around the EC to innervate perirhinal cortex and the medial aspect of the area TE (Amaral & Price, 1984). However, it is not excluded that some thalamic axons also end in the MZ (Herkenham, 1978). In contrast, the AChE reactivity of the deep MZ is discontinuous, due to alternating AChE-positive and AChE-negative vertical zones. This type of reactivity remains in the adult brain. As the AChE-positive zones of fibers also contain stellate neuron islands, some of these fibers likely innervate these neurons. The finding that AChE positive labeling coincides with stellate cell "islands" has important comparative implications. In rodents, cholinergic innervation of the MEC targets calbindin-immunoreactive patches that originate from apical dendrites of pyramidal layer II cells, an organizational pattern that is found in both adults and at early postnatal stages (Ray et al., 2014; Ray & Brecht, 2016). In contrast, it has been shown that the human EC shows the opposite pattern, as the cholinergic innervation of MEC specifically avoids calbindin-enriched patches (Neumann et al., 2016). Our data are in agreement with these later findings, as reelin-expressing stellate cells constitute a cell population distinct from the calbindin-immunoreactive pyramidal cells.

Based on studies of afferent fibers from the tegmentum (Collier & Routtenberg, 1977; Fallon et al., 1978; Lindvall & Björklund, 1974) that described the dopaminergic innervation of EC layer II stellate neuron islands it can be assumed that the AChE-positive zones are formed by dopaminergic in-growing axon bundles. As the deep portion of layer III in the rostral EC is innervated by radially oriented bundles of amygdaloid fibers that extend into superficial layer III and further through the cell-free spaces of layer II (Amaral, 1986), the AChE-negative vertical zones could correspond to projection fibers from the amygdala (Amaral & Insausti, 1992; Insausti et al., 1987a; Krettek & Price, 1977; Saunders & Rosene, 1988) and thalamus (Herkenham, 1978). A special fiber system accesses the lateral part of the EC through the external capsule – the lateral pathway of the basal nucleus complex (Saper & Chelimsky, 1984). The origin of these fibers is probably from the basal telencephalon because there is a continuity of AChE reactivity with the external capsule that can be considered the main projection system of the basal telencephalon (Šimić et al., 1999; Boban et al., 2006; Raghanti et al., 2011). Unlike the medial pathway fibers of the basal nucleus complex that enter the fornix from the medial septal and diagonal band nuclei, these fibers may arise from cholinergic neurons in the lateral part of the basal nucleus. The lateral part of the basal nucleus includes the human-specific subputaminal nucleus that has already been shown to innervate the cortical Broca area associated with speech and language production as well as the cingulate gyrus and amygdala (Šimić et al., 1999), traveling laterally within the anterior commissure from the basal nucleus into the temporal lobe (Mesulam et al., 1983). Because cholinergic fibers in the angular bundle are much more abundant than those arising in the MEC (contained in the alvear path), the layer II/III cells in the LEC are probably the main input region for cholinergic innervation of the EC (De Lacalle et al., 1994). AChE-positive neurons, which most likely originate from the SP, are also observed in the white matter of the EC in the adult human (Kostović & Rakic, 1980). There are also AChE-positive perikarya in the layer II cellular islands of the adult human EC.

4.3 Growth of afferent fiber systems into the EC in the developing human fetus and their functional relevance

The early development of the MZ, SP, and LDs with the development of AChE-positive reactivity in the EC around 22 w.g., as well as early synaptogenesis in the cortex (Molliver et al., 1973), suggest the precise order with which different classes of afferent fibers reach the EC. This is relevant not only in the context of the origins of these projections but also when considering critical periods in the development of individual afferent pathways (Radoš et al., 2006). In this context, Nobin & Björklund (1973) showed that ascending monoaminergic fibers from the mesencephalic tegmentum are seen in the basal telencephalon as early as 12 w.g., suggesting that tegmental afferent systems form one of the earliest afferent systems in the human fetal EC. The next fiber system most likely comes from the thalamus (Lorente de Nó, 1933), while the origin of other fiber systems, commissural and association, remains unexplored. A comparable order of afferent axons in-growth has been described for afferent systems to the frontal cortex of the human fetus (Vasung et al., 2010), as well as in experimental animals (Goldman & Nauta, 1977; Wise & Jones, 1978; Goldman-Rakic, 1978, 1981).

The periods of growth and differentiation of the EC in the human fetus largely coincide with the periods of differentiation of other cortical areas. The onset of the first period of early histogenetic differentiation falls between 10 and 14 w.g., which may represent a period of high vulnerability to genotoxic agents. The second period of intensive development is when afferent systems grow into the EC. This period starts after the 20th week of pregnancy (Hevner & Kinney, 1996), especially for AChE-positive fibers, as shown

by research on other areas of the fetal cortex (Krsnik et al., 2017). At the same time, the main (temporoammonic) branch of the PP grows through the subiculum and stratum lacunosum-moleculare of the Ammon's horn into the DG. This projection does not go not through the hippocampal sulcus, thus taking this other (longer) route before the 20th w.g. (Hevner & Kinney, 1996). The crossing of PP fibers through the hippocampal sulcus occurs only about two to three weeks later (at 23 w.g.), which suggests protracted development of the entorhino-hippocampal projection and also the probable importance of the direct connections. In this respect, it needs to be pointed out that granule cells in rhesus monkey's DG are the last neuronal type that still divides and differentiates (Rakic & Nowakowski, 1981) and that there is a progressive increase in synaptic density in the molecular layer of the DG along the second half of gestation (Eckenhoff & Rakic, 1991). Therefore, the period after the 20th w.g. can be considered critical for the development of the human cerebral cortex. The growth and development of commissural and association fibers allow higher EC functions that develop only in the prematurity period i.e. before 37 w.g., and which may be important for interpreting fine damage to the cerebral cortex of a child. Namely, it is known that premature newborns of low birth weight are particularly susceptible to respiratory difficulties and intracerebral hemorrhage, which can compromise the development of thalamic, commissural, and association connections (Ballabh, 2014; Žunić Išasegi et al., 2018). Therefore, it can be assumed that the action of pathogenetic factors in this period leads to lasting consequences for EC function.

4.4. Concluding remarks

A major reason for undertaking this study was that a detailed analysis of human EC neurogenesis and the developmental laminar pattern is unavailable. In addition to the challenges in obtaining high-quality fetal human brain specimens, it is difficult to subdivide the developing EC regions and layers solely based on Nissl stain. Such anatomical delineations can be only improved by a combined analysis of Nissl and AChE staining, and gene expression patterns (Ding et al., 2022). Early thymidine autoradiography studies of neuronal migration in rats (e.g. Bayer et al., 1993), as well as a few recent studies in mice (Donato et al., 2017) and pigs (Liu et al., 2021), revealed that EC development does not conform to the classical inside-out pattern as the rest of the neocortex and that the early birth of large "promoter" neurons at shallow subpial depths is a pivotal event in the EC neurogenesis (Kostović et al., 1993). The early cytoarchitectural differentiation of the EC, which significantly precedes that of the neighboring cortical areas, is paralleled by the neurochemical development, e.g. somatostatin innervation, where somatostatin-immunoreactive fibers in the EC MZ and the SP are first detected at E56 in the rhesus monkey (Berger et al., 1993). In mice, early-born stellate neurons in dorsomedial EC drive the maturation of other components of the entorhinal-hippocampal circuitry (Donato et al., 2017). Our results obtained with NeuN immunohistochemistry (Figure 12), also clearly refute the development of the EC in humans in an inside-out manner and support the early development of layer II and a key role of the large "promoter" neurons appearing in that layer first in the rostromedial parts of the EC at about 13-13.5 w.g. (Kostović et al., 1993), followed by the other layers, possibly in a "parallel" pattern as described by Liu et al. (2021), and possibly also with a "sandwich" gradient described by Bayer et al. (1993), which suggests that after layer II and layers V/VI, layer III forms last (Bayer et al., 1993). Altogether, these findings suggest that the final thickness and arrangement of EC layers in its different subfields along with the presence or absence, and position of LD, can not be simply calculated based on the number of neurons in each radial unit,

differential time of origin, and rate of migration along the radial glial cells (Rakic, 1988). In this context, it is relevant to note that the laminar patterning of cortical neurons mainly emphasizes the generation of glutamatergic neurons arising from onsite neurogenesis and movement along the growing cortex by radial migration. In addition, GABAergic neurons originate from neural progenitors of the medial and caudal ganglionic eminence and migrate to the pallium until arriving in either the MZ or the SP from where they finally get the corresponding fate inside the CP (Marín & Rubenstein, 2001, 2003). It would thus be of interest to study the development of GABAergic neurons as well to see whether and how their distribution influences the model proposed here, and to which extent it is supported by the above-mentioned studies in mice and pigs (Donato et al., 2017; Liu et al., 2021).

The major developmental events in EC structure and connectivity have broad implications for understanding its normal function, hemispheric asymmetry, modular variability, age-related changes (Šimić et al., 2005) as well as deficits in brain diseases, such as epilepsy, autism spectrum disorder, schizophrenia, or Alzheimer's disease (Šimić et al., 1997, 2000, 2009, 2014, 2016, 2017; 2019; Palmen et al., 2004; Polšek et al., 2011; Špeljko et al., 2011; Jazvinšćak Jembrek et al., 2015; Mladinov et al., 2016; Mihelčić et al., 2017; Španić et al., 2019; Bažadona et al., 2020; Babić Leko et al., 2021; Kobro-Flatmoen et al., 2021). The two main critical periods of EC development in human fetuses are the first period of intensive early histogenetic differentiation between 10 and 14 w.g., and the second period of intensive development of EC afferent systems, which takes place from the 20th w.g. until birth. Precise knowledge of histogenetic processes during these critical periods is important for interpreting developmental impairments, such as hypoxic-ischemic damage, of higher-order cognitive functions mediated by the EC, including self-awareness (Chavoix & Insausti, 2017). One of the most obvious instances of the importance of the knowledge of histogenetic processes in the development of the human EC is in their regard to the development of schizophrenia, as in this disease the organization of layer II neurons seems to be often disrupted (Arnold et al., 1997; Falkai et al., 2000; Muraki & Tanigaki, 2015).

Finally, further exploration of the intriguing AchE-positive bands of the EC that we observed in tangential sections (illustrated in Figure 23) has potential relevance for elucidating and deeper understanding of the EC functions. As these conspicuous bands resemble modular organization in other parts of the cerebral cortex (such as somatosensory and visual cortex), it would be of interest to explore whether they are composed of neuropil, neurons, or both, as well as their relationships to the local microvasculature, such as local meshworks of pial capillaries (Solodkin & van Hoesen, 1996; Šimić et al., 2005), and how they relate to the islands of layer II cells, particularly concerning metabolic demands of functionally diverse neuron types (Hafting et al., 2005; Brecht, 2017; Nilssen et al., 2018). In this context, the present study provides a foundation for a more detailed analysis of EC development using genetic and advanced cellular and brain imaging approaches in experimental animals and humans.

Acknowledgments

This work is the result of the efforts of many colleagues who have been involved in the collection, processing, analysis, storage, and digitization of the postmortal human brain material in the Zagreb Neuroembryological Collection over the past 50 years. The authors wish to thank all of them. The work was funded by The Croatian Science Foundation grant IP-2019-04-3584 to GŠ and by the Scientific Centre of Excellence for Basic, Clinical, and Translational Neuroscience CoRE-NEURO ("Experimental and clinical

research of hypoxic-ischemic damage in perinatal and adult brain"; GA KK01.1.1.01.0007 funded by the European Union through the European Regional Development Fund). Menno project number??

Conflict of interest

The authors do not report a conflict of interest.

Author contributions

GŠ, ZK, and PRH conceived the manuscript. GŠ and ZK wrote the manuscript. GŠ, VK, ZK, ŽK, and MR performed the research. GŠ, ŽK, VK, EŠ, and DM prepared images and microphotographs for publication. All authors edited the manuscript, contributed important intellectual content, and approved its final version.

Ethical statement

All procedures were conducted with the permission of the Central Ethical Committee of the University of Zagreb Medical School. All postmortem brain tissue collected is a part of the Zagreb Neuroembryological Collection at the Croatian Institute for Brain Research.

Data availability statement

All the data reported are available on request from the corresponding author.

References

Albanese, A., & Butcher, L. L. (1979). Locus coeruleus somata contain both acetylcholinesterase and norepinephrine: direct histochemical demonstration on the same tissue section. *Neuroscience Letters*, *14*(1), 101-104. https://doi.org/10.1016/0304-3940(79)95352-7

Albanese, A., & Butcher, L. L. (1980). Acetylcholinesterase and catecholamine distribution in the locus coeruleus of the rat. *Brain Research Bulletin*, *5*(2), 127-134. https://doi.org/10.1016/0361-9230(80)90184-7

Alexander, A. S., Robinson, J. C., Dannenberg, H., Kinsky, N.R., Levy, S.J., Mau, W, Chapman, G. W., Sullivan, D.W., & Hasselmo, M.E. (2020). Neurophysiological coding of space and time in the hippocampus, entorhinal cortex, and retrosplenial cortex. *Brain and Neuroscience Advances*, *4*, 2398212820972871. https://doi.org/10.1177/2398212820972871

Amaral, D. G. (1986). Amygdalohippocampal and amygdalocortical projections in the primate brain. *Advances in Experimental Medicine and Biology*, *203*, 3-17. https://doi.org/10.1007/978-1-4684-7971-3-1

Amaral, D. G., & Insausti, R. (1990). Hippocampal formation. In: Paxinos, G. (ed.) *The human nervous system*. London: Academic Press, 711-755.

Amaral, D. G., & Insausti, R. (1992). Retrograde transport of D-3H-aspartate injected into the monkey amygdaloid complex. *Experimental Brain Research*, *88*(2), 375-388. https://doi.org/10.1007/BF02259113

Amaral, D. G., Insausti, R., & Cowan, W. M. (1987). The entorhinal cortex of the monkey: I. Cytoarchitectonic organization. The *Journal of Comparative Neurology*, *264*(3), 326-355. https://doi.org/10.1002/cne.902640305

Amaral, D. G., & Price, J. L. (1984). Amygdalo-cortical projections in the monkey (*Macaca fascicularis*). *The Journal of Comparative Neurology*, *230*(4), 465-496. https://doi.org/10.1002/cne.902300402

Apergis-Schoute, J., Pinto, A., & Paré, D. (2006). Ultrastructural organization of medial prefrontal inputs to the rhinal cortices. *European Journal of Neuroscience*, *24*(1), 135-144. https://doi.org/10.1111/j.1460-9568.2006.04894.x

Arnold, S. E., Ruscheinsky, D. D., & Han, L-Y. (1997). Further evidence of abnormal cytoarchitecture of the entorhinal cortex in schizophrenia using spatial point pattern analyses. *Biological Psychiatry*, *42*(8), 639-647. https://doi.org/10.1016/S0006-3223(97)00142-X

Ballabh, P. (2014). Pathogenesis and prevention of intraventricular hemorrhage. *Clinical Perinatology*, *41*(1), 47-67. https://doi.org/10.1016/j.clp.2013.09.007

Bayer, S. A. (1980). Development of the hippocampal region in the rat. I. Neurogenesis examined with ^{3}H-thymidine autoradiography. *The Journal of Comparative Neurology*, *190*(1), 87-114. https://doi.org/10.1002/cne.901900107

Bayer, S. A., Altman, J., Russo, R. J., Zhang, X. (1993). Timetables of neurogenesis in the human brain based on experimentally determined patterns in the rat. *Neurotoxicology*, *14*(1), 83-144.

Babić Leko, M., Hof, P. R., & Šimić, G. (2021) Alterations and interactions of subcortical modulatory systems in Alzheimer's disease. *Progress in Brain Research*, *261*, 379-421. https://bs.pbr.2020.07.016

Bažadona, D., Fabek, I., Babić Leko, M., Bobić Rasonja, M., Kalinić, D., Bilić, E., Raguž, J. D., Mimica, N., Borovečki, F., Hof, P. R., & Šimić, G. (2020). A non-invasive hidden-goal test for spatial orientation deficit detection in subjects with suspected mild cognitive impairment. *Journal of Neuroscience Methods*, *332*(2), 108547. https://doi.org/10.1016/j.jenumeth.2019.108547

Berger, B., Alvarez, C., & Goldman-Rakic, P. S. (1993). Neurochemical development of the hippocampal region in the fetal rhesus monkey. I. Early appearance of peptides, calcium-binding proteins, DARPP-32, and monoamine innervation in the entorhinal cortex during the first half of gestation (E47 to E90). *Hippocampus*, *3*(3), 279-305. https://doi.org/10.1002/hipo.450030305

Boban, M., Kostović, I., & Šimić, G. (2006). Nucleus subputaminalis: neglected part of the basal nucleus of Meynert. *Brain*, *129*(4), E42. https://doi.org/10.1093/brain/awl025

Braak, H. (1972). Zur Pigmentarchitektonik der Groβhirnrinde des Menschen. I. Regio entorhinalis. *Zeitschrift für Zellforschung und mikroskopische Anatomie*, *127*, 407-438. https://doi.org/10.1007/BF00306883

Braak, H., & Braak, E. (1992). The human entorhinal cortex: normal morphology and lamina-specific pathology in various diseases. *Neuroscience Research*, *15*(1-2), 6-31. https://doi.org/10.1016/0168-0102(92)90014-4

Brecht, M. (2017). The body model theory of somatosensory cortex. *Neuron*, *94*(5), 985-992. https://doi.org/10.1016/j.neuron.2017.05.018

Broca, P. (1878). Anatomie comparée des circonvolutions cérébrales: le grande lobe limbique et la scissure limbique dans la série des mammifères. *Revue d'Antropologie*, *1*(2), 385-498.

Broderson, S. H., Westrum, L. E., & Sutton, A. E. (1974). Studies on the direct coloring thiocholine method for localizing cholinesterase activity. *Histochemistry*, *40*(1), 13-23. https://doi.org/10.1007/BF00490269

Brodmann, K. (1909). *Vergleichende Lokalisationslehre der Groβhirnrinde ini hren Prinzipien dargestellt auf Grund des Zellenbaues*. Leipzig: J. A. Barth.

Burwell, R. D., & Amaral, D. G. (1998). Cortical afferents of the perirhinal, postrhinal, and entorhinal cortices of the rat. *The Journal of Comparative Neurology*, *398*(2), 179-205. https://doi.org/10.1002/(sici)1096-9861(19980824)398:2<179::aid-cne3>3.0.co;2-y

Butcher, L. L. (1977). Nature and mechanisms of cholinergic-monoaminergic interactions in the brain. *Life Sciences*, *21*(9): 1207-1226. https//doi.org/10.1016/0024-3205(77)90001-7

Butcher, L. L., & Talbot, K. (1978). Acetylcholinesterase in rat nigroneostriatal neurons: experimental verification and evidence for cholinergic-dopaminergic interactions in the substantia nigra and caudate-putamen complex. In L. L. Butcher (Ed.) *Cholinergic-monoaminergic interactions in the brain*. New York: Academic Press; pp. 25-95.

Buzsáki, G., & Tingley, D. (2018). Space and time: the hippocampus as a sequence generator. *Trends in Cognitive Sciences*, *22*(10): 853-869. https://doi.org/10.1016/j.tics.2018.07.006

Canto, C. B., Wouterlood, F. G., & Witter, M., P. (2008). What does the anatomical organization of the entorhinal cortex tell us? *Neural Plasticity*, *2008*, 381243. https://doi.org/10.1155/2008/381243

Chavoix, C., & Insausti, R. (2017). Self-awareness and the medial temporal lobe in neurodegenerative diseases. *Neuroscience and Biobehavioral Reviews*, *78*(7), 1-12. https://doi.org/10.1016/j.neubiorev.2017.04.015

Collier, T. J., & Routtenberg, A. (1977). Entorhinal cortex: catecholamine fluorescence and Nissl staining of identical Vibratome sections. *Brain Research*, *128*(2): 354-360. https://doi.org/10.1016/0006-8993(77)91001-0

De Lacalle, S., Lim, S., Sobreviela, T., Mufson, E. J., Hersch, L. B., & Saper, C. B. (1994). Cholinergic innervation in the human hippocampal formation including the entorhinal cortex. *The Journal of the Comparative Neurology*, *345*(3), 321-344. https://doi.org/10.1002/cne.903450302

Ding, S.-L., & Van Hoesen, G. W. (2010). Borders, extent, and topography of human perirhinal cortex as revealed using multiple modern neuroanatomical and pathological markers. *Human Brain Mapping*, *31*(9), 1359-1379. https://doi.org/10.1002/hbm.20940

Ding, S.-L., & Van Hoesen, G. W. (2015). Organization and detailed parcellation of human hippocampal head and body regions based on a combined analysis of cyto- and chemoarchitecture. *The Journal of Comparative Neurology*, *523*(15), 2233-2253. https://doi.org/10.1002/cne.23786

Ding, S.-L., Royall, J. J., Lesnar, P., Facer, B. A. C., Smith, K. A., Wei, Y., Brouner, K., Dalley, R. A., Dee, N., Dolbeare, T. A., Ebbert, A., Glass, I. A., Keller, N. H., Lee, F., Lemon, T. A., Nyhus, J., Pendergraft, J., Reid, R., Sarreal, M., Shapovalova, N. V., Szafer, A., Phillips, J. W., Sunkin, S. M., Hohmann, J. G., Jones, A. R., Hawrylycz, M. J., Hof, P. R., Ng, L., Bernard, A., & Lein, E. S. (2022). Cellular resolution anatomical and molecular atlases for prenatal human brains. *The Journal of Comparative Neurology*, *530*(1), 6-503. https://doi.org/10.1002/cne.25243

Donato, F., Jacobsen, R., I., Moser, M-B., & Moser, E. I. (2017). Stellate cells drive maturation of the entorhinal-hippocampal circuit. *Science*, *355*(6330), eaai8178. https://doi.org/10.1126/science.aai8178

Duque, A., Krsnik, Ž., Kostović, I., & Rakic, P. (2016). Secondary expansion of the transient subplate zone in the developing cerebrum of human and nonhuman primates. *Proceedings of the National Academy of Sciences of the U S A*, *113*(35), 9892-9897. https:/doi.org/10.1073/pnas.1610078113

Eckenhoff, M. F., & Rakic, P. (1991). A quantitative analysis of synaptogenesis in the molecular layer of the dentate gyrus in the rhesus monkey. *Developmental Brain Research*, *64*(1-2), 129-135. https://doi.org/10.1016/0165-3806(91)90216-6

Fallon, J. H., Koziell, D.A., & Moore, R. Y. (1978). Catecholamine innervation of the basal forebrain. II. Amygdala, suprarhinal cortex and entorhinal cortex. *The Journal of Comparative Neurology*, *180*(3), 509-532. https://doi.org/10.1002/cne.901800308

Falkai, P., Schneider-Axmann, T., & Honer, W. G. (2000). Entorhinal cortex pre-alpha cell clusters in schizophrenia: quantitative evidence of a developmental abnormality. *Biological Psychiatry*, *47*(11), 937-943. https://doi.org/10.1016/s0006-3223(99)00250-4

Filimonoff, I. N. (1947). A rational subdivisions of the cerebral cortex. *Archives of Neurology and Psychiatry*, *58*(3), 296-311. https://doi.org/10.1001/archneurpsyc.1947.02300320047002

Filogamo, G., & Marchisio, P. C. (1971). Acetylcholine system and neural development. *Neuroscience Research*, *4*, 29-64. https://doi.org/10.1016/B978-0-12-512504-8.50008-1

García-Cabezas, M. Á., Barbas, H., & Zikopoulos, B. (2018). Parallel development of chromatin patterns, neuron morphology, and connections: potential for disruption in autism. *Frontiers in Neuroanatomy*, *12*, 70. https://doi.org/10.3389/fnana.2018.00070

Goldman, P. S., & Nauta, W. J. H. (1977). Columnar distribution of cortico-cortical fibers in the frontal association, limbic and motor cortex of the developing rhesus monkey. *Brain Research*, *122*(3), 393-413. https://doi.org/10.1016/0006-8993(77)90453-x

Goldman-Rakic, P. S. (1978). Neuronal plasticity in primate telencephalon: anomalous crossed cortico-caudate projections induced by prenatal removal of frontal association cortex. *Science*, *202*(4369), 768-770. https://doi.org/10.1126/science.102031

Goldman-Rakic, P. S. (1981). Development and plasticity of primate frontal association cortex. In F. O. Schmitt, & F. G. Worden, Dennis, S. G., Adelman, G. (Eds.): Organization of the cerebral cortex. The MIT Press, Cambridge, MA, USA, pp. 69-97.

Guthman, E. M., Garcia, J. D., Ma, M., Chu, P., Baca, S. M., Smith, K. R., Restrepo, D., & Huntsman, M. M. (2020). Cell-type-specific control of basolateral amygdala neuronal circuits via entorhinal cortex-driven feedforward inhibition. *eLife*, *9*(1), e50601. https://doi.org/10.7554/eLife.50601

Hafting, T., Fyhn, M., Sturla, M., Moser, M-B., & Moser, E. I. (2005). Microstructure of a spatial map in the entorhinal cortex. Nature, 436(7052), 801-806. https://doi.org/10.1038/nature03721

Herkenham, M. (1978). The connections of the nucleus reuniens thalami: evidence for a direct thalamo-hippocampal pathway in the rat. *The Journal of Comparative Neurology*, *177*(4), 589-610. https://doi.org/10.1002/cne.901770405

Hevner, R. F., & Kinney, H. C. (1996). Reciprocal entorhinal-hippocampal connections established by human fetal midgestation. *The Journal of Comparative Neurology*, *372*(3), 384-394. https://doi.org/10.1002/(SICI)1096-9861(19960826)372:3<384::AID-CNE4>3.0.CO;2-Z

Hsu, S. M., Raine, L., & Fanger, H. (1981). Use of avidin-biotin-peroxidase complex (ABC) in immunoperoxidase techniques: a comparison between ABC and unlabeled antibody (PAP) procedures. *Journal of Histochemistry and Cytochemistry*, *29*(4), 557-580. https://doi.org/10.1177/29.4.6166661

Hubel, D. H., & Wiesel, T. N. (1969). Anatomical demonstration of columns in the monkey striate cortex. *Nature*, *221*(5182), 747-750. https://doi.org/10.1038/22747a0

Huntgeburth, S. C., & Petrides, M. (2012). Morphological patterns of the collateral sulcus in the human brain. *European Journal of Neuroscience*, *35*(8), 1295-1311. https://doi.org/10.1111/j.1460-9568.2012.08031.x

Insausti, R., Amaral, D. G., & Cowan, W. M. (1987a). The entorhinal cortex of the monkey: II. Cortical afferents. *The Journal of Comparative Neurology*, *264* (3), 356-395. https://doi.org/10.1002/cne.902640306

Insausti, R., Amaral, D. G., & Cowan, W. M. (1987b). The entorhinal cortex of the monkey: III. Subcortical afferents. *The Journal of Comparative Neurology*, *264*(3), 396-408. https://doi.org/10.1002/cne.902640307

Insausti, R., Córcoles-Parada, M., Ubero, M. M., Rodado, A., Insausti, A. M., & Muñoz-López, M. (2019). Cytoarchitectonic areas of the *Gyrus ambiens* in the human brain. *Frontiers in Neuroanatomy*, *13*, 21. https://doi.org/10.3389/fnana.2019.00021

Insausti, R., Muñoz-López, M., Insausti, A. M., & Artacho-Pérula, E. (2017). The human periallocortex: layer pattern in presubiculum, parasubiculum and entorhinal cortex. A review. *Frontiers in Neuroanatomy*, *11*, 84. https://doi.org/10.3389/fnana.2017.00084

Insausti, R., Tuñón, T., Sobreviela, T., Insausti, A. M., & Gonzalo, L. M. (1995). The human entorhinal cortex: a cytoarchitectural analysis. *The Journal of Comparative Neurology*, *355*(2), 171-198. https://doi.org/10.1002/cne.903550203

Isaacson, R. L. (1982). *The limbic system* (2nd ed.). New York: Springer.

Jazvinšćak-Jembrek, M., Hof, P.R., & Šimić, G. (2015). Ceramides in Alzheimer's disease: key mediators of neuronal apoptosis induced by oxidative stress and Aβ accumulation. *Oxidative Medicine and Cellular Longevity*, *2015*, 346783. https://doi.org/10.1155/2015/346783

Judaš, M., Sedmak, G., & Pletikos, M. (2010). Early history of subplate and interstitial neurons: from Theodor Meynert (1867) to the discovery of the subplate zone (1974). *Journal of Anatomy*, *217*(4), 344-367. https://doi.org/10.1111/j.1469-7580.2010.01283.x

Judaš, M., Šimić, G., Petanjek, Z., Jovanov-Milošević, N., Pletikos, M., Vasung, L., Vukšić, M., & Kostović, I. (2011). The Zagreb Collection of human brains: a unique, versatile, but underexploited resource for the neuroscience community. *Annals of the New York Academy of Sciences, 1225*(Suppl. 1), E105-130. https://doi.org/10.1111/j.1749-6632.2011.05993.x

Kahle, W. (1969). *Die Entwicklung der menchlichen Grosshirnhemisphäre*. Neurology Series, Bd. 1. Berlin: Springer Verlag.

Karczmar, A. G., Nishi, S., Minota, S., Kindel, G. (1980). Electrophysiology, acetylcholine and acetylcholinesterase of immature spinal ganglia of the rabbit – an experimental study and a review. *General Pharmacology*, *11*(1), 127-134. https://doi.org/10.1016/0306-3623(80)90021-X

Karczmar, A. G., Srinivansan, R., Bernsohn, J. (1973). Cholinergic function in the developing fetus. In L. Boréus (Ed.) *Fetal pharmacology*. New York: Raven Press; 127-177.

Karnovsky, M. S., & Roots, L. (1964). A "direct coloring" thiocholine method for cholinesterases. *Journal of Histochemistry and Cytochemistry*, *12*(3), 219-221. https://doi.org/10.2478/s11686-006-0022-8

Knezović, V. (2020). Histological, MRI, and transcriptome analysis of the reorganizational processes in the developing human hippocampus (Doctoral dissertation, University of Zagreb Medical School, Zagreb, Croatia). Retrieved from: https://repozitorij.mef.unizg.hr/islandora/object/mef:2884

Kobro-Flatmoen, A., Lagartos-Donate, M. J., Aman, Y., Edison, P., Witter, M. P., & Fang, E. F. (2021). Re-emphasizing early Alzheimer's disease pathology starting in select entorhinal neurons, with a special focus on mitophagy. *Ageing Research Reviews*, *67*(5), 101307. https://doi://10.1016/j.arr.2021.101307

Köhler, C., Chan-Palay, V., Haglund, L., & Steinbusch, H. (1980). Immunohistochemical localization of serotonin terminals in lateral entorhinal cortex of the rat: demonstration of two separate patterns of innervation from the median raphe. *Anatomy & Embryology (Berlin)*, *160*(2): 121-129. https://doi.org/10.1007/BF00301855

Kondo, H., & Witter, M. P. (2014). Topographic organization of orbitofrontal projections to the parahippocampal region in rats. *The Journal of Comparative Neurology*, *522*(4), 772-793. https://doi.org/10.1002/cne.23442

Kostović, I. (1975). The correlation between distribution of synapses and Nissl-Golgi architectonics in hippocampus of 15 week human fetus. *Anatomical Record*, *181*(2), 536.

Kostović, I. (2020). The enigmatic fetal subplate compartment forms an early tangential cortical nexus and provides the framework for construction of cortical connectivity. *Progress in Neurobiology*, *194*, 101883. https://doi.org/j.pneurobio.2020.101883

Kostović, I., & Molliver, M. E. (1974). A new interpretation of the laminar development of cerebral cortex: synaptogenesis in different layers of neopallium in the human fetus. *Anatomical Record*, *178*(2), 395.

Kostović, I., & Rakic, P. (1980). Cytology and time of origin of interstitial neurons in the white matter in infant and adult human and monkey telencephalon. *Journal of Neurocytology*, *9*(2), 219-242. https://doi.org/10.1007/BF01205159

Kostović, I., Seress, L., Mrzljak, L., & Judaš, M. (1989). Early onset of synapse formation in the human hippocampus: a correlation with Nissl-Golgi architectonics in 15- and 16.5-week-old fetuses. *Neuroscience*, *30*(1), 105-116. https://doi.org/10.1016/0306-4522(89)90357-6

Kostović, I., & Rakic, P. (1990). Developmental history of the transient subplate zone in the visual and somatosensory cortex of the macaque monkey and human brain. *The Journal of Comparative Neurology*, *297*(3), 441-470. https://doi.org/10.1002/cne.902970309

Kostović, I., Judaš, M., Kostović-Knežević, Lj., Šimić, G., Delalle, I., Chudy, D., Šajin, B., & Petanjek, Z. (1991). Zagreb research collection of human brains for developmental neurobiologists and clinical neuroscientists. *International Journal of Developmental Biology*, *35*(3), 215-230.

Kostović, I., Petanjek, Z., & Judaš, M. (1993). Early areal differentiation of the human cerebral cortex: entorhinal area. *Hippocampus*, *3*(4), 447-458. https://doi.org/10.1002/hipo.450030406

Kostović, I., Sedmak, G., & Judaš, M. (2019). Neural history and neurogenesis of the human fetal and infant brain. *Neuroimage*, *188*(12), 743-773. https://doi.org/10.1016/j.neuroimage.2018.12.043

Kostović-Knežević, Lj., Kostović, I., Krmpotić-Nemanić, J., & Kelović, Z. (1979). Acetylcholinesterase (AchE) staining in the growing telencephalic structures of the human fetus. *Verhandlungen der Anatomischen Gesellschaft*, *73*, 667-669.

Krettek, J. E., & Price, J. L. (1977). Projections from the amygdaloid complex and adjacent olfactory structures to the entorhinal cortex and to the subiculum in the rat and cat. *The Journal of Comparative Neurology*, *172*(4), 723-752. https://doi.org/10.1002/cne.901720409

Krimer, L. S., Hyde, T. M., Herman, M. M., & Saunders, R. S. (1997). The entorhinal cortex: an examination of cyto- and myeloarchitectonic organization in humans. *Cerebral Cortex*, *7*(8), 722-731. https://doi.org/10.1093/cercor/7.8.722

Kropff, E., Carmichael, J. E., Moser, M. B., & Moser, E. I. (2015). Speed cells in the medial entorhinal cortex. *Nature*, *523* (7561), 419-424.

Krsnik, Ž., Majić, V., Vasung, L., Huang, H., & Kostović, I. (2017). Growth of thalamocortical fibers to the somatosensory cortex in the human fetal brain. *Frontiers in Neuroscience*, *11*, 233. https://doi.org/10.3389/fnins.2017.00233

Krušlin, B., Džombeta, T., Bezjak, M., Sedmak, G., Petanjek, Z., Šimić, G., Judaš, M., & Kostović, I. (2014). Congenital brain anomalies and chromosomal aberrations from the Zagreb Collection of the human brains. *Translational Neuroscience*, *5*(4), 293-301. https://doi.org/10.2478/s13380-014-0231-9

Leichnetz, G. R., & Astruc, J. (1976). The squirrel monkey entorhinal cortex: architecture and medial frontal afferents. *Brain Research Bulletin*, *1*(4): 351-358. https://doi.org/10.1016/0361-9230(76)90027-7

Lewis, P.R., & Schon, F. E. G. (1975). The localization of acetylcholinesterase in the locus coeruleus of the normal rat and after 6-hydroxydopamine treatment. *Journal of Anatomy*, *120*(2), 373-385.

Lindvall, O., & Björklund, A. (1974). The organization of the ascending catecholamine neuron systems in the rat brain as revealed by the glyoxylic acid fluorescence method. *Acta Physiologica Scandinavica Supplementum*, *412*: 1-48.

Liu, Y., Bergmann, T., Mori, Y., Vidal, J. M. P., Pihl, M., Vasistha, N. A., Thomsen, P. D., Seeman, S. E., Gorodkin, J., Hyttel, P., Khodosevich, K., Witter, M. P., & Hall, V. J. (2021). Development of the entorhinal cortex occurs via parallel lamination during neurogenesis. *Frontiers in Neuroanatomy*, *15*, 663667. https://doi.org/10.3389/fnana.2021.663667

Lorente de Nó, R. (1933). Studies on the structure of the cerebral cortex. I. The area entorhinalis. *The Journal of Psychology and Neurology (Leipzig)*, *45*, 381-438.

Lorente de Nó, R. (1934). Studies on the structure of the cerebral cortex. II. Continuation of the study of the Ammonic system. *The Journal of Psychology and Neurology (Leipzig)*, *46*, 113-177.

Loy, R. (1980). Development of afferent lamination in Ammon's horn of the rat. *Anatomy & Embryology (Berlin)*, *159*(5): 257-275. https://doi.org/10.1007/BF00317650

Maass, A., Berron, D., Libby, L., Ranganath, C., & Duzel, E. (2015). Functional subregions of the human entorhinal cortex. *eLife*, *4*, e06426. https://doi.org/10.7554/eLife.06426

Macchi, G. (1951). The ontogenetic development of the olfactory telencephalon in man. *The Journal of Comparative Neurology*, *95*(2), 245-305. https://doi.org/10.1002/cne.900950203

Marín, O., & Rubenstein, J. L. R. (2001). A long, remarkable journey: tangential migration in the telencephalon. *Nature Reviews Neuroscience 2*(11), 780-790. https://doi.org.10.1038/35097509

Marín, O., & Rubenstein, J. L. R. (2003). Cell migration in the forebrain. *Annual Review of Neuroscience 26*(2), 441-483. https://doi.org.10.1146/annurev.neuro.26.041002.131058

Meibach, R. C., & Weaver, L. M. (1979). Histochemical identification of acetylcholinesterase in dopaminergic nigrostriatal neurons. *Journal of Neural Transmission*, *44*(1-2), 87-96. https://doi.org/10.1007/BF01252704

Mesulam, M-M., Mufson, E. J., Wainer, B. H., & Levey, A. I. (1983). Central cholinergic pathways in the rat: an overview based on an alternative nomenclature (Ch1–Ch6). *Neuroscience*, *10*(4), 1185-1201. https://doi.org./10.1016/0306-4522(83)90108-2

Mihelčić, M., Šimić, G., Babić Leko, M., Lavrač, N., Džeroski, S., Šmuc, T. (2017). Using redescription mining to relate clinical and biological characteristics of cognitively impaired and Alzheimer's disease patients. *PLoS One*, *12*(10), e0187364. https://doi.org/10.1371/journal.pone.0187364

Mladinov, M., Sedmak, G., Fuller, H. R., Babić Leko, M., Mayer, D., Kirincich, J., Štajduhar, A., Borovečki, F., Hof, P. R., & Šimić, G. (2016). Gene expression profiling of the dorsolateral and medial orbitofrontal cortex in schizophrenia. *Translational Neuroscience*, *7*(1), 139-150. https://doi.org/10.1515/tnsci-2016-0021

Molliver, M. E., Kostović, I., & Van der Loos, H. (1973). The development of synapses in cerebral cortex of the human fetus. *Brain Research*, *50*(2), 403-407. https://doi.org/10.1016/0006-8993(73)90741-5

Muraki, K., & Tanigaki, K. (2015). Neuronal migration abnormalities and its possible implications for schizophrenia. *Frontiers in Neuroscience*, *9*(3), 74. https://doi.org/10.3389/fnins.2015.00074

Navarro Schröder, T., Haak, K. V., Zaragoza Jimenez, N. I., Beckmann, C. F., & Doeller, C. F. (2015). Functional topography of the human entorhinal cortex, *eLife*, *4*, e06738. https://doi.org/10.7554/eLife.06738

Nilssen, E.S., Jacobsen, B., Fjeld, G., Nair, R. R., Blankvoort, S., Kentros, C., & Witter, M. P. (2018). Inhibitory connectivity dominates the fan cell network in layer II of lateral entorhinal cortex. *Journal of Neuroscience*, *38*(45), 9712-9727. https://doi.org/10.1523/JNEUROSCI.1290-18.2018

Nilssen, E. S., Doan, T. P., Nigro, M. J., Ohara, S., & Witter, M. P. (2019). Neurons and networks in the entorhinal cortex: A reappraisal of the lateral and medial entorhinal subdivisions mediating parallel cortical pathways. *Hippocampus*, *29*(12), 1238-1254. https://doi.org/10.1002/hipo.23145

Nobin, A., & Björklund, A. (1973). Topography of the monoamine neuron systems in the human brain as revealed in fetuses. *Acta Physiologica Scandinavica Suppl*. *388*, 1-40.

Nowakowski, R. S., & Rakic, P. (1979). The mode of migration of neurons to the hippocampus: a Golgi and electron microscopic analysis in foetal rhesus monkey. *Journal of Neurocytology*, *8*(6), 697-718. https://doi.org/10.1007/BF01206671

Nowakowski, R. S., & Rakic, P. (1981). The place of origin and route and rate of migration of neurons to the hippocampal region of the rhesus monkey. *The Journal of Comparative Neurology*, *196*(1), 129-154. https://doi.org/10.1002/cne.901960110

Ohtake, T., & Yamada, H. (1989). Efferent connections of the nucleus reuniens and the rhomboid nucleus in the rat: an anterograde PHA-L tracing study. *Neuroscience Research*, *6*(6), 556-568. https://doi.org/10.1016/0168-0102(89)90044-8

Palmen, S. J. M. C., van Engeland, H., Hof, P. R., & Schmitz, C. (2004). Neuropathological finidings in autism. *Brain*, *127*(12), 2572-2583. https://doi.org/10.1093/brain/awh287

Pessoa, L., & Hof, P. R. (2015). From Paul Broca's great limbic lobe to the limbic system. *The Journal of Comparative Neurology*, *523*(17), 2495-2500. https://doi.org/10.1002/cne.23840

Pitkänen, A., Kelly, J. L., & Amaral, D. G. (2002). Projections from the lateral, basal, and accessory basal nuclei of the amygdala to the entorhinal cortex in the macaque monkey. *Hippocampus*, *12*(2), 186-205. https://doi.org/10.1002/hipo.1099

Polšek, D., Jagatic, T., Cepanec, M., Hof, P. R., & Šimić, G. (2011). Recent developments in neuropathology of autism spectrum disorders. *Translational Neuroscience*, *2*(3), 256-264. https://doi.org/10.2478/s13380-011-0024-3

Radoš, M., Judaš, M., & Kostović, I. (2006). *In vitro* MRI of brain development. *European Journal of Radiology*, *57*(2), 187-198. https://doi.org/10.1016/j.ejrad.2005.11.019

Raghanti, M. A., Šimić, G., Watson, S., Stimpson, C. D., Hof, P.R., Sherwood, C. C. (2011). Comparative analysis of the nucleus basalis of Meynert among primates. *Neuroscience*, *184*(6), 1-15. https://doi.org/10.1016/j.neuroscience.2011.04.008

Rakic, P. (1968). Studies of the processes of proliferation, migration, and differentiation of neuroblasts during mammalian neurogenesis. Ph.D. thesis. University of Belgrade Medical School.

Rakic, P. (1988). Specification of cerebral cortical areas. *Science*, *241*(4862), 170-176. https://doi.org/10.1126/science.3291116

Rakic, P., & Nowakowski R.S. (1981). The time of origin of neurons in the hippocampal region of the rhesus monkey. *The Journal of Comparative Neurology*, *196*(1), 99-128. https://doi.org/10.1002/cne.901960109

Ramón y Cajal, S. (1903). Studien über die Hirnrinde des Menschen, Heft 4: Die Riechrinde beim Menschen und Säugetier. Verlag von Johann Ambrosius Barth, Leipzig.

Ramón y Cajal, S. (1911). Histologie du Système Nerveux de l'Homme et des Vertebrés. Maloine, Paris. Translated from French by Swanson, N., & Swanson L.W. (1995) Oxford University Press, New York.

Ray, S., & Brecht, M. (2016). Structural development and dorsoventral maturation of the medial entorhinal cortex, *eLife, 5*, e13343. https://doi: 10.7554/eLife.13343

Ray, S., Naumann, R., Burgalossi, A., Tang, Q., Schmidt, H., & Brecht, M. (2014). Grid-layout and theta-modulation of layer 2 pyramidal neurons in medial entorhinal cortex. *Science*, *343*(6173), 891-896 https://doi: 10.1126/science.1243028

Rofsky, N. M., Lee, V. S., Laub, G., Pollack, M. A., Krinsky, G. A., Thomasson, D., Ambrosino, M. M., & Weinreb, J. C. (1999). Abdominal MRI imaging with a volumetric interpolated breath-hold examination. *Radiology*, *212*(3), 876-884. https://doi.org/10.1148/radiology.212.3.r99se34876

Rose, M. (1926). Über das histogenetische Prinzip der Einteilung der Grosshirnrinde (mit 16 Tafeln – Tafeln 7-22). *The Journal of Psychology and Neurology (Leipzig)*, *32*(3), 97-160.

Rose, M. (1927a). Der Allocortex beim Tier und Mensch. I. Teil (mit 21 Textabbildungen und 30 Doppeltafeln – Tafeln 1-30). *The Journal of Psychology and Neurology (Leipzig)*, *34*(1-2), 1-111.

Rose, M. (1927b). Die sogenannte Riechrinde beim Menschen und beim Affen. II. Teil des "Allocortex beim Tier und Mensch" (mit 13 Textabbildungen und 35 Doppeltafeln – Tafeln 42-76). *The Journal of Psychology and Neurology (Leipzig)*, *34*(6), 261-401.

Rose, M. (1935). Cytoarchitektonik und Myeloarchitektonik der Groβhirnrinde. In: Bumke, O., Foerster, O. (eds.) *Handbuch der Neurologie, Allgemeine Neurologie. 1. Anatomie*. Berlin: Springer, pp. 588-778.

Rowland, D. C., Roudi, Y., Moser, M.-B., & Moser, E. I. (2016). Ten years of grid cells. *Annual Review of Neuroscience*, *39*(7), 19-40. https://doi.org/10.1146/annurev-neuro-070815-013824

Saper, C. B., & Chelimsky, T. C. (1984). A cytoarchitectonic and histochemical study of nucleus basalis and associated cell groups in the normal human brain. *Neuroscience*, *13*(4), 1023-1037. https://doi.org/10.1016/0306-4522(84)90286-0

Sargolini, F., Fyhn, M., Hafting, T., McNaughton, B. L., Witter, M. P., Moser, M.B., & Moser, E. I. (2006). Conjunctive representation of position, direction, and velocity in entorhinal cortex. *Science*, *312*(5774), 758-762. https://doi.org/10.1126/science.1125572

Saunders, R. C., & Rosene, D. L. (1988). A comparison of the efferents of the amygdala and the hippocampal formation in the rhesus monkey: I. Convergence in the entorhinal, prorhinal, and perirhinal cortices. *The Journal of Comparative Neurology*, *271*(2), 153-184. https://doi.org/10.1002/cne.902710202

Schlessinger, A. R., Cowan, W. M., & Swanson, L. W. (1978). The time of origin of neurons in Ammon's horn and the associated retrohippocampal fields. *Anatomy & Embryology (Berlin)*, *154*(2): 153-173. https://doi.org/10.1007/BF00304660

Sgonina, K. (1938). Vergleichende Anatomie der Entorhinal- und Präsubikular region. *The Journal of Psychology and Neurology (Leipzig)*, *48*, 56-163.

Shatz, C. (1992). How are specific connections formed between thalamus and cortex? *Current Opinion in Neurobiology*, 2(*1*), 78-82. https://doi.org/10.1016/0959-4388(92)90166-i

Shi, C. J., & Cassell, M. D. (1999). Perirhinal cortex projections to the amygdaloid complex and hippocampal formation in the rat. *The Journal of Comparative Neurology*, *406*(3), 299-328. https://doi.org/10.1002/(sici)1096-9861(19990412)406:3<299::aid-cne2>3.0.co;2-9

Silver, A. (1974). *The biology of cholinesterases*. Amsterdam: North-Holland Publication Corporation.

Solstad, T., Boccara, C. N., Kropff, E., Moser, M. B., & Moser, E. I. (2008). Representation of geometric borders in the entorhinal cortex. *Science*, *322*(5909), 1865-1868. https://doi.org/10.1126/science.1166466

Suzuki, W. A., & Amaral, D. G. (1994). Topographic organization of the reciprocal connection between the monkey entorhinal cortex and the perirhinal and parahippocampal cortices. *Journal of Neuroscience*, *14*(3), 1856-1877. https://doi.org/10.1523/JNEUROSCI.14-03-01856.1994

Šimić, G., Babić, M., Borovečki, F., & Hof, P. R. (2014). Early failure of the default-mode network and the pathogenesis of Alzheimer's disease. *CNS Neuroscience & Therapy*, *20*(7), 692-698. https://doi.org/10.1111/cns.12260

Šimić, G., Babić-Leko, M., Wray, S., Harrington, C. R., Delalle, I., Jovanov-Milošević, N., Bažadona, D., Buée, L., de Silva, R., Di Giovanni, G., Wischik, C. M., & Hof, P. R. (2016). Tau protein hyperphosphorylation and aggregation in Alzheimer's disease and other tauopathies, and possible neuroprotective strategies. *Biomolecules*, *6*(1), 6. https://doi.org/10.3390/biom6010006

Šimić, G., Babić-Leko, M., Wray, S., Harrington, C. R., Delalle, I., Jovanov-Milošević, N., Bažadona, D., Buée, L., de Silva, R., Di Giovanni, G., Wischik, C. M., & Hof, P. R. (2017). Monoaminergic pathology in Alzheimer's disease. *Progress in Neurobiology*, *151*(4), 101-138. https://doi.org/10.1016/j.pneurobio.2016.04.001

Šimić, G., Bexheti, S., Kelović, Z., Kos, M., Grbić, K., Hof, P.R., & Kostović, I. (2005). Hemispheric asymmetry, modular variability and age-related changes in the human entorhinal cortex. *Neuroscience*, *130*(4), 911-925. https://doi.org.10.1016/j.neuroscience.2004.09.040

Šimić, G., & Hof, P. R. (2015). In search of the definitive Brodmann's map of cortical areas in human. *The Journal of Comparative Neurology*, *523*(1), 5-14. https://doi.org/10.1002/cne.23636

Šimić, G., Lucassen, P. J., Krsnik, Ž., Krušlin, B., Kostović, I., Winblad, B., Bogdanović, N. (2000). nNOS expression in reactive astrocytes correlates with increased cell death-related DNA damage in the hippocampus and entorhinal cortex in Alzheimer's disease. *Experimental Neurology*, *165*(1), 12-26. https://10.1006/exnr.2000.7448

Šimić, G., Mrzljak, L., Fučić, A., Winblad, B., Lovrić, H., & Kostović, I. (1999). Nucleus subputaminalis (Ayala): the still disregarded magnocellular component of the basal forebrain may be human specific and connected with the cortical speech area. *Neuroscience*, *89*(1), 73-89. https://doi.org/10.1016/s0306-4522(98)00304-2

Šimić, G., Stanić, G., Mladinov, M., Jovanov-Milošević, N., Kostović, I., & Hof, P. R. (2009). Does Alzheimer's disease begin in the brainstem? *Neuropathology Applied Neurobiology*, *35*(6), 532-554. https://doi.org/10.1111/j.1365-2990.2009.01038.x

Šimić, G., Španić, E., Langer Horvat L., & Hof, P.R. (2019). Blood-brain barrier and innate immunity in the pathogenesis of Alzheimer's disease. *Progress in Molecular Biology and Translational Science*, *168*, 99-145. https://10.1016/bs.pmbts.2019.06.003

Šimić, G., Tkalčić, M., Vukić, V., Mulc, D., Španić, E., Šagud, M., Olucha-Bordonau, F. E., Vukšić, M., Hof, P. R. (2021). Understanding emotions: origins and roles of the amygdala. *Biomolecules*, *11*(6), 823. https://doi.org/biom11060823

Šimić, G., Vukić, V., Kopić, J., Krsnik, Ž., & Hof, P.R. (2020). Molecules, mechanisms, and disorders of self-domestication: keys for understanding emotional and social communication from an evolutionary perspective. *Biomolecules*, *11*(1), 2. https://doi.org/10.3390/biom11010002

Šimić, G., Winblad, B., Kostović, I., & Bogdanović, N. (1997). Volume and number of neurons of the human hippocampal formation in normal aging and Alzheimer's disease. *The Journal of Comparative Neurology*, *379*(4), 482-494. https://doi.org/10.1002/(sici)1096-9861(19970324)379:4<482::aid-cne2>3.0co;2-z

Španić, E., Langer Horvat, L., Hof, P. R., & Šimić, G. (2019). Role of microglial cells in Alzheimer's disease tau propagation. *Frontiers in Aging Neuroscience*, *11*(4), 271. https://doi.org/10.3389/fnagi.2019.00271

Špeljko, T., Jutrić, D., & Šimić, G. (2011). HSV in Alzheimer's disease: myth or reality? *Translational Neuroscience*, *2*(1), 61-68. https://doi.org/10.2478/s13380-011-0009-2

Slotkin, T. A., Ryde, I. T., Wrench, N., Card, J.A., Seidler, F. J. (2009). Nonenzymatic role of acetylcholinesterase in neuritic sprouting: regional changes in acetylcholinesterase and choline acetyltransferase after neonatal 6-hydroxydopamine lesions. *Neurotoxicology and Teratology*, *31*(3), 183-186. https://doi.org/10.1016/j.ntt.2008.12.007

Solodkin, A., & Van Hoesen, G. W. (1996). Entorhinal cortex modules of the human brain. *The Journal of Comparative Neurology*, *365*(4), 610-627. https://doi.org/10.1002/(SICI)1096-9861(19960219)365:4<610::AID-CNE8>3.0.CO;2-7

Stephan, H. (1975). Allocortex. In: Bargmann, W. (ed.) *Handbuch der mikroskopischen Anatomie des Menschen*. 4. Band, 9. Teil. Berlin-Heidelberg-New York: Springer.

Swanson, L. W., Wyss, J. M., Cowan, W. M. (1978). An autoradiographic study of the organization of intrahippocampal association pathways in the rat. *The Journal of Comparative Neurology*, *181*(4), 681-716. https://doi.org/10.1002/cne.901810402

Tago, H., Kimura, H., & Maeda, T. (1986). Visualization of detailed acetylcholinesterase fiber and neuron staining in rat by a sensitive histochemical procedure. *Journal of Histochemistry and Cytochemistry*, *34*(11), 1431-1438. https://doi.org/10.1177/34.11.2430009

Van Hoesen, G. W., & Pandya, D. N. (1975). Some connections of the entorhinal area (area 28) and perirhinal (area 35) cortices of the rhesus monkey. I. Temporal lobe afferents. *Brain Research*, *95*(1), 1-24. https://doi.org/10.1016/0006-8993(75)90204-8

Van Hoesen, G. W., Pandya, D. N., & Butters, N. (1975). Some connections of the entorhinal (area 28) and perirhinal (area 35) cortices of the rhesus monkey. II. Frontal lobe afferents. *Brain Research*, *95*(1), 25-38. https://doi.org/10.1016/0006-8993(75)90205-X

Van Strien, N. M., Cappaert, N. L. M., & Witter, M. P. (2009). The anatomy of memory: an interactive overview of the parahippocampal-hippocampal network. *Nature Reviews Neuroscience*, *10*(4), 272-282. https://doi.org/10.1038/nrn2614
Vasung, L., Huang, H., Jovanov-Milošević, N., Pletikos, M., Mori, S., & Kostović, I. (2010). Development of axonal pathways in the human fetal fronto-limbic brain: histochemical characterization and diffusion tensor imaging. *Journal of Anatomy*, *217*(4), 400-417. https://doi.org/10.1111/j.1469-7580.2010.01260.x

Vertes, R. P., Hoover, W. B., Do Valle, A. C., Sherman, A., & Rodrigues, J. J. (2006). Efferent projections of reuniens and rhomboid nuclei of the thalamus in the rat. *The Journal of Comparative Neurology*, *499*(5), 768-796. https://doi.org/10.1002/cne.21135

Vogt, C., & Vogt, O. (1919). Allgemeinere Ergebnisse unserer Hirnforschung. *The Journal of Psychology and Neurology (Leipzig)*, *25*, 279-462.

Von Economo, C., & Koskinas, G. N. (1925). *Die Cytoarchitektonik der Hirnrinde des erwachsenen Menschen*. Wien: Springer.

Wahlstrom, K. L., Huff, M. L., Emmons, E. B., Freeman, J. H., Narayanan, N. S., McIntyre, C. K., LaLumiere, R. T. (2018). Basolateral amygdala inputs to the medial entorhinal cortex selectively modulate the consolidation of spatial and contextual learning. *Journal of Neuroscience*, *38*(11), 2698-2712. https://doi.org/10.1523/JNEUROSCI.2848-17.2018

Wiesel, T. N., Hubel, D. H., & Lam, D. M. (1974). Autoradiographic demonstration of ocular-dominance columns in the monkey striate cortex by means of transneuronal transport. *Brain Research*, *79*(2), 273-279. https://doi.org/10.1016/0006-8993(74)90416-8

Wise, S. P., & Jones, E. G. (1978). Developmental studies of thalamocortical and commissural connections in the rat somatic sensory cortex. *The Journal of Comparative Neurology*, *178*(2), 187-208. https://doi.org/10.1002/cne.901780202

Witter, M. P., Wouterlood, F. G., Naber, P. A., & Van Haeften, T. (2000). Anatomical organization of the parahippocampal-hippocampal network. *Annals of the New York Academy of Sciences*, *911*(6), 1-24. https://doi.org/10.1111/J.1749-6632.2000.Tb06716.X

Witter, M. P., Doan, T. P., Jacobsen, B., Nilssen, E. S., & Ohara, S. (2017). Architecture of the entorhinal cortex. A review of entorhinal anatomy in rodents with some comparative notes. *Frontiers in Systems Neuroscience*, *11*(6), 46. https://doi.org/10.3389/fnsys.2017.00046

Witter, M. P., & Amaral, D. G. (2021). The entorhinal cortex of the monkey: VI. Organization of projections from the hippocampus, subiculum, presubiculum, and parasubiculum. *The Journal of Comparative Neurology*, *529*(4), 828-852. https://doi.org/10.1002/cne.24983

Wouterlood, F. G., Saldana, E., & Witter, M. P. (1990). Projection from the nucleus reuniens thalami to the hippocampal region: light and electron microscopic tracing study in the rat with the anterograde tracer *Phaseolus vulgaris*-leucoagglutinin. *The Journal of Comparative Neurology*, *296*(2), 179-203. https://doi.org/10.1002/cne/902960202

Zimmer, J., & Haug, F. M. (1978). Laminar differentiation of the hippocampus, fascia dentata and subiculum in developing rats, observed with the Timm sulphide silver method. *The Journal of Comparative Neurology*, *179*(3), 581-617. https://doi.org/10.1002/cne.901790309

Žunić Išasegi, I., Radoš, M., Krsnik, Ž., Radoš, M., Benjak, V., & Kostović, I. (2018). Interactive histogenesis of axonal strata and proliferative zones in the human fetal cerebral wall. *Brain Structure & Function*, *223*(9), 3919-3943. https://doi.org/10.1007/s00429-018-1721-2

Table 1. Differences in the terminology of the laminar division of the EC among different authors.

Authors	Layers							Species
Ramón y Cajal (1903, 1911)	I plexiform	II stellate neurons	III pyramidal neurons	IV deep plexiform	V horizontal spindle cells	VI small pyramidal cells with recurrent axon	VII polymorphic and spindle cells	rodents, cats, human
Brodmann (1909)	I molecular	II external granular	III pyramidal	IV internal granular	V ganglionic		VI polymorphic	human
Rose (1927a,b, 1935)	I lamina zonalis	lamina principalis externa		LD	lamina principalis interna			mouse
von Economo and Koskinas (1925)	I molecular	II	III pyramidal (IIIa and IIIb in the area HA)	V (IV)	V ganglionic		VIa and VIb spindle cells	human
Lorente de Nó (1933, 1934)	I plexiform	II stellate neurons	III superficial pyramidal (+IIIa = LD)		IV (+IVa) deep pyramidal	V small pyramidal cells with recurrent axon	VI polymorphic cells	rodents, macaque monkeys
Blackstad (1956)	I lamina zonalis	II-III		IV				rat
Van Hoesen and Pandya (1975)	I outer plexiform zone	II large stellate cells	III mid-sized pyramidal cells	IV inner plexiform layer / LD	V small pyramidal cells and horizontal cells		VI multilaminar layer of polymorphic and spindle cells	primates
Stephan (1975)	1. stratum moleculare	2. stratum stellare	3. stratum pyramidale	3a. substratum dissecans	4. (4a) stratum magnocellulare	5. stratum parvocellulare	6. stratum multiforme	rodents, non-human primates, human
Braak (1972) Braak & Braak, 1992)	I molecular	external principal stratum subdivided into pre-α (II), and pre-β and pre-γ (III)		IV LD	internal principal stratum subdivided into pre-α (V) and pre-β and pre-γ (VI)		lamina cellularis profunda (within the underlying wm)	human
Amaral and Insausti (1990)	I	II	III	IV	V	VI		human

Abbreviations: LD, lamina dissecans; wm, white matter.

Table 2. Summary of the human fetal brains analyzed.

Cases	Age w.g./y	CRL (mm)	Nissl stain	AChE stain	Immuno-histochemistry	3 T MRI
F43	9	42	+			
F96	9	43	+			
F95	10	50	+			
F43	12	80	+			
F60	15	110	+			
F134	15.5	120	+			+
F125	17	120	+			
F627	20	170	+		MBP, SMI-312, NeuN, synaptophysin	+
F86	21	195	+			
F163	22	200	+			
F181	22	200	+	+		
F32	22	200	+			
F177	23	220	+	+		
F180	25.5	245	+	+		+
F182	28	270	+	+		
F205	30	late abortion	+			
F194	30	late abortion	+			
F209	33	late abortion 300 mm	+			
F207	36	late abortion	+			
F587	40	newborn	+	+	MBP, SMI-312	+
O34	26 y	adult	+	+		
O20	27 y	adult	+	+		

AChE, acetylcholinesterase; CRL, crown-rump length; MBP, myelin basic protein; MRI, magnetic resonance imaging; NeuN, neuronal nuclear antigen; SMI-312, a cocktail of monoclonal antibodies that react against all axons; w.g., weeks of gestation (w.g. - 2 weeks = postconceptional weeks, PCW).

Table 3. Light microscopy criteria to assess stages of cell differentiation (SD1-7) in Nissl-stained sections according to Rakic (1968).

Stage	Short description	Nucleus	Cytoplasm
SD1	Undifferentiated germ cells with a round shape	- very dark - granular basophilic chromatin	- not noticeable
SD2	Stage of chromatin segregation	- becomes larger and lighter in color than in the previous stage - the chromatin clusters in the form of 4-5 basophilic granules	- not yet pronounced
SD3	Stage of young neuroblast	- basophilic chromatin almost completely disappears (its remnant can only be seen on the periphery of the nucleus) - spongioblasts (the neuroglia precursor cells) cannot be differentiated from neuroblasts (the neural stem cells)	- unstained and yet not visible
SD4	Neuroblast stage with cytoplasmic crescent	- crescent-shaped part of the cytoplasm is at first seen on one half of the nucleus and then encompasses the whole nucleus - spongioblasts can be distinguished from neuroblasts	- a narrow, discrete crescent-shaped part of the cytoplasm appears
SD5	Early neuron stage	- both nucleus and cytoplasm increase in size - this is a transitional stage between a neuroblast and a mature neuron	- Nissl substance appears in the cytoplasm in the form of finely dispersed granules
SD6	Stage of partially mature neuron	- nucleus further increases in size, but its volume grows slower than the volume of the cytoplasm (the nucleocytoplasmic ratio changes in favor of the cytoplasm)	- the granules of Nissl's substance are larger and more noticeable - an axon hillock can be recognized
SD7	Stage of a fully differentiated neuron	- no significant qualitative change in comparison to the previous stage, only a quantitative increase in nucleus volume - neurons differ only quantitatively	- the volume of the cytoplasm still grows faster than the volume of the nucleus

Table 4. Summary of the major events in human EC prenatal development and their potential functional relevance. The last column describes the main events of hippocampal development in the same period.

Time of occurrence (w.g.)	Short description of the main events in the EC development	Potential functional relevance	Short description of the main events in the hippocampal development
10-13	The earliest cytoarchitectural differentiation of the EC and the appearance of the superficial magnocellular layer in the MZ, followed by the early condensation of the EC CP and simultaneous delamination of its deep part. The unique features of this process in the EC are the precocious onset of fiber in-growth into the CP, the incomplete spread of the CP, and the paucity of thalamocortical fibers.	The precocious lamination of the CP may be the crucial event in the histogenesis of the human EC, as this is the first pallial region that has the typical CP to differentiate. This may also explain the poor development of the SP and the paucity of thalamocortical fibers in the EC. This is also probably the first period highly vulnerable to (mostly environmental) genotoxic agents.	In this early fetal phase the hippocampus is characterized by about fifteen rows of dark densely packed VZ cells, absence of SVZ, IZ flooded with radially migrating neurons, scattered cells in the CP, and enlarged MZ. The rostral (septal) part of the hippocampus is still at the same level of development as the caudal part in the temporal lobe, the prospective retrocommissural hippocampus. The fimbria is present and in continuation with the primordial DG. As hippocampal neurons are still migrating toward CP, mature fimbria axons are likely either afferents from the septum, the monoaminergic fibers from the brainstem, or projections from the supramammillary nucleus of the hypothalamus (Knezović, 2020).
14-16	The appearance of the superficial LD and concurrent separation of the LPE in the rostral parts of the EC into islands of stellate cells, followed by the emergence of the deep LD in the LPI. In-growth of afferent fibers from the hippocampus (14 w.g.) and amygdala (16 w.g.).	The early differentiation of the large stellate cells ("promoter neurons") is important as they provide signals for sequential maturation of the intrinsic entorhino-hippocampal network (Donato et al., 2017), in concert with the in-growth of afferents from the hippocampus and amygdala in this period.	This stage is characterized by the early onset of synapse formation in the MZ and SP, which contain dendritic branches of pyramidal and large non-pyramidal neurons, with a much higher density of synapses in the MZ than in the SP, in contrast to the neocortex (Kostović et al., 1989). Accordingly, at this stage the MZ becomes rich in extracellular matrix molecules and characteristically enlarged, making about half of the thickness of the hippocampal wall, and is composed of five layers: 1. cell-poor marginal stripe (*Randstreifen*), 2. SGL, 3. MZ proper, 4. stratum lucidum, and 5. deep granular layer.
20	The penetration of the main (temporoammonic) branch of the PP into the subiculum by the 20th w.g., and its perforation of the hippocampal sulcus 2-3 weeks later. MBP-expressing oligodendrocytes first appear in the fimbria. NeuN immunoreactivity is most pronounced in the layer II cell islands. Inside-out migration and	The perforant path provides a connectional route from the EC to all fields of the hippocampal formation, including the DG, all CA fields (including CA1), and the subiculum. Cytoarchitecturally, for the first time, the EC	Compared to the periallocortex, the hippocampus has a much thicker MZ and thinner and loose CP. The DG primordium has developed into three conspicuous layers: molecular, dentate granule cells, and polymorphic layers. The layer of dentate granule cells is no longer in continuation with the Ammon's horn: the supra- and infrapyramidal parts of DG CP can be distinguished. The suprapyramidal blade and its synapses appear a week before

	differentiation gradients are seen in both the upper (LPE) and the lower (LPI) pyramidal layers, where less differentiated cells are found in the more superficial portions in each of these compartments.	adopts an adult-like organization.	infrapyramidal (20 w.g. vs 21 w.g.), both in an order inverse to that of the neocortex and Ammon's horn, which is in an outside-in manner (Knezović, 2020).
22-23	First in-growth of the AChE-positive fibers in the form of longitudinal strips in layers I and II. MBP-expressing myelin patches are present in the alveus.	The onset of the modular organization of the EC circuits.	A thin SP develops at 22 w.g. Synapses are present in all three DG layers. While both proliferative zones of the neocortex (VZ and SVZ) are still thick, in the hippocampus only a very thin VZ is present.
40	Patchy myelination of the PP. Based on MAP2 and NeuN immunoreactivity the EC neurons are more mature in their appearance, although there are still significant differences in their size: LPI consists of smaller neurons, with NeuN labeling being more pronounced in the deeper parts of the LPI, with few cells expressing MAP2 (Knezović, 2020). In addition to neurons, LPI is rich in dendrites and in-growing axons from the cerebral cortex as well as with efferent fibers. The LPE consists of large pyramidal neurons with long apical dendrites extending to the entorhinal islands and MZ. Towards pia, the size of pyramidal neurons decreases, and only a few are MAP2-immunoreactive (Knezović, 2020). EC islands are well-developed, with large NeuN-labeled nuclei in island neurons, while rare MAP2-expressing cells are seen in between. Small calretinin-expressing neurons are seen throughout the CP. A strong calretinin immunoreactivity is present in the MZ above islands, diminishing between the islands and spreading along the more superficial layer of pyramidal neurons. The MZ consists of the subpial granular layer with fewer cells than in previous stages, the MZ proper with CRC, and the fiber-abundant stratum lucidum.	Beginning of the establishment of functional entorhino-hippocampal circuits.	MBP-expressing and Gallyas-positive oligodendrocytes can be seen only in the region of the alveus (stratum oriens) and fimbria. The hippocampus is significantly larger, especially the head and uncus. The hippocampal fissure is deeper. VZ is extremely compact and forms a single layer of packed cells. The alveus takes an adult appearance. The pyramidal layer of CA3 and CA2 loses the superficial layer of immature cells, which are replaced by large pyramidal cells, whereas such small immature neurons with dark round nuclei are still present in the CA1 (Knezović, 2020). AChE reactivity is most pronounced in the stratum radiatum of CA3 and CA2 and is not that abundant in the CA1. Growth of the mossy fibers from granule cells of the DG can be tracked by MAP1b and NF200 immunoreactivity from 27 w.g. onwards (Knezović, 2020). The DG shape becomes more jagged.

	Synaptophysin is present in all layers except VZ and SVZ.		

Figure legends

Figure 1. Localization of the EC in humans (a-c) and rhesus monkeys (d). (a) Inferior view and (b) medial view of the EC subdivided into the three 'H' fields. (c) Divisions of the human EC into seven cytoarchitectural subfields. (d) Divisions of the EC in the rhesus monkey. OA, occipital lobe, area A; ots, occipitotemporal sulcus; pam, periamygdaloid cortex; ppc, prepiriform cortex; pr, prorhinal cortex; rs, rhinal sulcus. Scale bars: 2 mm.

Figure 2. Seven stages of neuronal differentiation in the EC as seen in Nissl-stained sections. (a) Most cells in the germinative layer (VZ and SVZ) are in SD1, some in SD2, and only rare in its upper part in SD3. (b) During radial migration through the IZ, many cells differentiate from SD2 into SD3. (c) In SD5 neurons begin to display regional and individual morphological differences in size, shape, and distribution of Nissl substance. (d) Stages SD5-SD7. Numbers represent stages of differentiation. See Table 2 for a more detailed description of each stage. IZ, intermediate zone; SD, stage of differentiation; SVZ, subventricular zone; VZ, ventricular zone. Scale bars: 20 µm.

Figure 3. The rostral part of the EC at 10 w.g. (CRL = 50 mm). (a) Borders of the EC are labeled with black arrows. Both the medial and lateral borders of the EC are defined by the presence of the superficial magnocellular layer of cells. The delamination of the deep CP (thick white arrow) can be seen progressing from the lateral to the medial part of the EC. Note that the superficial magnocellular zone (white notched arrow) is present in between the MZ and the CP along the whole width of the EC. (b) Superficial magnocellular zone (in between black arrows) between the MZ and the CP at higher magnification. (c) The superficial part of the CP in the rostral EC is compact, whereas the deep part of the CP is delaminated and appears stratified (white arrows). ACx, archicortex (archipallium); CP, cortical plate; IZ, intermediate zone; MZ, marginal zone; Neo, temporal neopallium. Scale bars: 1 mm (a), 100 µm (b, c).

Figure 4. Nissl staining of the EC at 12 w.g. (CRL = 80 mm). (a) Rostral part. Borders of EC with PAM and Neo are marked with black arrows. (b) Caudal part. Borders of the EC with the ACx and Neo are labeled with black arrows. Note delamination, or more stratified appearance, of the deep parts of the CP in the EC (white arrow). (c) The superficial part of the CP is compact, whereas the deep part of the CP is delaminated (white arrows). Note that the superficial magnocellular zone is missing. The seemingly smaller size of the EC in comparison to Figure 3 (EC at 10 w.g.) stems from the fact that this figure is composed of sections from the rostral tip of the EC, whereas Figure 3 contains sections from a more posterior level where the width of the EC is greater. ACx, archipallium (archicortex); CP, cortical plate; IZ, intermediate zone; MZ, marginal zone; Neo, temporal neopallium; PAM, periamygdaloid area; SVZ, subventricular zone, VZ, ventricular zone. Scale bars: 1 mm (a, b), 100 µm (c).

Figure 5. Nissl staining of the rostral part of the EC at 15 w.g. (CRL = 110 mm). (a) Borders of the EC with PAM and Neo are labeled with black arrows. The lateral border of the EC is determined by the disappearance of the superficial LD (dis 1). (b) Cytoarchitectural regions of the rostral EC: rostromedial (RM) and caudolateral (CL). The lateral border of the rostromedial EC region is determined by the

disappearance of the superficial part of the LPE (LPEs). The lateral border of the caudolateral part of the EC is determined by the disappearance of the LD (superficial LD, dis1). Borders are marked by black arrows. (c) Some islands of vertical cellular zones of the LPE are marked with black arrows. CL, caudolateral EC; dis 1, superficial LD; EC, entorhinal cortex; IZ, intermediate zone; LD, lamina dissecans; LPEd, lamina principalis externa - deep part; LPEs, lamina principalis externa – superficial part; LPI, lamina principalis interna; Neo, temporal neopallium; PAM, periamygdaloid area; RM, rostromedial EC. Scale bars: 1 mm.

Figure 6. Caudal part of the EC at 15-15.5 w.g. (CRL = 110-120 mm). (a) The borders of the EC with Neo and PaS are marked with thick black arrows. Note the compact cortical plate of EC and the very thin superficial LD (dis 1). (b) The border between the caudolateral and caudomedial EC is marked with a thin black arrow. Note that the CL part of EC contains one LD (dis 1), whereas the caudomedial part of the EC contains two LD (dis 1 + dis 2). (c) Note two LD in the EC – the superficial (dis 1) and the deep one (dis 2), where the deep LD (dis 2) continues into PaS. LPE, lamina principalis externa; LPI, lamina principalis interna; MZ, marginal zone; Neo, temporal neopallium; PaS, parasubiculum. Scale bars: 1 mm (a, b), 100 μm (c).

Figure 7. Rostral part of the EC at 15-15.5 w.g. (CRL = 110-120 mm). (a) The first appearance of the superficial LD (dis 1), which divides two main layers of the CP: LPE and LPI. Note that rostral EC is near the PAM. (b) The LPE at higher magnification. Vertical cellular zones in the superficial part of LPE (LPEs) are marked with arrows. (c) The LPE is made of highly differentiated cells (SD5) – marked with arrows, and small, undifferentiated cells (SD1-2). The LPEd is made of undifferentiated cells only. (d) Vertical cellular zones of the LPE, marked with arrows. (e) Vertical cellular zones of the LPE near the PAM, marked with arrows. IZ, intermediate zone; LPE, lamina principalis externa; LPEd, LPE – deep part , LPEs, LPE – superficial part; LPI, lamina principalis interna; PAM, periamygdaloid area; MZ, marginal zone. Scale bars: 100 μm.

Figure 8. Rostral EC at 17 w.g. (CRL = 120 mm). (a) Vertical cellular zones (islands) of the LPE are marked with triangular black arrows. (b) The superficial LD separates LPE from LPI. The LPE consists of a narrow, superficial cellular layer (thin red arrow) and a wider, deep cellular layer (thick red arrow). Both layers are organized into cellular islands. (c) Caudally from the section in (b), the LPE in the rostral EC still consists of a narrow, superficial cellular layer (thin red arrow) and a wider, deep cellular layer (thick red arrow), but is more continuous (fewer cell islands are seen). (d) The vertical, cell-dense zones (islands) of the LPE are indicated by white arrows. The thick red arrow shows the deep cellular layer of LPE, the thin red arrow shows the superficial (magnocellular) layer of the LPE. dis1, superficial LD; EC, entorhinal cortex; LPE, lamina principalis externa; LPI, lamina principalis interna; MZ, marginal zone; Neo, temporal neopallium; PAM, periamygdaloid area. Scale bars: 1 mm (a, b, c), 100 μm (d).

Figure 9. Rostral EC at 17 w.g. (CRL = 120 mm). (a) The vertical, cell-dense zones (islands) of the LPEd are indicated by white arrows. The horizontal red arrow indicates SGL. (b) Higher magnification of the islands of the superficial and deep cellular zones of the LPE from (a). The large, differentiated polymorphic

neurons (SD5) of the islands of the LPEs are indicated by arrows. Note that all cells in islands of the LPEd still have a low degree of differentiation (SD1-2). (c) In the caudal part of the EC at 17 w.g. the superficial and deep cellular zones of the LPE merge into a single layer. dis1, superficial LD; LPE, lamina principalis externa; LPEd, lamina principalis externa – deep part; LPEs, lamina principalis externa – superficial part; LPI, lamina principalis interna; MZ, marginal zone; SGL, subpial granular layer. Scale bars: 100 μm (a, b), 1 mm (c).

Figure 10. Visualization of the EC fiber pathways using the SMI-312 antibody at 20 w.g. (a) Low-power magnification microphotograph of the EC and hippocampal formation (the exact age is 19 w.g. + 5 d, which is 17 + 5 d PCW). The regions marked by rectangles in A represent the three enlarged insets in (b), (c), and (d). Panels (b) and (c) show the temporoammonic (temporodentate) branch of the PP as the main branch (asterisk). The asterisk indicates the place where the PP separates from the angular bundle and penetrates the CP of the subiculum. The temporoammonic branch of the PP targets the subiculum and CA1, but also travels through the stratum lacunosum-moleculare of CA2 and CA3 to reach the DG without piercing the hippocampal sulcus. The crossed temporoammonic pathway is marked with an arrowhead. These slanted fibers are visualized in a discontinuous manner due to their oblique orientation on this coronal section while traveling towards the fimbria. Later, they will cross sides within the commissure of the fornix. The well-developed AP is marked with a triangle. On (c), the angular bundle (below the asterisk) shows highly mixed fiber orientations in all directions, making it impossible to visualize continuous PP fibers from the EC layer II cells to the granule cells of the DG. (d) The temporoammonic (temporodentate) branch of the PP reaches the DG: in-growing PP fibers are just about to enter into the outer two-thirds of the molecular layer of the DG (small arrows). Note that the obliterated hippocampal sulcus is not yet penetrated by PP fibers, also seen in (b) and (c). ab, angular bundle; AP, alvear pathway; DG, dentate gyrus; PP, perforant pathway. Scale bars: 2.5 mm (a), 1 mm (b), 500 μm (c, d).

Figure 11. Visualization of the EC fiber pathways using the SMI-312 antibody at 23 w.g. + 3 days (21 PCW + 3 d). (a) Low-power magnification microphotograph of the coronal section of the human fetal brain. (b) Higher power magnification of the inset from (a). A triangle marks the place where axons of the PP perforate through the hippocampal sulcus (marked by a dashed line) and thus are directly approaching apical dendrites of the granule cells in the DG. (c) and (d) Higher power magnification of the upper and lower inset from (b), respectively. Arrows mark axons of the PP. DG, dentate gyrus; PP, perforant pathway. Scale bars: 5 mm (a), 1 mm (b), 50 μm (c), 250 μm (d).

Figure 12. Fetal EC at 20 w.g. (19 weeks + 5 days). (a) Nissl stain. The CP of the EC consists of a recognizable LPE with entorhinal islands. Below the LPE is the LD, and further the LPI. (b) Synaptophysin-immunoreactivity shows that synaptogenesis is most intense in the MZ and is positive throughout the thickness of the MZ, LD, and SP. At this stage, only the upper parts of EC islands are immunoreactive for synaptophysin. (c) NeuN immunohistochemistry shows the laminar organization of postmitotic neurons in the EC layers. NeuN-immunoreactivity is most pronounced in the layer II cell islands. Inside-out migration and differentiation gradients are seen in both the upper (LPE) and the lower (LPI) pyramidal layers as well as in layer II, where less differentiated cells are found in the more superficial portions in each of these compartments. The EC adopts for the first time an adult-like cytoarchitectural organization. (d) Postmortem MRI image of the rostral EC and hippocampus at 3 T. The thin VZ of the archicortex is not visible, but it is possible to recognize the superficial LD (dis 1, arrowhead). The intermediate zone, the

alveus, the stratum oriens, and the SP are seen as hypointense layers whose density is similar to the SP in the neocortex. The CP of the hippocampus appears as a hyperintense band ending in the dentate gyrus. CP, cortical plate; HIPP, hippocampus; LPE, lamina principalis externa; LPI, lamina principalis interna; MZ, marginal zone; SP, subplate zone. Scale bars: 200 μm.

Figure 13. The rostral part of the EC near the PAM at 22 w.g. (CRL = 200 mm). (a) The vertical cellular zones of the LPE are indicated by arrows. (b) Between the vertical cellular zones of the LPE indicated by arrows are the acellular zones that extend to different depths of the LPE. dis1, superficial lamina dissecans; LPE, lamina principalis externa; LPI, lamina principalis interna; MZ, marginal zone. Scale bars = 1 mm.

Figure 14. The rostral (a and b) part of the EC at high magnification and the caudal (c and d) part of the EC at low magnification at 22 w.g. (CRL = 200 mm). (a) The SGL of the EC is a part of the MZ and contains cells at a low degree of differentiation. The vertical cellular zones consist of islands of cells in the superficial cellular zone, the prospective layer II and vertical groups of cells in the superficial part of the deep cellular zone of the LPE (the future layer III). Between the vertical cellular zones are acellular zones (marked with asterisks), which represent afferent fiber bundles. The SGL is indicated by the hollow white arrow. (b) Two types of cells can be seen in the islands of the superficial cellular zone of the LPE: large differentiated cells (SD5) marked with arrows, and small, dark, undifferentiated cells (SD1-2). In the superficial parts of the vertical cellular zones of the prospective layer III, small undifferentiated cells (SD1-2) predominate. (c) Note the presence of two LD in the caudal part of EC. The vertical cellular zones of the LPE are indicated by arrows. (d) Note the disappearance of islands of cells of the superficial cellular zone of the LPE in the HB_1 subarea in the caudal EC. dis 1, superficial lamina dissecans; dis 2, deep lamina dissecans; HB, area parauncinata; HC, area rhinalis limitans; MZ, marginal zone; SGL, subpial granular layer. Scale bars: 100 μm (a, b), 1 mm (c, d).

Figure 15. Horizontal sections of the rostral part of the EC at 33 w.g. (CRL = 300 mm). (a) Horizontal section at low magnification reveals that the islands of the superficial LPE are composed of longitudinal strips of cells (cell zones) that are stretched predominantly in the rostrocaudal direction and separated by longitudinal acellular zones. (b) A horizontal section of the rostral part of the EC at higher magnification reveals that the longitudinal strips of cells (cell zones) anastomose with each other. Scale bars: 1 mm.

Figure 16. EC at 22 w.g. (CRL = 200 mm). AChE histochemistry. The boundary between the Neo and the EC is marked with the arrow. The AChE-positive reaction in the MZ and IZ zones is lost at the border of the temporal neopallium with the EC. CE, external capsule; CP, cortical plate; IZ, intermediate zone; MZ, marginal zone; Neo, temporal neopallium; OF, outer fiber zone of SVZ; SP, subplate zone; SVZ, subventricular zone.

Figure 17. EC at 23 w.g. (CRL = 220). (a) Coronal section through the rostral part of the EC. (b) Frontal section through the central part of the EC, caudal to (a). Cytoarchitectural subareas are marked with black

arrows. (c) The rostral part of the EC. Within the LPE, three layers of the EC can be distinguished (I-III). The surface part of the deep cellular zone of the LPE consists of undifferentiated cells (SD3/SD4 in Figure 2, in between the two white arrows). The horizontal white arrow indicates the SGL. (d) The cell islands of the LPE (superficial part of layer III, white arrow) correspond to vertical zones of increased AChE reactivity marked by black arrows in Figure 18. (e) A bundle of AchE-positive fibers in the MZ of the uncus. AChE, acetylcholinesterase; dis1, superficial LD; dis2, deep LD; HA, area uncinata; HB, area parauncinata; HC, area rhinalis limitans; LD, lamina dissecans; LPE, lamina principalis externa; LPI, lamina principalis interna; MZ, marginal zone; SGL, subpial granular layer. Scale bars: 1 mm (a, b, d, e), 100 µm (c).

Figure 18. AChE histochemistry of EC at 25.5 w.g. (CRL = 245 mm). Black arrows show the AChE-positive bands of in-grown AChE-positive axons into the islands of the cells of the LPE. A single white arrow indicates MZ. AChE, acetylcholinesterase; LPE, lamina principalis externa; MZ, marginal zone. Scale bar: 1 mm.

Figure 19. EC at 28 w.g. (CRL = 270 mm). (a) The rostral part of the EC. The vertical cellular zones of undifferentiated LPE cells are indicated by a series of black arrows. The RS is marked by the long arrow. (b) Rostral portion of EC adjacent to the PAM. The vertical cellular zones of the LPE that are also AChE-positive are indicated by arrows. AChE, acetylcholinesterase; dis1, superficial LD; LD, lamina dissecans; MZ, marginal zone; Neo, temporal neopallium; PAM, periamygdaloid area; RS, rhinal sulcus. Scale bars: 1 mm.

Figure 20. AChE histochemistry of the rostral part of EC at 28 w.g. (CRL = 270 mm). (a) Note the cessation of AChE reactivity of the SP near the RS. The vertical AChE-positive zones of the superficial part of the LPE are indicated by arrows. (b) The most intense AChE reactivity is present in the superficial part of the LPE (arrows). (c) The AChE-positive SP layer abruptly terminates at the border with the neopallium. (d) The rostral part of EC at the transition to the PAM. The most intense reactivity is present in the superficial part of the LPE. Arrows indicate AChE-positive vertical zones. (e) The rostral part of EC at the level of the uncus. Arrows indicate AChE-positive vertical zones. (f) The superficial part of the LPE. A dark, distinctly AChE-positive superficial part of the MZ and the AChE-positive vertical zones of the superficial part of the LPE can be identified. AChE-positive bodies of stellate neurons are indicated by single arrows. Two arrows mark two AChE-positive Cajal-Retzius cells in the MZ. AChE, acetylcholinesterase; LPE, lamina principalis externa; PAM, periamygdaloid area; MZ, marginal zone; RS, rhinal sulcus; SP, subplate zone. Scale bars: 1 mm (a, b), 100 µm (c-f).

Figure 21. AChE histochemistry of the rostral part of the EC at 28 w.g. (CRL = 270 mm). (a) Dark AChE-positive multipolar neurons in the deep LPE are marked with arrows. (b) Two types of AChE-positive neurons occur in LPEd, dark polymorphic neurons (double arrows) and weakly stained pyramidal neurons (single arrow). (c) AChE-positive polymorphic neurons below the CP in the SP (single arrow). (d) AChE-positive polymorphic neurons in the SP (single arrow). CP, cortical plate; LPEd, lamina principalis externa – deep part; SP, subplate zone. Scale bars: 100 µm.

Figure 22. Myelination of the EC fiber systems in the neonate, as revealed by MBP immunocytochemistry. (a) Low-power magnification microphotograph of a coronal section at 40 w.g. The ic is well myelinated as well as some angular bundle fibers. (b) Higher-power magnification of the left (upper) inset in (a), a place where the main branch of the perforant path fibers passes through the subiculum. A significant number of MBP-immunoreactive oligodendrocytes can be seen in the alveus and fimbria, but the perforant and alvear pathways are not yet myelinated. (c) Higher-power magnification of the right (lower) inset in (a). Patches of MBP-immunoreactive immature oligodendrocytes (arrows) and their processes along the temporoammonic branch of the PP in the subicular region can be seen. ab, angular bundle; ic, internal capsule; MBP, myelin basic protein. Scale bars: 5 mm (a), 250 µm (b), 100 µm (c).

Figure 23. AChE histochemistry on tangential sections from rostral EC (areas HA and HB) in a normal adult human brain. (a, b) Note the dark longitudinal AChE-positive bands (zones). (c) To some extent, AChE-positive bundles of axons (indicated by arrows) are extending from the uncus to the superficial layers of the EC. (d) Longitudinal AChE-positive bands in the rostral EC. (e) Longitudinal AChE-positive bands in the central EC (area HB). (f) A reconstruction of a series of serial tangential sections through the EC in areas HA and HB. Note that cell islands in layer II (macroscopically seen as verrucae, Šimić et al., 2005) are always surrounded by capillaries (round empty spaces in a, b, d, e; compare with Fig. 3 in Solodkin and Van Hoesen, 1996). AChE, acetylcholinesterase; HA, area uncinata; HB, area parauncinata; HC, area rhinalis limitans. Scale bars: 1 mm (a-f).

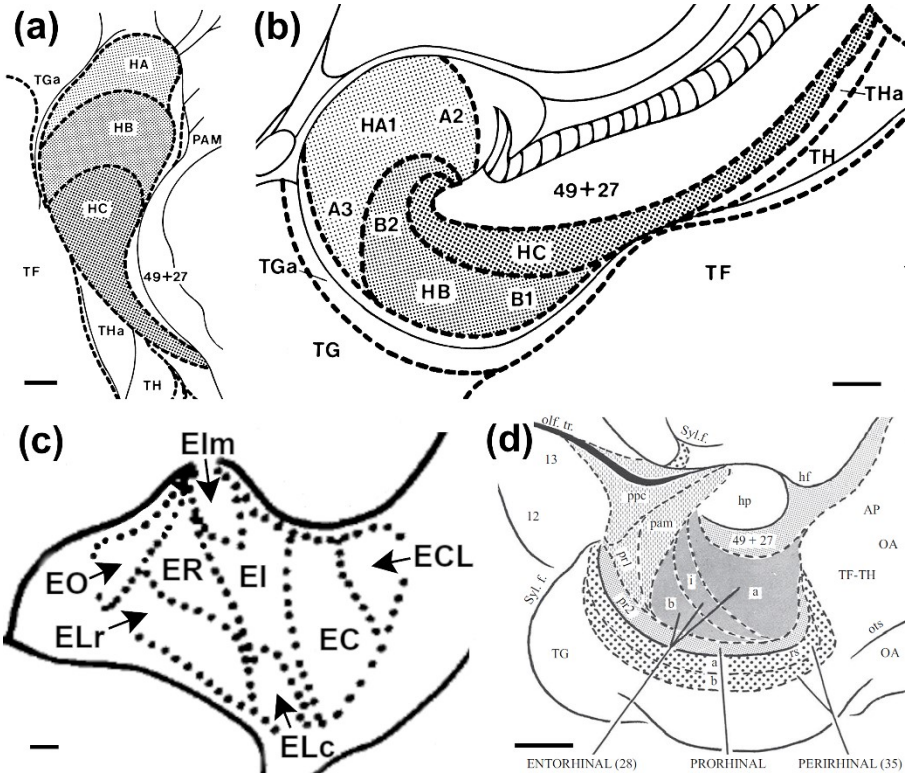
(a)
TGa
HA
HB
PAM
HC
TF
49+27
THa
TH
(b)
HA1
A2
A3
B2
HC
HB
B1
TGa
TG
49+27
THa
TH
TF
(c)
Elm
EO
ER
EI
ECL
ELr
EC
ELc
(d)
olf. tr.
Syl.f.
13
ppc
hf
hp
AP
12
pam
49 + 27
OA
prl
TF-TH
Syl. f.
pr.3
f
a
b
TG
ots
OA
ENTORHINAL (28)
PRORHINAL
PERIRHINAL (35)

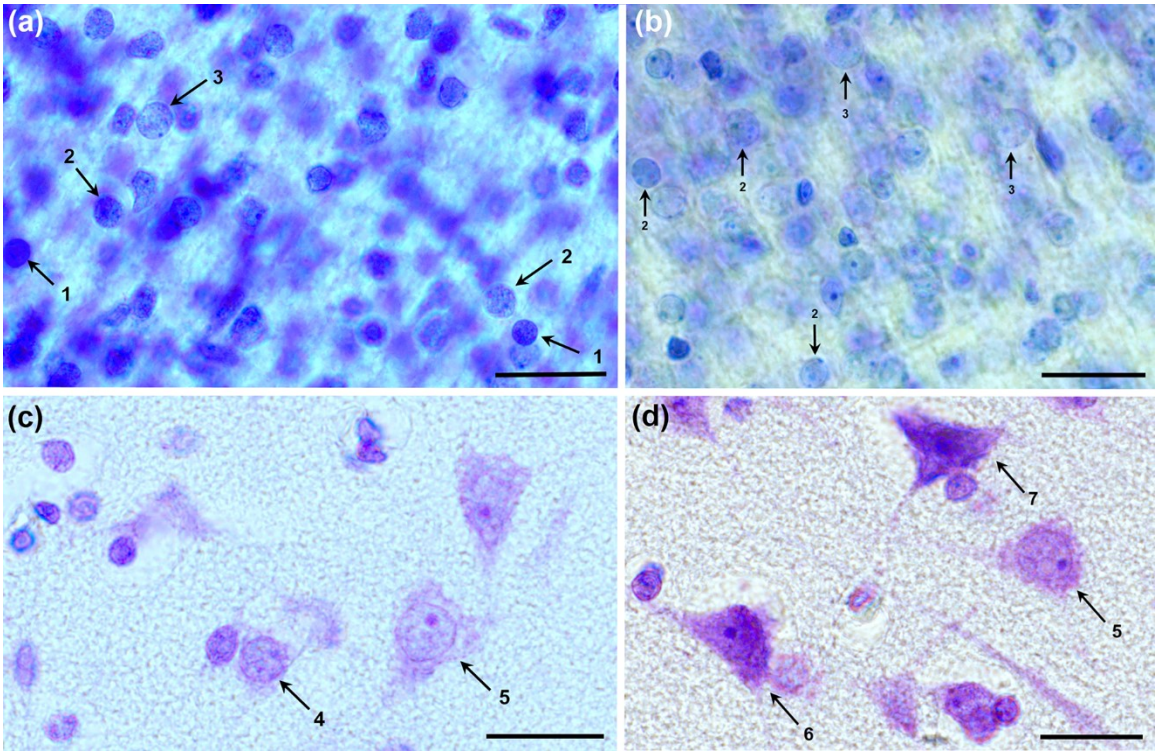
(a)
3
2
1
2
1
(b)
3
2
3
2
2
(c)
4
5
(d)
7
5
6

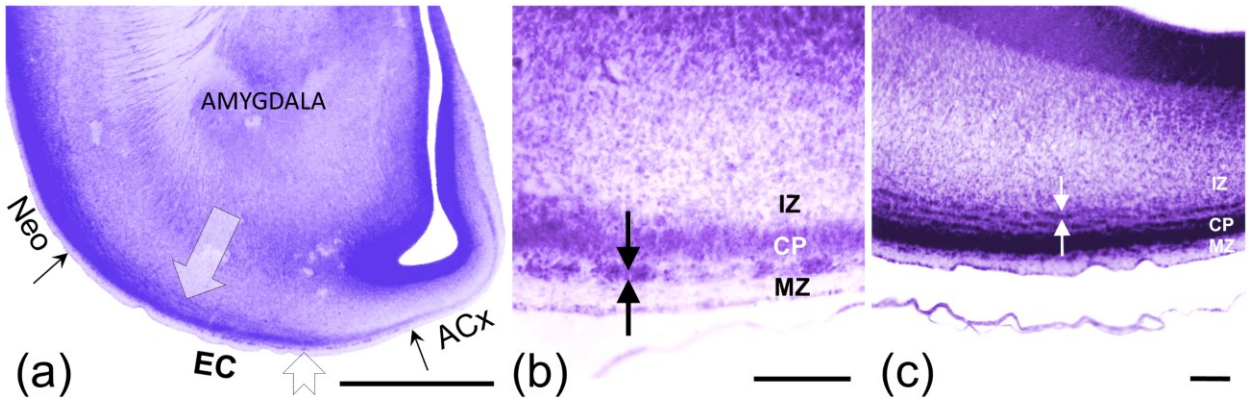
AMYGDALA
Neo
ACx
EC
(a)
IZ
CP
MZ
(b)
IZ
CP
MZ
(c)

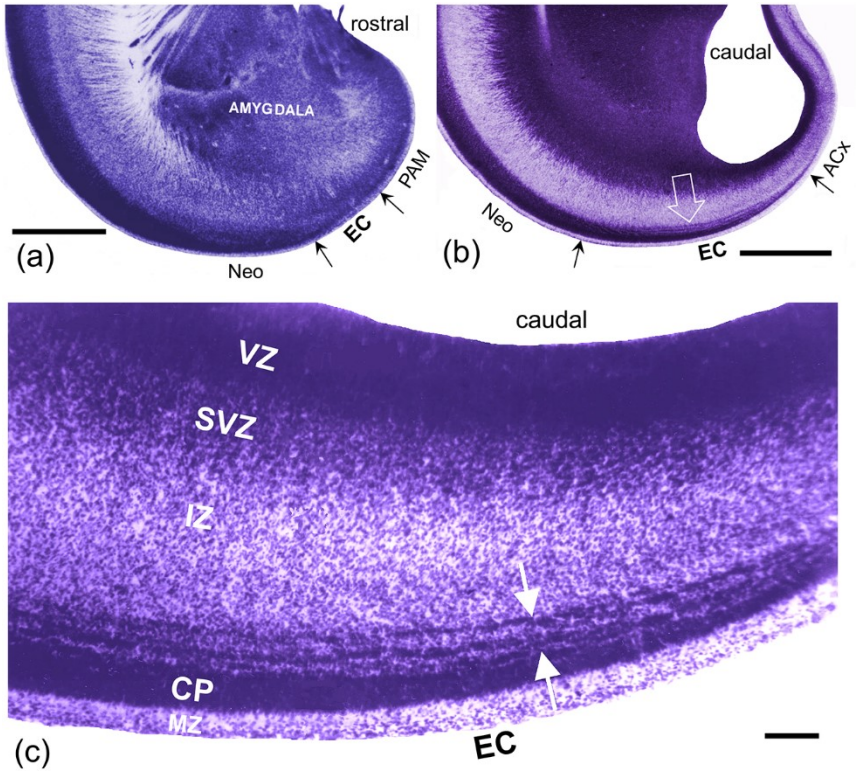
rostral
AMYGDALA
PAM
EC
(a)
Neo
caudal
ACx
Neo
(b)
EC
caudal
VZ
SVZ
IZ
CP
MZ
(c)
EC

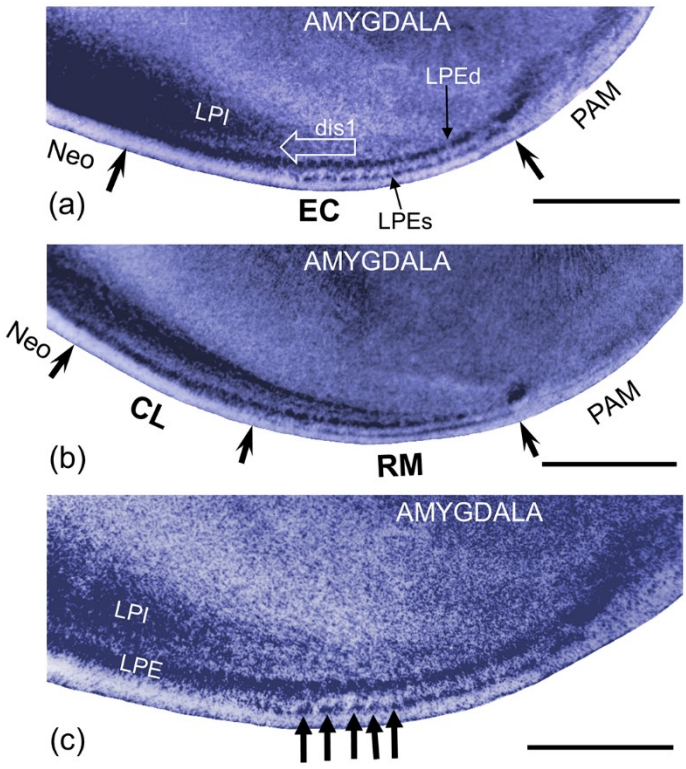
AMYGDALA
LPI
LPEd
dis1
PAM
Neo
(a)
EC
LPEs
AMYGDALA
Neo
CL
PAM
(b)
RM
AMYGDALA
LPI
LPE
(c)

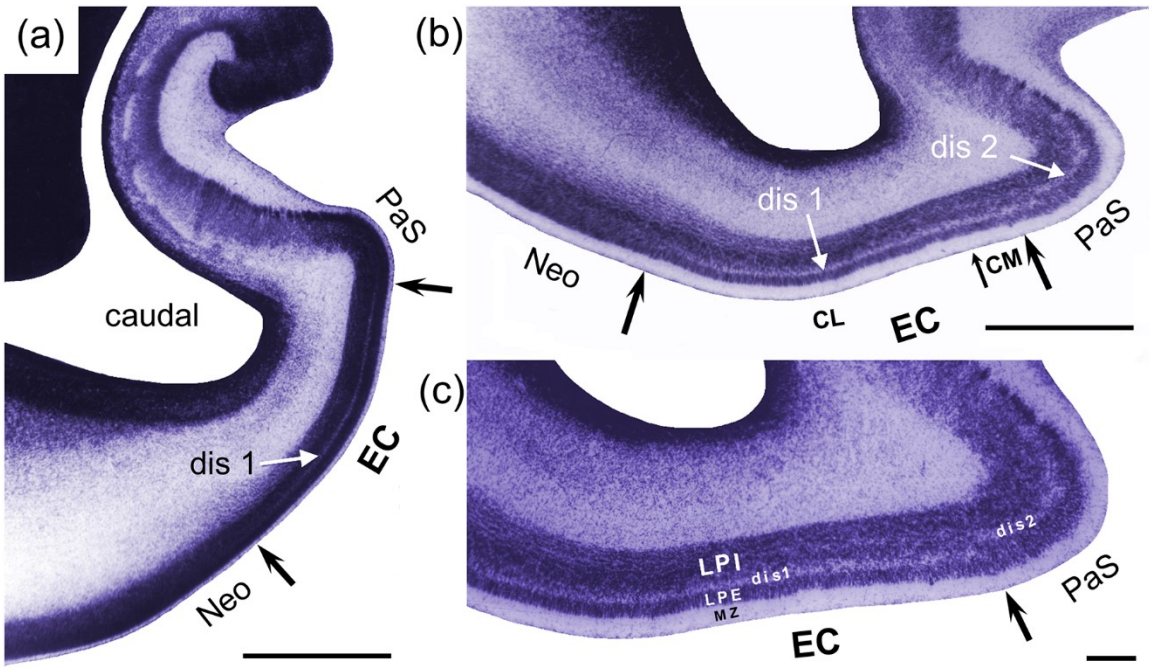
(a)
caudal
PaS
dis 1
EC
Neo
(b)
dis 2
dis 1
Neo
CL
EC
CM
PaS
(c)
LPI
dis1
LPE
MZ
dis2
EC
PaS

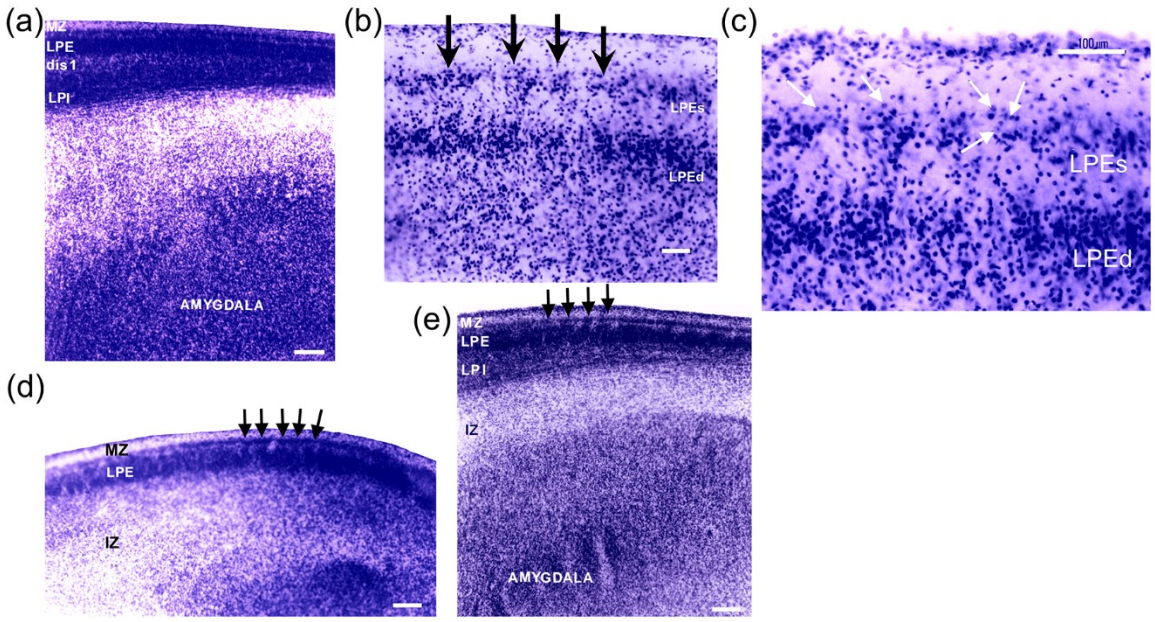
(a)
MZ
LPE
dis 1
LPI
AMYGDALA
(b)
LPEs
LPEd
(c)
100μm
LPEs
LPEd
(d)
MZ
LPE
IZ
(e)
MZ
LPE
LPI
IZ
AMYGDALA

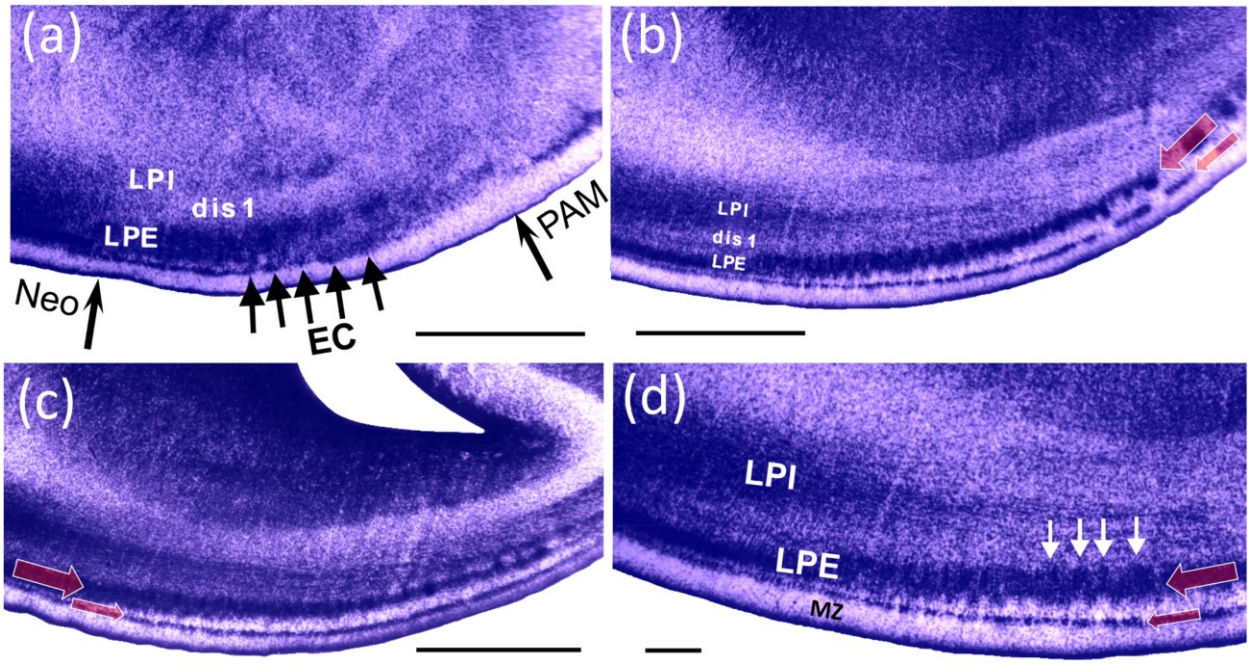
(a)
LPI
dis 1
LPE
PAM
Neo
EC
(b)
LPI
dis 1
LPE
(c)
(d)
LPI
LPE
MZ

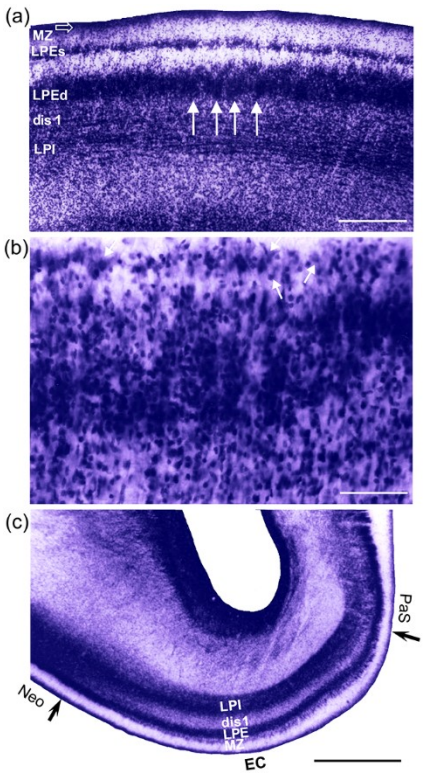
(a)
MZ
LPEs
LPEd
dis 1
LPI
(b)
(c)
PaS
Neo
LPI
dis1
LPE
MZ
EC

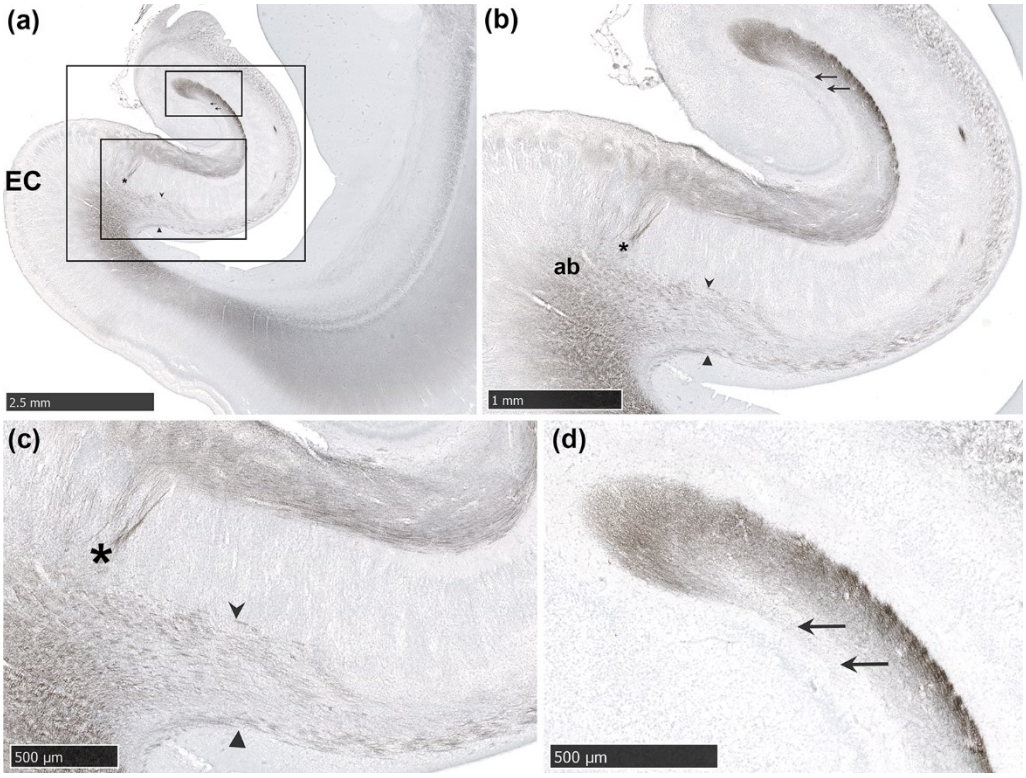
(a)
EC
2.5 mm
(b)
ab
1 mm
(c)
500 µm
(d)
500 µm

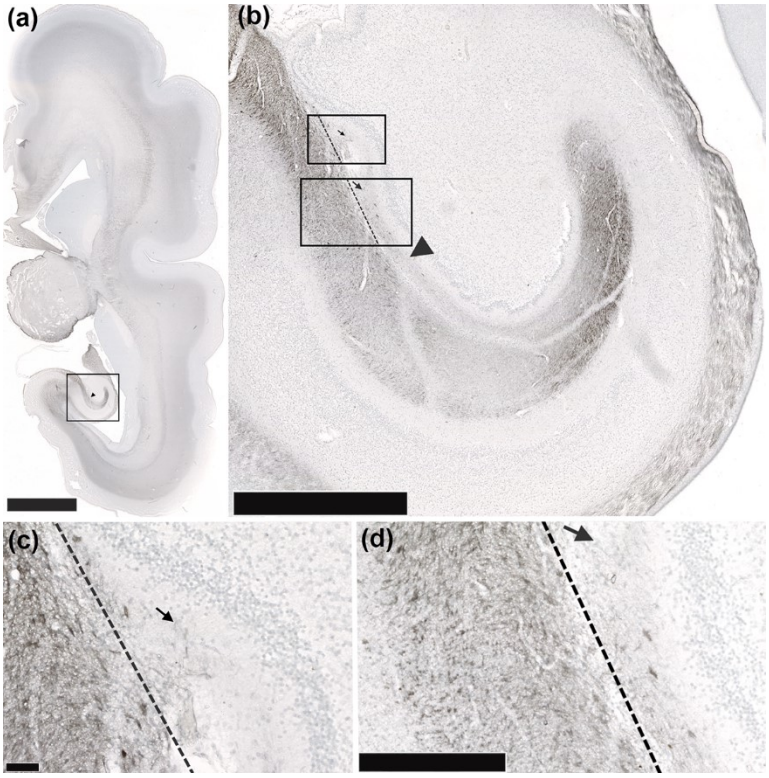
(a)
(b)
(c)
(d)

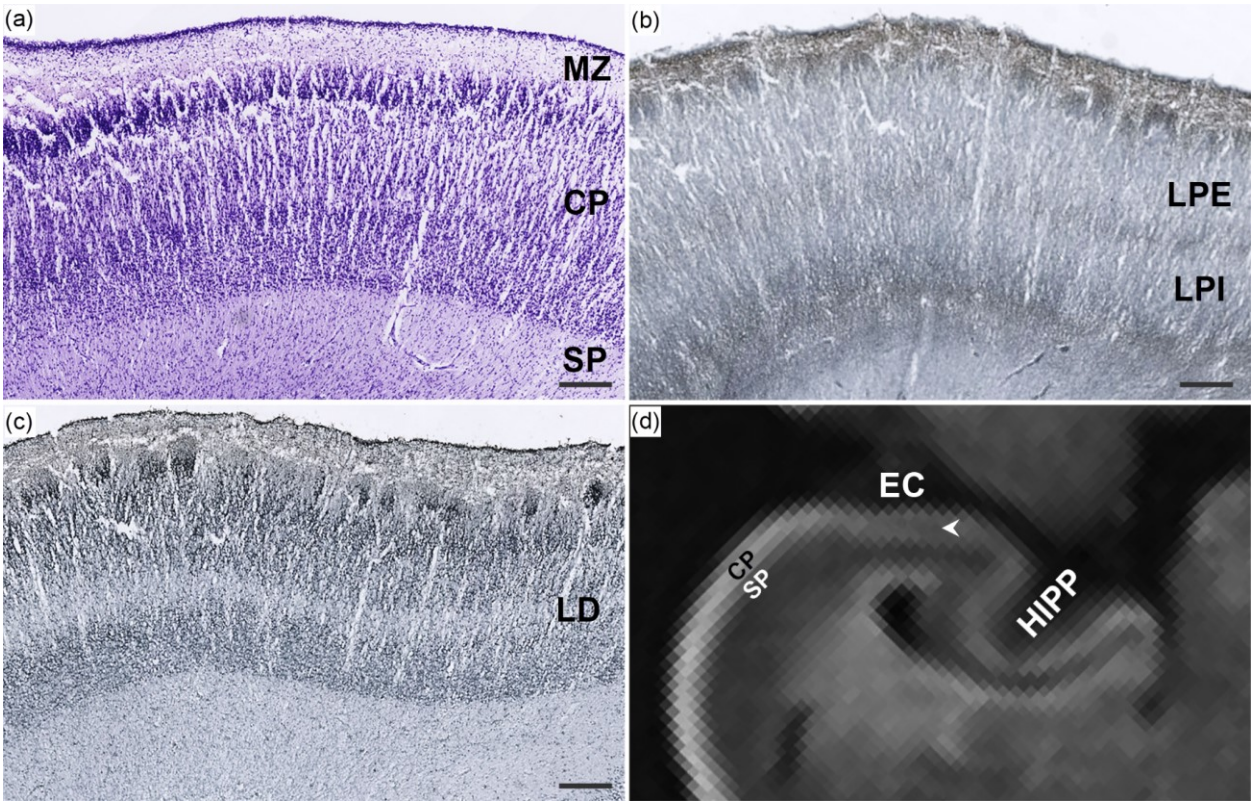
(a)
MZ
CP
SP
(b)
LPE
LPI
(c)
LD
(d)
EC
CP
SP
HIPP

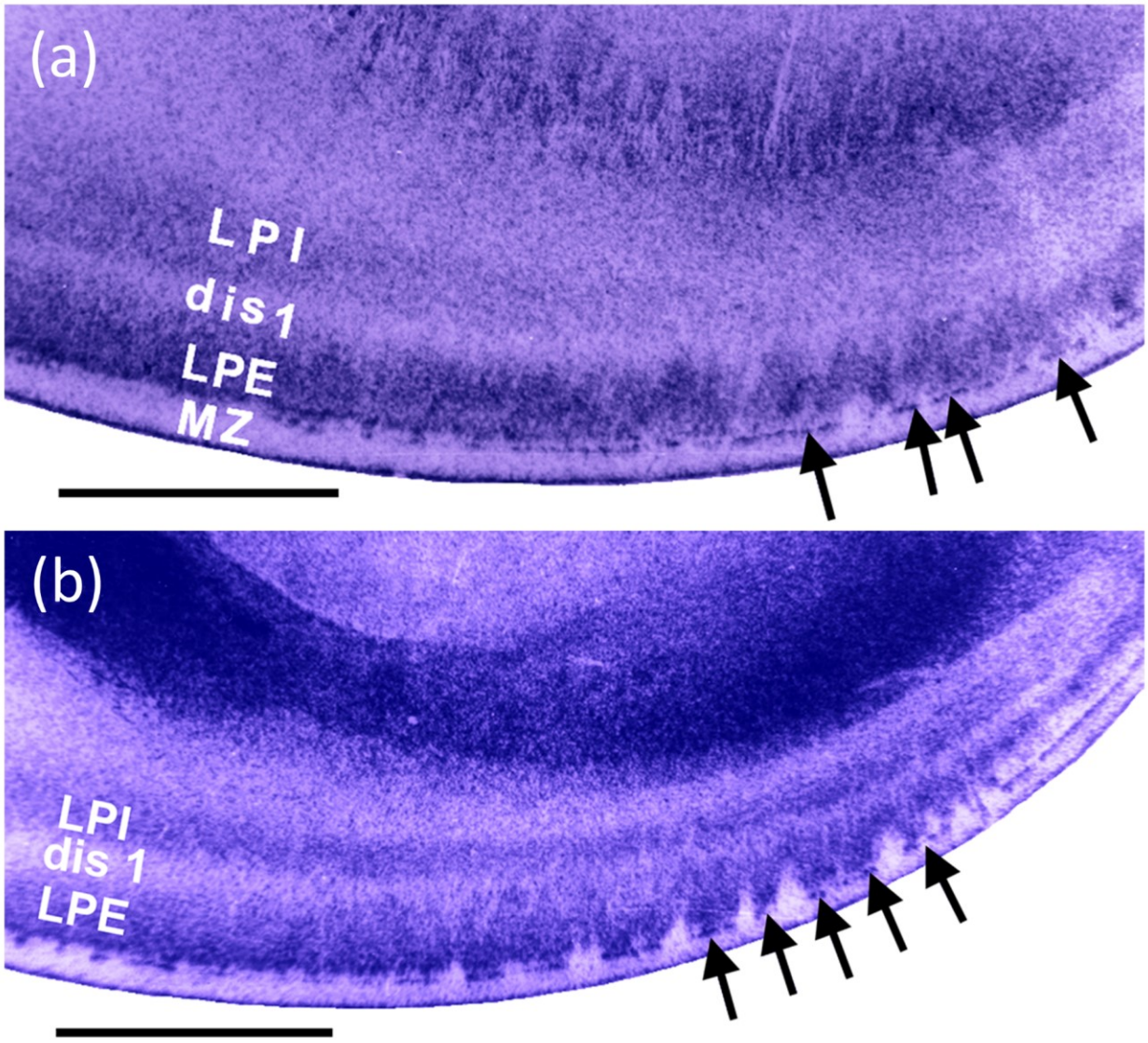
(a)
LPI
dis 1
LPE
MZ
(b)
LPI
dis 1
LPE

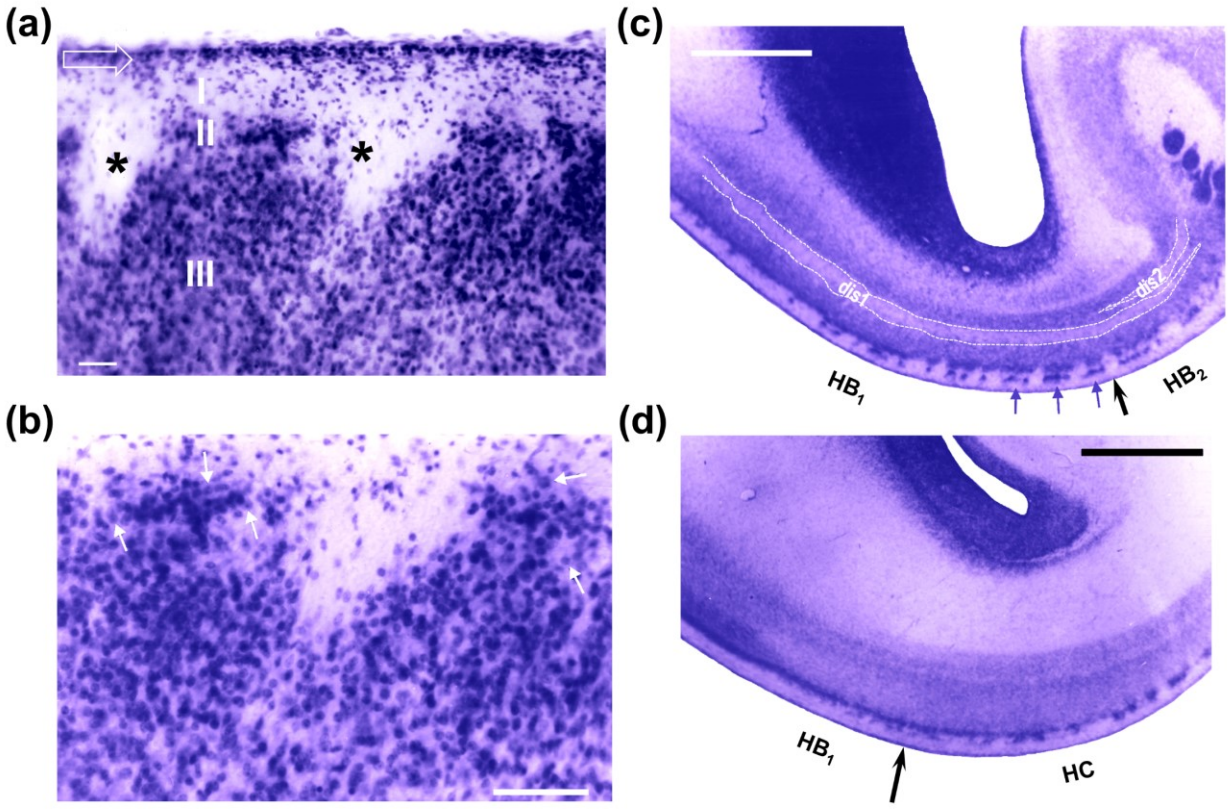
(a)
I
II
III
*
*
(b)
(c)
dis1
dis2
HB1
HB2
(d)
HB1
HC

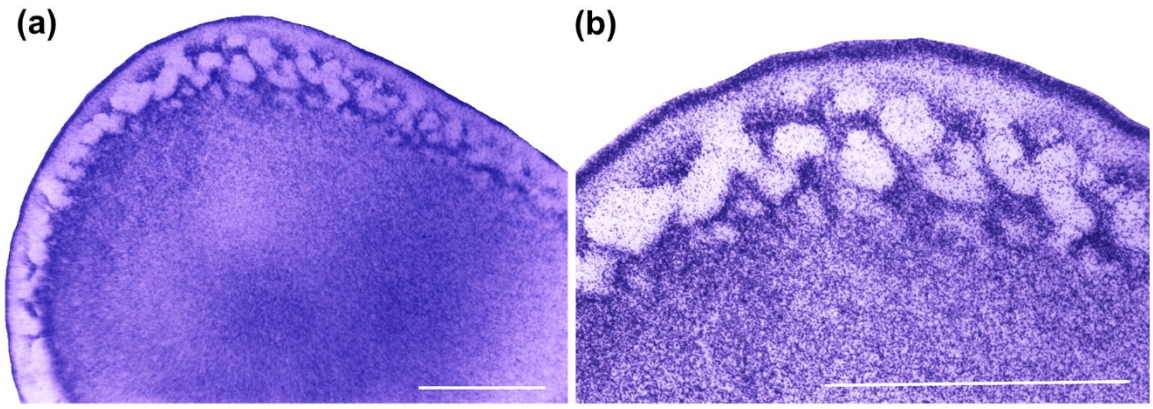
(a)
(b)

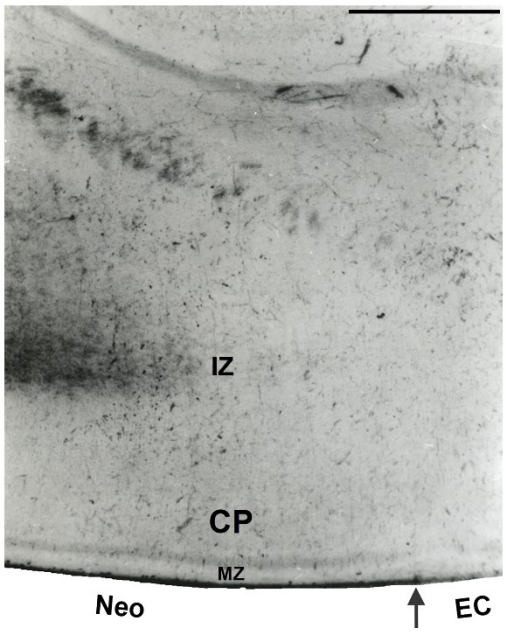
IZ
CP
MZ
Neo
EC

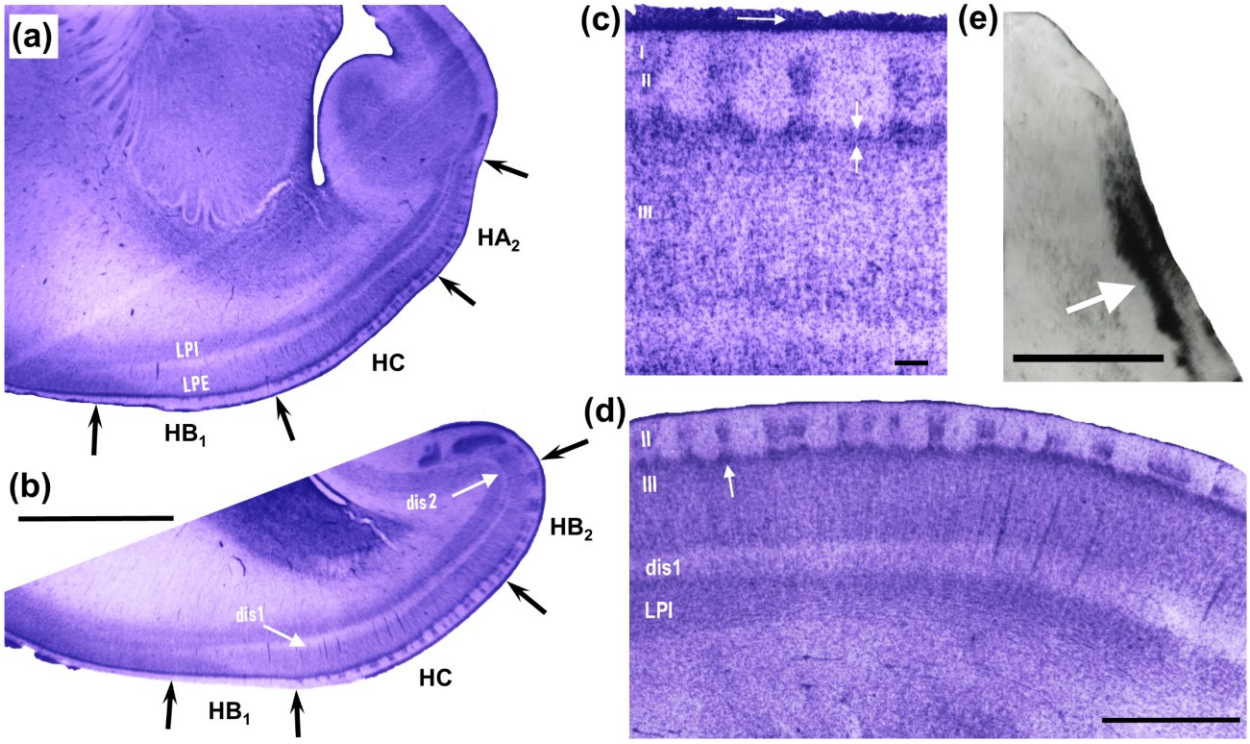
(a)
HA2
LPI
LPE
HC
HB1
(b)
dis2
HB2
dis1
HC
HB1
(c)
I
II
III
(d)
II
III
dis1
LPI
(e)

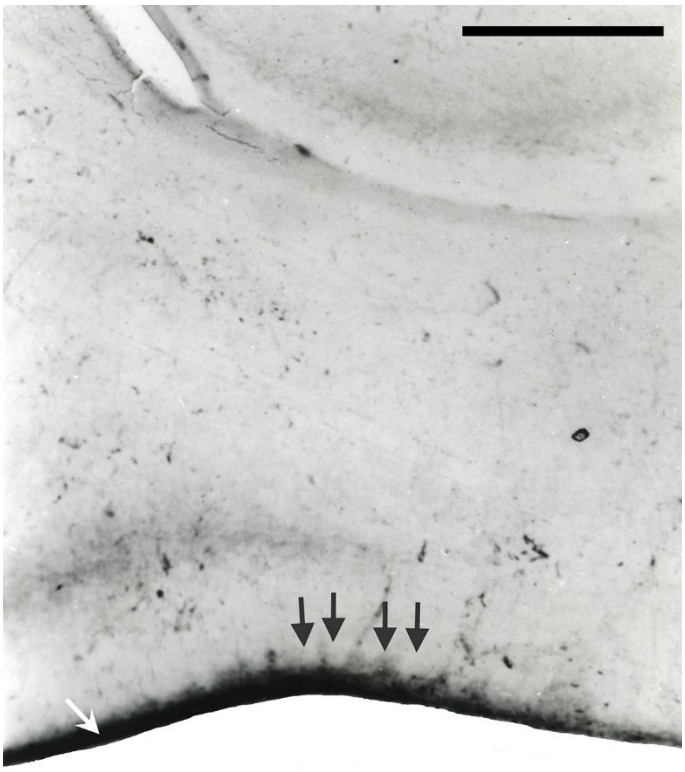

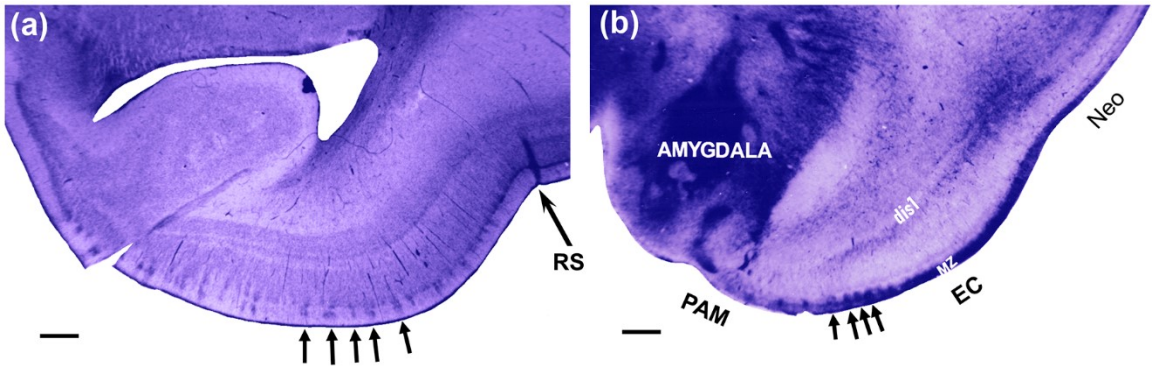
(a)
RS
(b)
AMYGDALA
dis1
MZ
Neo
PAM
EC

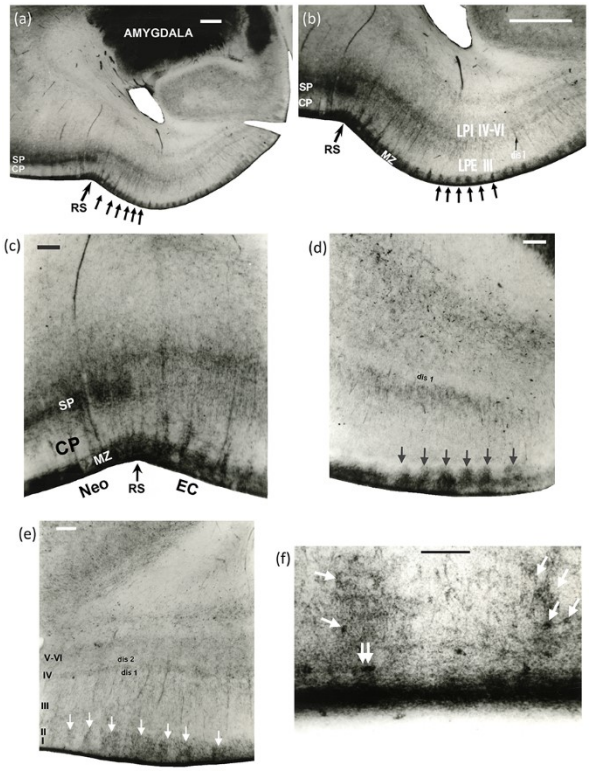
(a)
AMYGDALA
SP
CP
RS
(b)
SP
CP
RS
MZ
LPI IV-VI
LPE III
(c)
SP
CP
MZ
Neo
RS
EC
(d)
dis 1
(e)
V-VI
IV
III
II
I
dis 2
dis 1
(f)

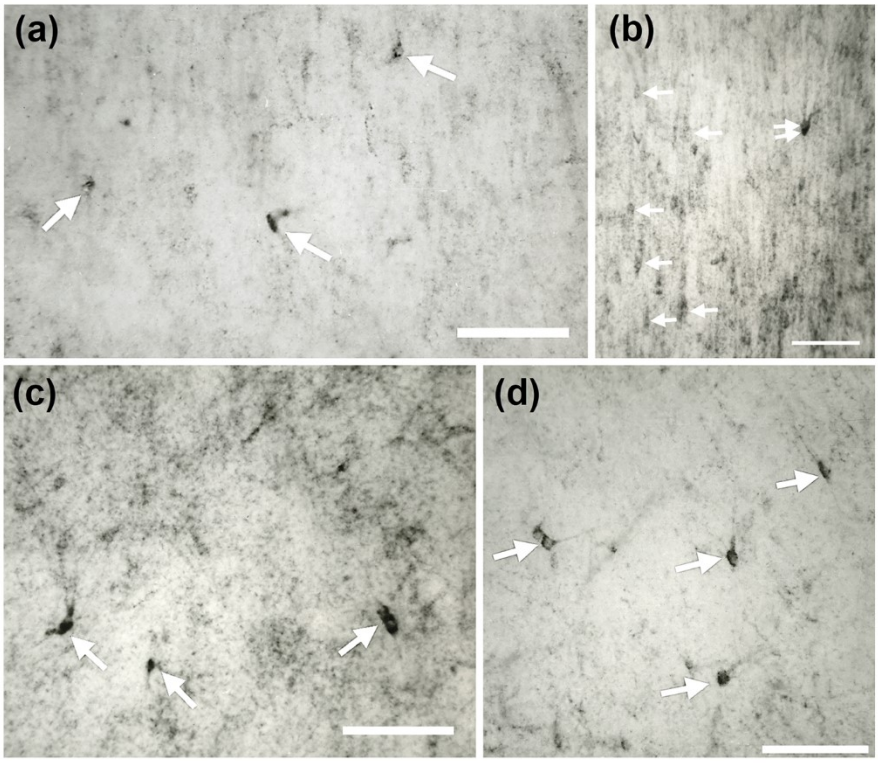
(a)
(b)
(c)
(d)

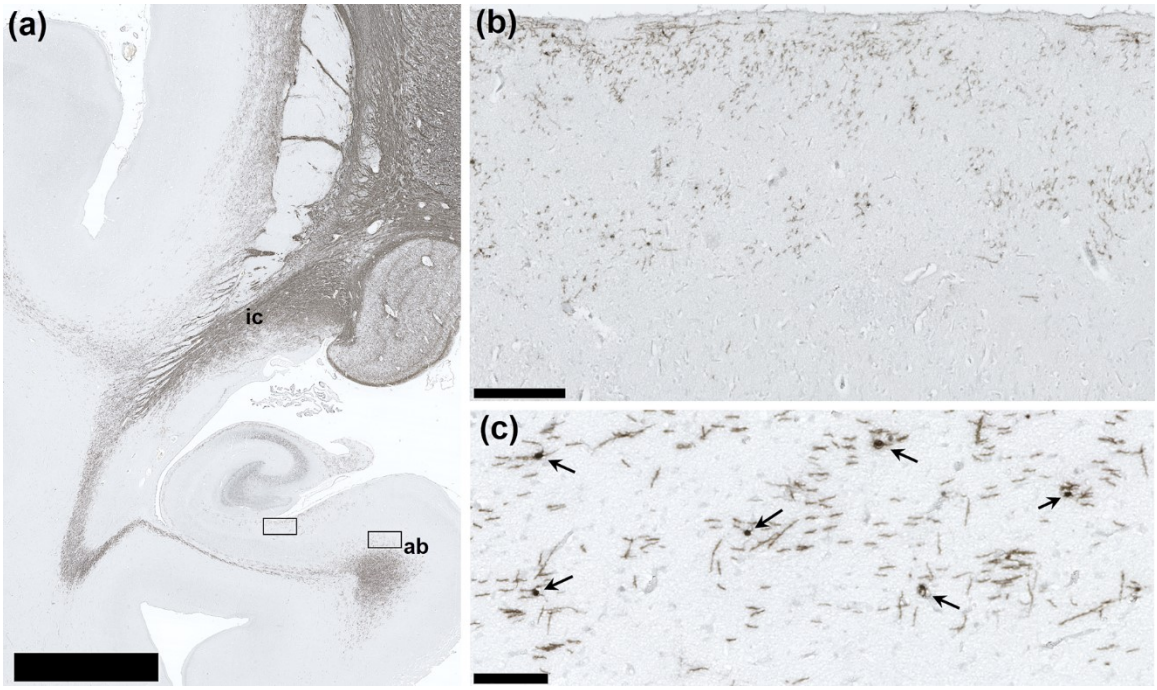
(a)
ic
ab
(b)
(c)

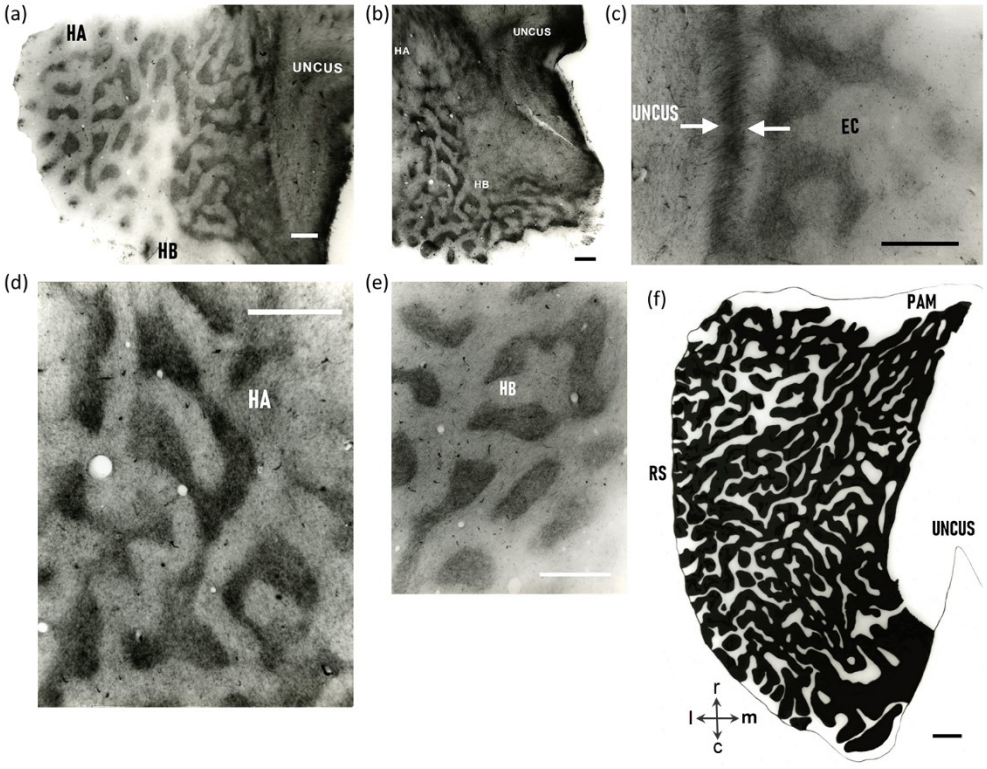
(a)
HA
UNCUS
HB
(b)
UNCUS
HA
HB
(c)
UNCUS
EC
(d)
HA
(e)
HB
(f)
PAM
RS
UNCUS
r
l
m
c